PREPARATION AND PROPERTIES OF REACTIVELY SPUTTERED COPPER OXIDE FILMS

by

Vladimir F. Drobny

Dipl. Ing. 1969

Slovak Technical University

A THESIS SUBMITTED IN PARTIAL FULFILMENT OF

THE REQUIREMENT FOR THE DEGREE OF

DOCTOR OF PHILOSOPHY

in

THE FACULTY OF GRADUATE STUDIES

(Department of Electrical Engineering)

We accept this thesis as conforming to

the required standard

THE UNIVERSITY OF BRITISH COLUMBIA

August, 1978

In presenting this thesis in partial fulfilment of the requirements for an advanced degree at the University of British Columbia, I agree that the Library shall make it freely available for reference and study. I further agree that permission for extensive copying of this thesis for scholarly purposes may be granted by the Head of my Department or by his representatives. It is understood that copying or publication of this thesis for financial gain shall not be allowed without my written permission.

Vladimir F. Drobny

Department of Electrical Engineering

The University of British Columbia
2075 Wesbrook Place
Vancouver, Canada
V6T 1W5

Date October 16, 1978

ABSTRACT

The deposition of thin copper oxide films by reactive sputtering has been investigated from both experimental and theoretical standpoints. Experimental work utilized both r.f. and d.c. sputtering in argon/oxygen mixtures. The film properties of [O]/[Cu] compositional ratio, optical constants and resistivity were experimentally determined. The composition of the films was found to change with increasing oxygen partial pressure in the following manner

$$Cu \rightarrow Cu + Cu_2O \rightarrow Cu_2O \rightarrow Cu_2O + CuO \rightarrow CuO$$

The above trend could also be observed at a given oxygen partial pressure by varying the metal deposition rate. This observation led to the postulate that the film compositional ratio was determined by the relative magnitudes of the fluxes of copper and oxygen atoms incident on the substrate plane. Based on this postulate a comprehensive theory describing film deposition by reactive sputtering was developed. The theory is sufficiently general to apply to any metal - elemental reactive gas system. Good agreement was obtained between the predictions of the theory and the phase composition of copper oxide films deposited over a wide range of experimental conditions. Correlation of theoretical and practical data also allowed determination of the sticking coefficient for oxygen on copper-coated surfaces. The theory also served to guide experiments in producing, in a very reproducible manner, copper oxide films with a wide range of optical and electrical properties. The optical constants of complex refractive index and absorption coefficient were determined for the first time for reactively-sputtered films of $Cu + Cu_2O$, Cu_2O, $Cu_2O + CuO$ and CuO. The presence of Cu_2O was found to be characterized by a peak in the real part of the refractive index

(n = 3.36) occurring at a wavelength of 0.48μm. Evidence of free carrier absorption and acceptor level - conduction band transitions was obtained for Cu_2O films of various stochiometry. The resistivity of the Cu_2O films depended strongly on the stochiometry and values as low as 30 ohm cm could be easily obtained. Such low values of resistivity are not readily obtainable by other preparative techniques and allow Cu_2O to be considered as a semiconductor material for a variety of applications. One such application, namely Cu_2O/Si heterojunction solar cells, was investigated in the present work.

TABLE OF CONTENTS

LIST OF TABLES

LIST OF ILLUSTRATIONS

LIST OF SYMBOLS

a	-	ratio of the initial copper thickness to the thickness of resulting Cu_2O
A	-	surface area of the regions of the evacuated enclosure coated by sputtered deposits
A_M	-	area coated by metal
A_{Mo}	-	area coated by metal oxide species
A_S	-	substrate table area
A_T	-	target area
b	-	constant, see definition in chapter 2.2
B	-	re-emission rate of reactive gas atoms
C	-	compositional ratio
C_1	-	compositional ratio contributed from reactive gas in atomic form
C_2	-	compositional ratio contributed from reactive gas in molecular form
d	-	film thickness
d_s	-	substrate thickness
$d_{(h_i k_i l_i)}$	-	interplanar spacing
D	-	deposition rate
E_f	-	Fermi level in the metal
E_{fn}	-	quasi-fermi level for electrons in the semiconductor
E_{oo}	-	characteristic energy
$f(P_o)$	-	normalized sputtering rate
F	-	constant, see definition in chapter 2.2
FF	-	fill factor
$G(P)$	-	incident flux of reactive gas atoms at partial pressure P

$G(P_o)$ - incident flux of reactive gas atoms at partial pressure P_o

h - conduction hole

I - electric current

I_o - incident light intensity

I_o - saturation current (chapter 6)

I_r - reference beam intensity

I_R - reflected light intensity

E_{RO} - intensity of light reflected from a reference aluminum mirror

I_T - transmitted light intensity

J_{SC} - short circuit current density

k - Boltzmann's constant

k - extinction coefficient (chapter 5)

K - isobaric thermal constant

L - variable oxygen leak rate

L - effective specimen - plate distance (Chaper 4)

L - characteristic length (chapter 6)

M - molecular weight

n - number of oxygen atoms in a volume V (chapter 2.2)

n - order of the reaction (chapter 2.1)

n - refractive index (chapter 5)

$\tilde{n}$ - complex refractive index

n_s - refractive index of the substrate

N - number of sites at the target occupied by reactive gas species

N_A - Avogadro's number

N_e - number of empty sites at the substrate

N_M - number of metal atoms in one molecule of compound

N_s - total number of sites at the substrate at which reactive gas species might bond

$N_t(x)$ - trap density

N_{ts} - trap density at the surface of silicon

N_T - total number of sites at the target at which reactive gas species might bond

O.D. - optical density

P - partial pressure of reactive gas during sputtering

P_{eff} - effective partial pressure of reactive gas

P_L - constant related to limiting pressure

P_o - initial partial pressure of reactive gas

q - electronic charge

Q_d - gas contributed from outgassing processes

Q_{lk} - gas contributed from air leakage, steady-state permeation and other constant vapor emissions

r(T) - specific rate of reactive species arrival from the gas phase

$r_{(h_i k_i l_i)}$ - radius on the diffraction pattern of the ring representing a particular crystalographic plane $(h_i k_i l_i)$

R - reflectance from film side

R' - reflectance from substrate side

$R(P_o)$ - sputtering rate at initial partial pressure P_o

R_M - sputtering rate of metal from clean metallic target

R_{ox} - sputtering rate of metal from target fully covered by reactive gas

R_{Tg} - sputtering rate from the target of atomic oxygen

R_{TMo} - fraction of oxygen sputtered from the target in the form of molecular species

$R0(\lambda)$ - reflectance of the reference aluminium mirror

R.O.D. - optical density for reflectance

s - specific density

S	-	pumping speed
t	-	time
T	-	absolute temperature
T	-	optical transmittance (chapter 4 and 5)
T_s	-	rate of sorption of reactive gas by sputtered metal deposits
T_T	-	rate of sorption of reactive gas by the target
T.O.D.	-	optical density for transmittance
V	-	voltage
V_{oc}	-	open circuit voltage
$[V_{cu}^{-}]$	-	copper ion vacancy
W	-	film thickness
x	-	distance from the surface
α	-	sticking coefficient
α	-	absorption coefficient for light (chapter 5)
α_o^T	-	sticking probability for reactive gas at the target
α_o	-	sticking coefficient of oxygen at the substrate
α_M	-	sticking coefficient of metal at the substrate
α_{Mo}	-	sticking coefficient of metal oxide species at the substrate
α_M^*	-	sticking coefficient of metal species at the substrate
β	-	constant, see definition in chapter 2.2
β'	-	constant, see definition in chapter 2.2
β''	-	constant, see definition in chapter 2.2
γ	-	maximum composition ratio available for particular metal-oxygen system
Δ_M	-	rediffusion coefficient for metal species
Δ_M^*	-	effective rediffusion coefficient for metal species
Δ_{Mo}	-	rediffusion coefficient for molecular species

ε - constant, see definition in chapter 2.2

ε_a - thermal activation energy for conductivity

ε' - constant, see definition in chapter 2.2

ζ - ratio of the sputtering rate of metal in molecular form to the total sputtering rate of metal from compound target

η - efficiency (chapter 6.1)

η - diode quality factor (chapter 6.4)

θ - target surface coverage by reactive gas atoms

ξ - proportionality constant relating the effective gettering rate of sputtered deposits to the sputtering rate of metal

λ - wavelength of electrons (chapter 4)

λ - wavelength of light

ρ - electrical resistivity

σ - electrical conductivity

ϕ_{Bo} - barrier height

ψ - ratio of partial pressure of oxygen to the sputtering rate of copper

ω - constant, see definition in chapter 2.2

ACKNOWLEDGEMENT

I thank my research supervisor, Dr. David L. Pulfrey, for his encouragement, support and careful guidance throughout the course of this research.

Special thanks are due to Dr. L. Young, Dr. D. Tromans, Mr. H. Hogenboom and Mr. A. Lacis for numerous helpful discussions and to Mr. J. Stuber and Mr. D. Fletcher for technical assistance. The financial support of the National Research Council of Canada is gratefully acknowledged.

Finally, I would like to thank my fellow graduate students in the Solid-State group for helpful discussions and also Miss Lisa Ohrling for typing this thesis.

1. INTRODUCTION

It is becoming increasingly clear that the methods presently used for the large scale generation of electricity will need to be augmented by other, so-called non-conventional methods, if future, major crises in the supply of electricity are to be avoided. One of the possible methods that is receiving much attention is photovoltaics. The goal for cost-effective electricity generation by this method is a solar array cost of $500 for each rated peak kilowatt of photovoltaically-produced electricity [1]. The cost of solar cell arrays has fallen from $30,000/kW$_{pk}$ to 6,000/kW$_{pk}$ in the last four years and intensive research and development efforts around the world are seeking to further reduce this figure. One approach is to utilize large area, flat plate solar cells fabricated from thin film semiconductors. Various candidate materials being investigated are Cu_2S, CdS, Si, GaAs, CdZnS, CdTe, Zn_3P_2, InP, $CuInSe_2$ and several organics [2]. Another material that has only received little attention is Cu_2O [3-6]. It is perhaps surprising that more work has not been carried out on this material as it can be formed by the simple thermal oxidation of an abundant and inexpensive metal. Also the bandgap of Cu_2O is 2.04 eV and is direct, thus suggesting use of Cu_2O either as a window material in a heterojunction structure with lower bandgap semiconductor partners, or as a short wavelength absorbing component in a tandem cell arrangement [2]. The traditional method of thermal oxidation of Cu to Cu_2O may be suited to cells of the latter type, provided stable material of resistivity considerably lower than presently attainable ($\sim$ 2500 ohm-cm) can be achieved. However this does not appear too likely in view of the difficulties involved in doping thermally grown Cu_2O [7]. The effect of doping by substitutional impurities on Cu_2O conductivity is presently not known and thus only a defect doping effect

resulting from a Cu_2O nonstochiometry has so far been utilized in lowering the resistivity of Cu_2O material used in solar cell experiments. The usual doping procedure for thermally grown Cu_2O involves the saturation of Cu_2O by oxygen at high temperature ($\sim$ 1100°C) followed by an abrupt cooling of the sample to $\sim$ 25°C resulting in a freezing-in of copper ion vacancies. Various quenching procedures have been tried [8,9] but all have so far failed to produce Cu_2O material with resistivity low enough to make it practical for solar cell use. The limitations would appear to be the nature of the annealing and quenching processes in as much as they restrict the amount of excess oxygen that can be incorporated in the sample and the crystalline perfection respectively. Thus, to realize the photovoltaic potential of Cu_2O, formation technologies other than thermal oxidation need to be developed. In particular to fully realize the thin film capability of Cu_2O a method of depositing the material on a desirable substrate would be preferable to a method limited to "growing" the film on a copper substrate. Deposition of copper oxide films by reactive sputtering is one possibility and this method has received some attention in the past in studies on the fundamental processes involved in both r.f. [24] and d.c. [28] reactive sputtering. As would be expected, the composition of the deposited oxide is a function of the oxygen partial pressure in the sputtering discharge, although the previous works are not in agreement as to the relationship between these two properties. It was postulated by the present author that this control over the material composition ratio may lead to a convenient method of effectively doping cuprous oxide and thus achieving the desired low values of resistivity. Accordingly the reactive sputter deposition of thin films of copper oxide was investigated in detail in this thesis.

The results obtained led to postulation of a comprehensive theory of film deposition by reactive sputtering based on the premise that the deposited film compositional ratio is related to the magnitudes of the fluxes of reactive gas species and sputtered metal species at the substrate plane. This theory is described in chapter 2, both from a general standpoint and for the particular case of the copper-oxygen system.

Chapter 3 describes substrate preparation techniques and the sputtering system used in the experiments. General considerations related to film preparation techniques leading to a high reproducibility of experimental data are also discussed in this chapter.

The ultimate aim of this program on copper oxide thin films is to produce acceptably efficient (5 - 10%) solar cells, but before this can be achieved a number of relevant material properties of the deposited films have to be firmly established. This task formed the main part of the experimental work described in this thesis and is recorded in chapters 4 and 5. In chapter 4 measurements of phase composition, optical transmittance, electrical resistivity and thermal activation energies for conductivity of copper oxide films are presented. Experiments designed to directly test the proposed theory on reactive sputtering are also described, and the agreement obtained is very good. The theoretical treatment is then used in conjunction with the experimental data to determine the sticking coefficient of reactive gas at the substrate, so illustrating a novel way of determining this parameter. Chapter 5 is devoted to describing the method used and the results obtained in determining the optical constants of the thin copper oxide films. Knowledge of the optical constants is of importance not only for assessing the photovoltaic potential of copper oxide films but also for establishing a fundamental property of these films.

The measured electrical and optical properties of the copper oxide films suggest that, as far as photovoltaic applications are concerned, a heterojunction diode solar cell structure involving Cu_2O and a lower bandgap semiconductor is worthy of study. Accordingly the technology of preparation of Cu_2O/Si heterojunction diodes is described in chapter 6. First results of I-V measurements both in the dark and under simulated sunlight are presented.

The conclusions to be drawn from this work are presented in chapter 7 and suggestions for further work are made.

2. THEORY OF REACTIVE SPUTTERING

2.1 INTRODUCTION

There has recently been much discussion on the fundamental aspects of reactive sputtering, especially concerning the mechanism of film formation and the particular location at which the film-building species are formed [10-16]. All three possible locations have been considered; namely the target surface, the vapor phase and the substrate. At pressures in the range typically used for r.f. and d.c. diode sputtering the mean free path of sputtered atoms is large ($\sim$ 1 cm). Therefore, when a low partial pressure of reactive gas is used ($\sim$ 1% of total pressure), the number of collisions between sputtered metal species (M) and the reactive gas species (O) will be small. Thus the rate of creation of M-O species in the vapor phase is likely to be much less than the rate of arrival of either reactive species at the target or reactive and metal species at the substrate. Obviously the probability of formation of more complicated species, such as MO_2, M_2O etc., is even lower. Also the probability of a synthesis reaction in the gas phase is very low because some means for the release of the energy of reaction as well as the kinetic energy of the atoms is necessary to prevent a spontaneous decomposition [10]. Thus at the low total pressures and reactive gas concentrations used in reactive sputtering the possibility of forming the film-building species in the gas phase would appear to be very unlikely.

It is known that when sputtering metallic targets in a reactive gas mixture, an abrupt decrease in the deposition rate takes place above a certain value of reactive gas partial pressure [17- 21]. This has been

attributed to a reaction taking place at the target surface. It has been assumed that, above a certain critical pressure of reactive gas, the target becomes partially or fully, depending on the pressure, covered by the compound formed by reaction between the reactive gas species and the target. Usually, especially in the case of oxides, these compounds have much lower sputtering yields than their parent metals, resulting in a deposition rate which decreases in proportion to the area of target covered by the compound. During the last decade several models of reactive sputtering have been published which seek to explain the processes occurring at the target's surface [17-21], with the aim of modelling and predicting the changes of sputtering rate with partial pressure of reactive gas. Heller [21] first presented a model, in which the rapid decrease of the sputtering rate above a certain pressure of reactive gas was explained in terms of the difference between the sputtering and oxidation rate at the target surface as a function of the partial pressure of reactive gas. Later Abe and Yamashina [18] further developed this model and were able to calculate the deposition rate at any partial pressure of reactive gas for a particular metal-reactive gas system, provided some constants were determined experimentally. They expressed the normalized sputtering rate in terms of the incident flux of reactive gas atoms G (P_o) [$m^{-2}sec^{-1}$], the re-emission rate of reactive gas atoms B [$m^{-2}sec^{-1}$], the sticking coefficient α, the initial (i.e. before energizing the plasma) partial pressure of reactive gas P_o [Pa], and the constant P_L [Pa] related to some limiting pressure, by the following relations:

$$f(P_o) = \frac{R(P_o) - R_{ox}}{R_M - R_{ox}} = 1 - \frac{(\alpha/B)(P_o/P_L)^n \, G(P_o)}{1 + (\alpha/B)(P_o/P_L)^n G(P_o)} \qquad (2.1)$$

where $R(P_o)$ is the sputtering rate at a given initial partial pressure of reactive gas P_o, R_M the sputtering rate from a clean metallic target, and R_{ox} the sputtering rate of the metal from the target fully covered by a reactive gas species. The values for α/B, P_L and n (the so-called order of the reaction [18]) can be determined from experimental data for $R(P_o)$, R_M and R_{ox} respectively. The limiting pressure P_L refers to the value of partial pressure of reactive gas at which the reduction in the sputtering rate, due to compound formation at the target, starts to be significant. P_L is certainly a function of the metal sputtering rate but no attempt was made to relate these two properties. The model also did not account for the reduction in the pressure of reactive gas during sputtering due to its absorption by deposits and the target.

A similar model published in the same year by Shinoki and Itoh took into consideration the absorption of reactive gas by sputtered metal deposits at the substrate, and the effective partial pressure of reactive gas during sputtering was expressed by the following equation [19] :

$$P_{eff} = P_o - \frac{\xi}{S} R_M A_T \left(1 - \frac{N}{N_T} \right) \qquad (2.2)$$

where P_o and R_M are as defined in equation (2.1), A_T is the target area, S is the pumping speed, N_T is the total number of sites on the target at which reactive gas species might bond, N is the number of sites on the target actually occupied by a reactive gas species and ξ is a proportionality constant which relates the effective gettering rate of sputtered deposits to the sputtering rate of the metal. However, in the above model no mathematical expression was given for the determination of ξ, neither was this factor correlated in a physical sense with other variables. This model also did not account for the reduction of reactive

gas pressure stemming from absorption by the target. Target absorption becomes important when a large number of reactive gas species are sputtered from the target in molecular form (MO, M_2O etc.)

In all the above models it has been assumed that the effective metal sputtering rate is a function of the target's surface coverage by a reactive gas species. To express this mathematically let θ be the target surface coverage by reactive gas atoms ($\theta = N/N_T$), R_M^* the effective sputtering rate of metal at a target surface with coverage θ, R_M and R_{ox} the sputtering rates when $N/N_T = 0$ (clean metallic target surface) and $N/N_T = 1$ (the target surface fully covered by reactive species) respectively. The effective sputtering rate of metal is then given by a linear combination of R_M and R_{ox}, namely

$$R_M^* = R_M - (R_M - R_{ox})\ \theta \qquad [m^{-2}\ sec^{-1}] \qquad (2.3)$$

Another expression involving θ stems from consideration of the rate of change of the number of sites at the target occupied by reactive gas species, i.e.

$$\frac{dN}{dt} = \alpha_o^T G(P)\ (1 - \theta\ ) - B\ \theta \qquad (2.4)$$

where α_o^T is the sticking probability for reactive gas at the target and B is the reemission rate of reactive gas atoms when the target is fully covered by reactive species $[m^{-2}sec^{-1}]$. The first term on the right hand side of equation (2.4) expresses the rate of reactive gas trapping on the target surface and the second term the rate of reactive gas removal from the target surface. For steady state conditions at the target, $dN/dt = 0$ and from Equation (2.4).

$$\theta = \frac{\alpha_o^T\ G(P)}{B + \alpha_o^T\ G(P)} \qquad (2.5)$$

Thus this value of θ can be substituted into Eq. (2.3) and R_M^* calculated as R_M and R_{ox} can be easily determined experimentally.

The above models are useful in describing conditions at the target during reactive sputtering and as such form a basis for developing a more complete model and theory of reactive sputtering that would relate sputtering conditions to the properties of sputter-deposited films. Such a theory is proposed and described in the next section. Following this the theory is applied to a particular system (copper-oxygen) thus providing theoretical results for the composition of deposited copper oxides which can then be used to guide experiments and to compare with experimental data (chapter 4).

2.2 PROPOSED THEORY OF REACTIVE SPUTTERING

In the following treatment reactive sputtering in a diode arrangement is considered. Discharge pressure is taken to be controlled on a dynamic basis and the mode of energizing the plasma is not specified (i.e. it is not considered to be significant whether a d.c. or an r.f. energizing source is used). The target is taken to be metal and the reactive gas species is taken, for definiteness, to be oxygen but the theory so developed is relevant to other elemental reactive gases, e.g. N_2, H_2 etc.

It is first proposed that the reaction site for the film-building species is the substrate and that the deposited film composition is determined by the relative magnitudes of the fluxes of metal and oxygen species sorbed thereat. The arrival of metal species at the substrate continually creates sites at which oxygen may be sorbed. Thus the film builds up and under these circumstances the film composition ratio can be expressed as

$$C = \frac{[O]}{[M]} = \frac{\text{oxygen flow sorbed by the film}}{\text{metal flow sorbed by the film}}$$

$$= \frac{\alpha_o G(P)\ (N_e/N_s) + \Delta_{Mo}\alpha_{Mo}\zeta\theta R_{ox}}{\Delta_M^* \alpha_M^* R_M^*} \qquad (2.6)$$

where α_o, α_{Mo} and α_M^* are the sticking coefficients at the substrate of oxygen, metal oxide and metal species respectively, N_s is the total number of active sites on the substrate created per unit time which can be occupied by reactive atoms [$m^{-2}sec^{-1}$], and N_e is the number of these sites which remains empty per unit time [$m^{-2}sec^{-1}$], G(P) is the flux of oxygen species to the substrate when the discharge is on [$m^{-2}sec^{-1}$], Δ_M^* is the effective rediffusion coefficient for metal sputtered species and Δ_{Mo} is the rediffusion coefficient for molecular sputtered species, θ (as in eqn.2.5) is the fraction of the target covered by oxygen atoms, ζ is the ratio of the sputtering rate of molecular species to the total sputtering rate (i.e. of atomic and molecular species). A measure of ζ has been obtained by Coburn, Taglauer and Kay [23] for various metal oxide targets using glow discharge spectrometry (GDS). It was found that ζ increased with the binary M-O bond energy. Because more complex species such as MO_2^+ or M_2O^+ were only occasionally observed and at very low intensities [23], these species, or more specifically the neutrals MO_2, M_2O, are neglected in the present treatment and only MO formation is considered. The coefficents Δ_M^* and Δ_{Mo} which appear in Eq. (2.6) express the proportions of the total sputtered metal or metal oxide species respectively that impinge on the substrate table, under the condition of equal areas of the target and the substrate table. The coefficients Δ_M^* and

Δ_{Mo} arise from the diffusive nature of sputtered species as they are transported towards the substrate at pressures typically used in r.f. and d.c. diode sputtering [26]. However in most cases, when the target-substrate distance is much smaller than the target diameter, $\Delta^*_{M,}$ Δ_{Mo} can both be taken as approximately equal to unity, especially at the centre portion of the substrate table.

The first term in the numerator of Eq.(2.6) represents the amount of oxygen sorbed by the substrate from the gas phase, while the second term ($\Delta_{Mo}\,\alpha_{Mo}\,\zeta\,\theta\,R_{ox}$) arises because the target can be expected to become partially covered with oxide [18-21], and sputtering from this oxide will yield molecular species as well as atomic oxygen and metal species. The contribution of the latter two components to their respective particle fluxes are included in Eq.(2.6) via G(P) and R^*_M respectively. The effective sputtering rate of metal is defined as the total number of metal species leaving a unit area of target in unit time, and thus the metal deposition rate at the substrate can be described by the following relation:

$$\Delta^*_M\alpha^*_M R^*_M = \Delta_M\alpha_M\,(1-\theta)R_M + \Delta_M\alpha_M(1-\zeta)\theta R_{ox} + \Delta_{Mo}\alpha_{Mo}\zeta\theta R_{ox} \quad \ldots\ldots$$

$$\ldots\ldots [m^{-2}sec^{-1}] \qquad (2.7)$$

where Δ_M is the rediffusion coefficient for sputtered atomic metal species. The first two terms on the right hand side of equation (2.7) represent metal species sorbed upon the substrate in their elemental form. The last term denotes a contribution from the metal species arriving in a bonded metal-oxygen form. Note that G(P) represents the flux of elemental oxygen species to the substrate under deposition conditions, i.e. when the actual partial pressure of oxygen P [Pa] will be somewhat different from that pressure P_o [Pa] established prior to initiation of the sputtering discharge. Thus,

from the kinetic theory of gases we can write

$$G(P) = \frac{5.25 \times 10^{24} P}{(MT)^{1/2}} = r(T)\ P \qquad [\text{atoms } m^{-2} sec^{-1}] \tag{2.8}$$

where M is the molecular weight of oxygen (31.9988), T the gas temperature [K] and r(T) the specific rate of reactive species arrival from the gas phase [$m^{-2} sec^{-1} Pa^{-1}$] [22].

To develop the theory further it is necessary to express the actual pressure P in terms of the measured initial partial pressure P_o. This can be achieved by considering the system equation prior to sputtering, i.e.

$$V \frac{dP_o}{dt} = - P_o S + L \tag{2.9}$$

where V is the system volume [m^3], S the pumping rate [$m^3 sec^{-1}$] and L the variable oxygen leak rate [$m^3 Pa\ sec^{-1}$]. In the steady state $dP_o/dt = 0$ and thus

$$P_o = \frac{L}{S} \tag{2.10}$$

Now, on allowing sputtering to commence the surfaces within the bell jar will become coated with metal atoms, leading to the possibility of oxygen sorption and hence a reduction in the effective oxygen partial pressure. Also some oxygen is sorbed by the target. Thus the new system equation becomes

$$\frac{dn}{dt} = - \frac{n}{V} S + \frac{L}{kT} - A_T(T_T - R_{Tg}) - AT_s \tag{2.11}$$

where A_T, A are the surface areas of the target and of the regions of the evacuated enclosure coated by sputtered deposits respectively [m^2]; T_T, T_s are the rates of sorption of oxygen by the target and by sputtered metal on the substrate respectively [$m^{-2} sec^{-1}$]; R_{Tg} is the sputtering rate from the target of atomic oxygen [$m^{-2} sec^{-1}$]; k is Boltzmann's constant [joules K^{-1}]

and n the number of oxygen atoms in a volume V corresponding to the pressure P assuming ideal gas behavior, i.e.

$$PV = nkT \tag{2.12}$$

When steady state conditions prevail at the target the rate of oxygen reemission from the partially oxidized target will equal the rate of sorption of oxygen at the target (i.e. θ reaches a constant value). It is obvious that all oxygen sorbed at the target surface arrives from the gas phase. On the other hand the oxygen species reemitted from the target are in both atomic and molecular (MO) form and the ratio of their relative fluxes depends on an M-O bond energy as discussed above. Thus the steady state oxygen balance at the target can be described by the following relation:

$$T_T - (R_{Tg} + R_{TMo}) = 0,$$

or

$$R_{TMo} = T_T - R_{Tg} \quad \ldots\ldots \ [m^{-2}sec^{-1}] \quad \ldots\ldots \tag{2.13}$$

where R_{TMo} is the fraction of oxygen sputtered from the target in the form of molecular (MO) species. It is obvious that this fraction of oxygen does not return to the gas phase and thus causes a reduction in oxygen partial pressure. The molecular fraction R_{TMo} can be related to R_{ox}, θ and ζ by the following relationship:

$$R_{TMo} = \theta\zeta R_{ox} \tag{2.14}$$

Inserting Eq. (2.13) into Eq. (2.11) and assuming that the whole sputtering process is in a steady state (dn/dt = 0) one can write that

$$0 = -\frac{n}{V} S + \frac{L}{kT} - A_T R_{TMo} - AT_s \tag{2.15}$$

The rate at which oxygen in the gas phase is sorbed by deposits is given by

$$T_s = \alpha_o G(P) \left(\frac{N_e}{N_s}\right) \tag{2.16}$$

Combining equations (2.6 and 2.16) the expression for T_s emerges as

$$T_s = \Delta_M^* C \alpha_M^* R_M^* - \Delta_{Mo} \alpha_{Mo} \zeta \theta R_{ox} \tag{2.17}$$

Let us assume that no metal and MO species leave the sputtering chamber during sputtering and also that the deposited material, regardless of its location, has a uniform composition. Then in terms of A_M and A_{Mo}, the areas coated by metal and metal oxide species respectively, using Eqns. (2.17) and (2.14) it follows that

$$AT_s = A_M \Delta_M^* C \alpha_M^* R_M^* - A_{Mo} \Delta_{Mo} \alpha_{Mo} \zeta \theta \, R_{ox} \tag{2.18}$$

because all deposits within the vacuum chamber are active in the gettering process.

Inserting equations (2.14 and 2.18) into equation (2.15), then using the relations given by Eqns. (2.10 and 2.12), and then solving for the partial pressure of oxygen P the following relation can be obtained:

$$P = P_o - \frac{A_T kT \zeta \theta R_{ox}}{S} - \frac{A_M kTC \alpha_M^* R_M^* \Delta_M^*}{S} + \frac{A_{Mo} kT \alpha_{Mo} \zeta \theta R_{ox} \Delta_{Mo}}{S} \tag{2.19}$$

If no metal and metal-oxide species leave the sputtering chamber, it is obvious that

$$A_T R_M^* = A_M \Delta_M^* \alpha_M^* R_M^* \tag{2.20a}$$

and

$$A_T \zeta\theta R_{ox} = A_{Mo} \Delta_{Mo} \zeta\theta \alpha_{Mo} R_{ox} \tag{2.20b}$$

Then, when the target area is taken to equal the substrate area ($A_T = A_s$)

$$A_M = \frac{A_s}{\Delta_M^* \alpha_M^*} \tag{2.21a}$$

and

$$A_{Mo} = \frac{A_s}{\Delta_{Mo} \alpha_{Mo}} \tag{2.21b}$$

Substituting the relations for A_M and A_{Mo} given by equations (2.21a and 2.21b) into Eq.(2.19) and again taking $A_T = A_s$ the following relation for the reduced partial pressure of oxygen can be obtained:

$$P = P_o - \frac{A_s kTCR_M^*}{S} \quad [Pa] \tag{2.22}$$

By substituting Eq.(2.22) into Eq.(2.6) using Eq. (2.8) and solving for the composition ratio C we have:

$$C = \frac{P_o}{R_M^*}\left[\frac{1 + \frac{\Delta_{Mo}\alpha_{Mo}\zeta\theta}{\alpha_o r(T)}\left(\frac{R_{ox}}{P_o}\right)\left(\frac{N_s}{N_e}\right)}{\left(\frac{N_s}{N_e}\right)\frac{\Delta_M^*\alpha_M^*}{\alpha_o r(T)} + \frac{A_s kT}{S}}\right] \qquad (2.23)$$

A particular metal oxide film will be characterised by a particular value of (N_e/N_s). Thus for a given composition ratio, temperature, pumping speed and for sticking coefficients independent of oxygen partial pressure and metal sputtering rate, it follows that the denominator in the square bracketed term in Eq.(2.23) is a constant. Assuming the same sputtering power dependence for both R_{ox} and R_M^* the numerator in the square bracketed term will also remain constant for a given ratio of P_o/R_M^*. Note that if the ratio R_M/R_{ox} is independent of sputtering power then the ratio R_M/R_M^* automatically remains constant, see Eq.(2.3). Hence Eq.(2.23) predicts that for preparation of films of a given composition ratio the discharge conditions must be such that the ratio P_o/R_M is kept constant. This situation of keeping a constant value of P_o/R_M for a range of P_o and R_M is difficult to realize in practice as, for example, changes in P_o are not likely to leave the sticking coefficients unaltered and changing R_M will affect the gas and substrate temperatures (and hence $\alpha_o, \alpha_M^*, \alpha_{Mo}$ also). However the appropriateness of equation (2.23) to describing the reactive sputtering of metal oxides can be appreciated by assuming that R_M^* is given by the sputtering rate R_M from a clean metal target in pure argon, and that changes in R_M (caused by adjusting the r.f. power level for instance) require corresponding changes in initial oxygen partial pressure P_o to produce films of a given composition ratio, (see section 4.6).

To find an absolute relationship between the oxygen partial pressure, metal sputtering rate and film composition ratio, N_e/N_s has to be computed. The number of empty sites within a film is given by the difference between the total number of sites able to bond oxygen and the number of oxygen species absorbed by film. Thus during a growth period $t_1 \rightarrow t_2$ we have

$$\int_{t_1}^{t_2} N_e dt = \int_{t_1}^{t_2} N_s dt - \alpha_o G(P) \int_{t_1}^{t_2} \frac{N_e}{N_s} dt \qquad (2.24)$$

The total number of sites N_s available for bonding oxygen can be described as the difference between the number of metal species sorbed by the film during its growth, multiplied by γ (the maximum number of available bonds per metal atom, i.e. γ is equivalent to the maximum composition ratio available for a particular metal-oxygen system), and the number of sites filled during the growth by oxygen arriving in molecular (MO) form. Thus

$$N_s = \gamma \Delta_M^* \alpha_M^* R_M^* - \Delta_{Mo} \alpha_{Mo} \zeta \theta R_{ox} \qquad (2.25)$$

Assuming that the effective deposition rate of metal R_M^*, the pressure P and the N_e/N_s ratio remain constant during a deposition process (i.e. the conditions necessary for obtaining a uniform composition through the film thickness), then by combining equations (2.24 and 2.25) and solving for N_s/N_e one can obtain

$$\frac{N_s}{N_e} = 1 + \frac{\alpha_o r(T)\ P}{\gamma \Delta_M^* \alpha_M^* R_M^* - \Delta_{Mo} \alpha_{Mo}\ \zeta \theta R_{ox}} \qquad (2.26)$$

Substituting Eq.(2.22) for P in Eq.(2.26) and then by inserting Eq.(2.26) into Eq.(2.23) and solving for the composition ratio C the following equation can be obtained

$$C = \frac{1}{2}\left(\gamma + \gamma\omega\varepsilon + \omega\frac{P_o}{R_M^*} - \omega\varepsilon'\zeta\theta\frac{R_{ox}}{R_M^*}\right) - \frac{1}{2}\left[\left(\gamma + \gamma\omega\varepsilon + \omega\frac{P_o}{R_M^*} - \omega\varepsilon'\zeta\theta\frac{P_o}{R_M^*}\right)^2 - 4\omega\left(\gamma\frac{P_o}{R_M^*} + \gamma\varepsilon'\zeta\theta\frac{R_{ox}}{R_M^*} - \varepsilon'\beta''\zeta^2\theta^2\frac{R_{ox}^2}{R_M^{*2}}\right)\right]^{\frac{1}{2}} \tag{2.27}$$

where

$$\omega = \frac{S}{A_s kT}\ ; \qquad \beta = \frac{\alpha_o}{\Delta_M^* \alpha_M^*}\ ; \qquad \beta' = \frac{\alpha_o}{\Delta_{Mo}\alpha_{Mo}}\ ; \qquad \beta'' = \frac{\Delta_{Mo}\alpha_{Mo}}{\Delta_M^* \alpha_M^*}\ ;$$

$$\varepsilon = \frac{1}{\beta r(T)}\ ; \qquad \varepsilon' = \frac{1}{\beta' r(T)}\ .$$

Obviously if Eq.(2.27) is to be used to guide experiments in preparing films of a required C all parameters in the equation have to be known or experimentally controllable. Of these parameters the two likely to give most difficulty in determination are θ and R_M^*. Determination of these is addressed below.

Regarding θ,

$$\theta = \frac{R_M - R_M^*}{R_M - R_{ox}} \tag{2.28}$$

In many cases θ can be approximated, namely; at high partial pressures of reactive gas, when $R_M^* \simeq R_{ox}$ then $\theta \simeq 1$; at very low partial pressures, when

$R_M^* \simeq R_M$ then $\theta \simeq 0$. However at medium partial pressures, when neither of these conditions is fulfilled a simple approximation does not work and R_M^* has to be determined experimentally or calculated theoretically, see below.

As mentioned in section 2.1, when steady state conditions prevail at the target, the rate of oxygen sorption by the target is equal to the rate of oxygen removal from the target, i.e. from Eq.(2.4)

$$\alpha_o^T \, r(T)P(1 - \theta) = B\theta \tag{2.29}$$

B was originally defined as the reemission rate of reactive gas atoms from the target when it was fully covered by the reactive gas species. However the reemission rate B can also be described as the sputtering rate of oxygen atoms from the target fully covered by oxygen atoms. Thus, assuming the same sputtering power dependence (or discharge current dependence in the d.c. sputtering case) for both, R_{ox} and B, one can simply relate B to R_{ox} by some constant b

$$B = bR_{ox} \tag{2.30}$$

Inserting Eq.(2.30) into Eq.(2.29) and solving for θ the following relationship can be obtained:

$$\theta = \frac{Fr(T)P}{R_{ox} + Fr(T)P} = 1 - \frac{R_{ox}}{R_{ox} + Fr(T)P} \tag{2.31}$$

where

$$F \doteq \frac{\alpha_o^T}{b}$$

The relation for the effective sputtering rate of the metal at a particular partial pressure can then be obtained by combining Eqns.(2.3, 2.22 and 2.31),

i.e.

$$R_M^* = R_{ox}\left[1 + \frac{R_M - R_{ox}}{R_{ox} + Fr(T)(P_o - \frac{C}{\omega} R_M^*)}\right] \qquad (2.32)$$

The effective sputtering rate of metal R_M^* can be calculated directly from Eq.(2.32), if C and F are known. In most cases, however, C is unknown. It is then necessary to substitute Eq.(2.28) for θ into Eq.(2.27) and Eq.(2.27) for C into Eq.(2.32) and then solve the complete set of equations iteratively. In the cases when F is unknown, it can be determined experimentally for a given metal-oxygen system by depositing a film of known composition and thickness. Then the number of metal atoms within a film per unit area can be calculated. Dividing this value by a deposition time in seconds the effective sputtering rate of metal can be obtained. By substitution of R_M^* and C values into Eq.(2.32) the value of F can be calculated.

For some metal-oxygen systems having an M-O binary bond energy so small that the contribution of MO species to film formation can be neglected (i.e. the number of MO species is only a very small fraction of the total number of sputtered metal species), Eqns(2.23 and 2.27) can be simplified by omitting all terms containing ζ. Such a system, which can be classified as the low M-O bond energy system, will be discussed in the next section.

Note that Eqns(2.23 and 2.27) can also be used for calculation (or estimation) of the concentration in a deposited film of impurities from the gas phase. In this case P_o can be replaced by P_o', the initial partial pressure of impurity gas. Also γ in this case would now represent either a maximum composition ratio or solubility for a particular impurity gas-deposited metal (or metal oxide) system.

2.3 APPLICATION OF THE THEORY TO THE REACTIVE SPUTTERING OF COPPER IN OXYGEN

To complement the experimental work on the preparation of reactively sputtered thin copper oxide films as described elsewhere in this thesis the above general theory was applied to the particular case of the Cu-O system.

It has already been mentioned in section 2.2 that the molecular to atomic sputtering ratio decreases as the value of binary M-O bond energy decreases [23]. Also when the elemental partners in the oxide have a high mass ratio, the molecular to atomic sputtering ratio tends to have lower values than expected from the pure M-O bond energy view point [23]. The molecular bond energy for the Cu-O system is low ($\sim$ 90 Kcal/mole [25]) and thus the species ejected from the target will more likely be atomic than molecular. From the data of Coburn et al. [23] it can be inferred that, for a completely oxidized copper target $\zeta \simeq 0.02$. This is in a good agreement with results of Purdes, Bolker,Bucci and Tisone [24] for the case of a copper target reactively sputtered in an oxygen-neon r.f. plasma. The latter workers studied the nature of the species coming from the target using GDS techniques and found that the CuO^+ signal was about two orders of magnitude lower than that of Cu^+. For cases where such a low value of ζ applies Eqns.(2.23 and 2.27) can be simplified, as is shown below.

Let us rewrite Eq. (2.6) in the following form:

$$C = \frac{\alpha_o r(T) P N_e}{\Delta_M^* \alpha_M^* R_M^* N_s} + \frac{\Delta_{Mo} \alpha_{Mo} \zeta \theta R_{ox}}{\Delta_M^* \alpha_M^* R_M^*} = C_1 + C_2 \qquad (2.33)$$

For values of $\zeta << 1$ the second term on the right hand side of Eq. (2.33) can be neglected in comparison with the first term provided $\Delta_M^* \alpha_M^* R_M^*$ is never much less than $\Delta_{Mo} \alpha_{Mo} \theta R_{ox}$. To show that this inequality is unlikely to be

violated in the system under discussion, consider the following two extreme cases. Firstly, when the partial pressure of reactive gas is so high that the target is fully covered by reactive species ($\theta = 1$) then $R_M^* = R_{ox}$. Thus

$$C = C_1 + \zeta \frac{\Delta_{Mo}\alpha_{Mo}}{\Delta_M^* \alpha_M^*} \tag{2.34}$$

If $\zeta << 1$, most of the metal is sputtered in the form of atomic species. Thus obviously $\Delta_M^* \simeq \Delta_M$, see Eq.(2.7). Both Δ_M and Δ_{Mo} depend on the mean free path of sputtered metal atoms and sputtered metal oxide species respectively. The mean free path of sputtered species decreases with their increasing mass and diameter [26]. Because the masses of Cu and CuO species do not differ significantly, and the CuO diameter is larger than that of Cu, the mean free path of sputtered CuO species is smaller than that of Cu species. Thus energies of CuO species will be reduced to the thermal energy of the sputtering gas at shorter distances from the target than energies of Cu species [26], resulting in $\Delta_{Mo} < \Delta_M$. The values of α_M^* and α_{Mo} at the substrate temperature used (<50°C) are approximately equal to unity and thus

$$\frac{\Delta_{Mo}\alpha_{Mo}}{\Delta_M^* \alpha_M^*} \simeq \frac{\Delta_{Mo}\alpha_{Mo}}{\Delta_M \alpha_M^*} < 1$$

Thus at high partial pressures of oxygen, where $\theta \simeq 1$ and CuO is being deposited, we have $C \simeq 1$; i.e. from Eq.(2.34) $C_1 >> \zeta$, and hence from Eq.(2.33)

$$\frac{\alpha_o r(T) P N_e}{\Delta_M^* \alpha_M^* R_M^* N_s} >> \frac{\Delta_{Mo}\alpha_{Mo}\zeta\theta R_{ox}}{\Delta_M^* \alpha_M^* R_M^*}$$

or

$$\alpha_o r(T) P_o \left(\frac{N_e}{N_s}\right) > \alpha_o r(T) P \left(\frac{N_e}{N_s}\right) >> \Delta_{Mo}\alpha_{Mo}\zeta\theta R_{ox} \qquad (2.35)$$

From Eq. (2.35) one can see that the right hand side term in the numerator in the square brackets of Eq.(2.23) is much smaller than unity and therefore can be neglected. Eqns (2.23 and 2.27) can then be rewritten respectively in the form

$$C = \frac{P_o}{R_M^*}\left[\frac{1}{\frac{N_s \alpha_M^* \Delta_M}{N_e \alpha_o r(T)} + \frac{A_s kT}{S}}\right] \qquad (2.36)$$

and

$$C = \frac{1}{2}\left(\gamma + \gamma\omega\varepsilon + \omega\frac{P_o}{R_M^*}\right) - \frac{1}{2}\left[\left(\gamma + \gamma\omega\varepsilon + \omega\frac{P_o}{R_M^*}\right)^2 - 4\omega\gamma\frac{P_o}{R_M^*}\right]^{\frac{1}{2}} \qquad (2.37)$$

At low partial pressures of oxygen, when Cu_2O is being formed for example, $\theta << 1$, and thus then the term involving θ and ζ in Eq.(2.35) becomes even less significant than in the high pressure case and can be neglected.

It is encouraging that Eq.(2.36), as obtained by reduction from the general analysis, is identical to that previously derived by Drobny and Pulfrey [27] from an analysis that used Cu-O system parameters at the outset.

It follows from Eq. (2.36) that a particular copper oxide film will be characterized by a particular value of N_e/N_s, thus for a given composition ratio, temperature, pumping speed and for sticking coefficients independent of oxygen pressure and copper sputtering rate, it follows that the term in the square brackets in Eq.(2.36) remains constant. Hence Eq.(2.36) predicts that for preparation of copper oxide films of a given composition ratio the discharge

conditions must be such that the ratio P_o/R_M is constant. This dependence of composition ratio on P_o and R_M was utilized experimentally to prepare, in a very reproducible fashion, copper oxide films with C ranging, as desired, from 0 to 1 (see chapter 4.). Also precise measurements on films of a particular composition ratio ($0.5 \equiv Cu_2O$) allowed determination of the sticking coefficient α_o and the constant F (see section 4.5).

3. COPPER OXIDE FILM PREPARATION

3.1. GENERAL CONSIDERATIONS

Because of the large amount of heat dissipation and the chance of ionic bombardment of any plasma-exposed surfaces, there is usually considerably more outgassing in sputtering systems than in comparable evaporation systems. Thus serious contamination of sputtered deposits can result. In order to avoid or reduce this effect, a high background vacuum in the range of 10^{-7} Torr or less should be attained before admitting the sputtering gas. The initial pressure of contaminant gases should be thus quite low. Initial presputtering, with the substrate being protected by a shutter should take care of additional gases freed by ion bombardment and thermal outgassing from surfaces adjacent to the plasma. Presputtering utilizes the fact that a deposited film is an active getter for impurities. It has been found [12] that reactive gases such as oxygen, nitrogen and water vapor show a fast decrease in concentration as soon as sputtering is initiated due to the gettering action of fresh metal deposits. Note that outgassing can be minimized by cooling and grounding all plasma-exposed surfaces.

There are basically two methods which can be used to maintain a required pressure during sputtering. One is to use a sealed (closed) system arrangement, where the sputtering chamber is first pumped down to the desired pressure ($\sim 10^{-7}$ Torr) in the high vacuum range. Then the sputtering gas is admitted through a metering valve into the chamber to build-up the desired pressure for sputtering. A closed system method requires the sputtering chamber to be perfectly leak proof (a very unlikely event) if one wants to avoid a further pressure build-up and contamination of sputtered deposits.

This method, however, is not suitable for reactive sputtering because the reactive gas consumed in deposited films is not replenished, resulting in a continuously decreasing partial pressure of reactive gas. This in turn will cause a change in the flux of reactive species to the substrate, thus resulting in compositional variation through the film thickness. Despite this drawback the closed system has been used in early work where throttling of the diffusion pump was presumably not available [28]. The other, more common, practice is to have a continuously pumped system, where the desired pressure is maintained by an adjustable leak of reactive gas. Here, however, one should be aware that at the relatively high pressures used during r.f. and d.c. sputtering the diffusion pump is very inefficient, unstable and a significant backstreaming of diffusion pump oil will most likely occur. This is avoidable by throttling the diffusion pump either by only partially opening the high vacuum valve or by utilizing an additional throttle valve. The pressure in the vacuum chamber P, the variable leak L and a throttled pumping speed S are related by

$$P = \frac{L}{S} + \frac{Q_{lk}}{S} + \frac{Q_d(t)}{S} \tag{3.1}$$

where Q_{lk} is the gas contributed from air leakage, steady-state permeation or other constant vapor emissions and $Q_d(t)$ is the gas contributed from outgassing processes. It is clear that the concentration of impurities within the vacuum chamber decreases with increasing pumping rate S. However this is only useful if the sputtering gas used is of high purity. If the concentration of impurities in the sputtering gas is the dominant factor which determines the number of impurity species in the sputtering atmosphere, then sputtering pressures as low as possible should be used. An additional effect

of high system throughput is an improved cooling of elements and fixtures exposed to heating by the plasma. Considering conventional d.c. or r.f. diode sputtering arrangements, the minimum value of discharge pressure is given either by a minimum value of pressure at which the discharge of a particular excitation type can be maintained, or by a minimum pressure at which a desired deposition rate can be obtained. Thus as far as the purity of deposited films is concerned, films of better quality can be obtained by r.f. rather than by d.c. sputtering.

3.2 THE SPUTTERING SYSTEM

The basic sputtering system used in all experiments reported in this work was a Perkin Elmer Randex type 3140 - 6J system. The evacuation unit comprised a 6 - inch 2500 l/sec diffusion pump (Varian), ballasted 500 l/min mechanical pump (Sargent Welch), 1.5" I.D. foreline and roughing tubing system and an automatically operated solenoid-pneumatic valve system. The cryo-baffle in this arrangement was placed between the diffusion pump and the baseplate throat of the sputtering unit. During a sputtering process the diffusion pump was throttled by means of a throttling valve placed in the baseplate throat, (see Fig. 3.1). It is noteworthy that for an optimum sputtering system the cryo-baffle should be placed above the throttling valve in order to have maximum pumping speed for water vapors liberated during the sputtering process. The system was equipped with a semiautomatic gauge monitoring system with digital readout. In the system as supplied it was possible to continuously monitor the reading of the thermocouple gauge A, which served also as the sensor for the automatic valve control system, and any one of either the two thermocouple gauges B and C or the ionization gauge D. The base pressure, which the system regularly achieved after

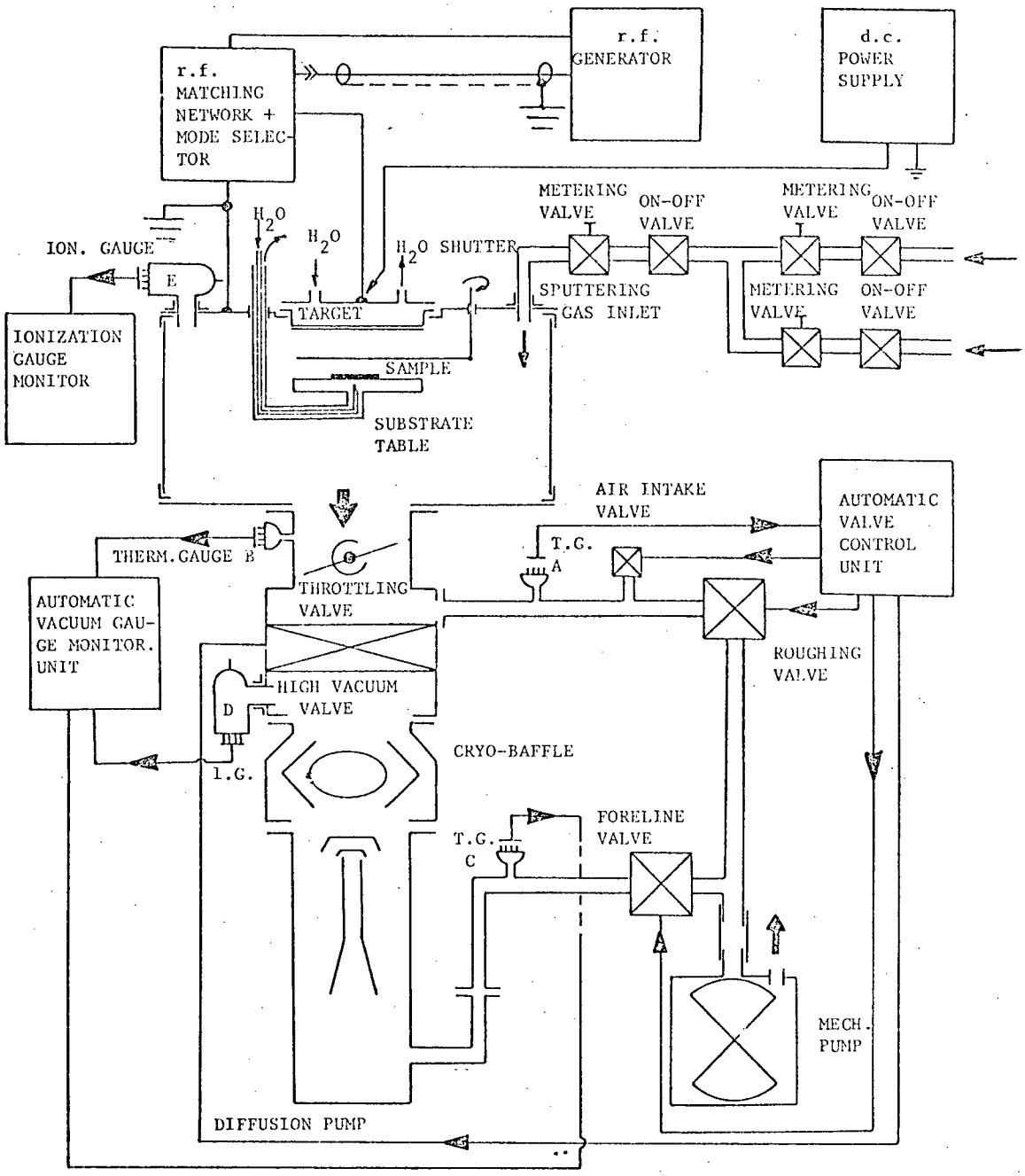

Fig. 3.1 Schematic diagram of reactive sputtering system used for copper oxide film deposition

overnight pumping was in the order of 4×10^{-8} Torr. The sputtering unit had a single target 6 inches in diameter. Both the target and substrate table were watercooled. The system's mode selector switch enabled the energizing r.f. voltage to be switched to the target solely (sputter-depositon mode), or to the substrate table solely (sputter-etch mode) or to both the target and the substrate (bias-sputter mode). In the present work only the sputter-deposition mode was used. The as-supplied r.f. network was used for r.f. sputtering. By removing the final connection to the target the latter could also then be energized from a separate high voltage d.c. source, thus permitting d.c. sputtering. In order to measure the necessarily low pressure of reactive gas (oxygen), deliberately admitted to the sputtering chamber, an additional ionization gauge E was coupled directly to the sputtering chamber. The gas distribution system, comprising metering valves, on-off valves, mixing chamber, and conduits was made from stainless steel. The schematic drawing of the whole system can be seen on Fig. 3.1.

3.3. SUBSTRATE PREPARATION

The basic properties of the copper oxide films of interest in the present work were composition, electrical resistivity and optical properties (see chapters 4 and 5).

Transmission electron microscopy was used to provide information on film phase composition and the substrates used in this application consisted of a fine copper mesh (Fig. 3.2) supporting an amorphous carbon film. The carbon film was prepared by evaporating carbon onto a microscope glass slide. The film was then stripped from the glass slide by immersing it in water. The floating carbon film was then picked up by the copper mesh and allowed to dry.

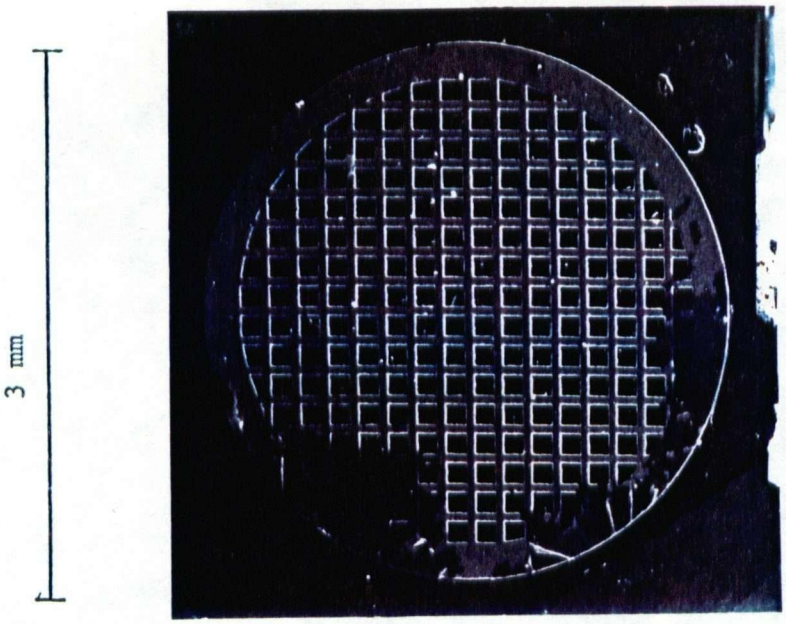

Fig. 3.2 3mm diameter 150 mesh EM copper grid.

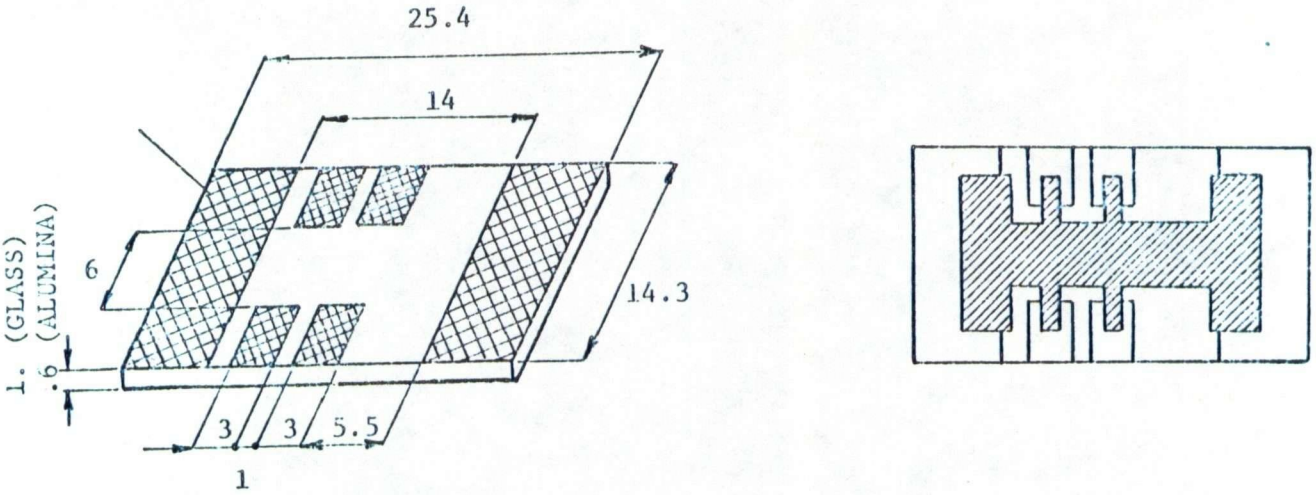

Fig. 3.3a Substrate with contact areas used for preparation of samples for determination of the thermal activation energies of conductivity. All dimensions are in millimeters.

Fig. 3.3b Sample for thermal activation energy of conductivity measurements.

Films intended for transmittance and resistivity evaluation were deposited onto Corning 2947 3"x1" glass slides. Glass slides were precleaned at a temperature between 70 - 80 °C in a glass cleaning solution of 2% (by weight) of chromium trioxide (CrO_3) in sulfuric acid for 3 minutes, followed by rinsing in deionized water and blowing dry in nitrogen. In some cases, when some traces of impurities remained on the slides, the procedure was repeated. The glass cleaning solution was prepared by dissolving chromic trioxide in the minimum amount of deionized water necessary to dissolve the crystals completely. Then the sulfuric acid was added.

The measurement of activation energies was done on Hall effect shaped films deposited on either glass or alumina substrates (Fig. 3.3), with the sample contacts prepared beforehand. This contacting method was found to be fast and reliable because the sample was ready for measurement immediately following a copper oxide film deposition. It also avoided the contamination of the film or its exposure to an undesired temperature treatment, that may have resulted, if the contacting procedure had followed the film deposition procedure. Substrates were prepared by sputtering first a $\sim$ 200 Å thick chromium film onto the glass or alumina slide followed by a $\sim$ 2000 Å thick gold film. The purpose of the chromium layer was to assure a good adherence of the gold film to the substrate. The substrate was then scribed into individual samples of required size (1" x 9/16"). The contact area was defined by photolithography, using a positive Waycoat photoresist. (The complete photoresist process is described in chapter 6). The gold film was then etched away in a solution of KI + I_2 in deionized water. The solution was made from 400g KI, 100g I_2 and 400 ml of deionized water. Subsequently, chromium was etched off in a solution prepared from 330 g of ceric ammonium nitrate ($(NH_4)_2Ce(NO_3)_6$) and 100 ml of perchloric acid ($HClO_4$) made up to a

volume of 2 litres with deionized water. (Note, when resolution better than 50μm is required, the solution should be filtered).

The measurement of reflectance and transmittance of films for determination of optical constants was done on Suprasil 2 (fused quartz-fused silica material made by Amersil Inc.) substrates. The Suprasil 2 substrates were precleaned by using the same procedure as used for glass slides.

Copper oxide films were also deposited onto Si substrates in order to form heterojunction diodes. The substrate preparation procedure for this case is described in Chapter 6.

3.4 DEPOSITION CONDITIONS

Most of the experimental work was performed using r.f. reactive sputtering but, as described in Chapter 4.,d.c. reactive sputtering was also investigated. The general procedure for reactive sputtering with either voltage source was very similar and is described below.

The target used was made of 14 mil thick 99.999% copper foil fastened to the water cooled copper target holder by four screws. The target-anode distance was fixed at 5cm. It follows from the theoretical results of Chapter 2 that the film composition is determined by the relative magnitudes of the fluxes of copper and oxygen species at the substrate. It is also known that the sputtering yield from a particular target material depends on the condition of its surface. It was observed that, for given deposition conditions, a new copper target with a smooth surface always showed a somewhat higher sputtering rate than a target exhibiting the surface texture developed by prolonged sputtering. Therefore, whenever a new target was used, intensive presputtering had to be carried out to ensure attainment of characteristic surface texture and thus the stabilization of the sputtering yield from the target

and the reproducibility of the deposited films. Another parameter which can significantly change the ratio of fluxes of copper and oxygen species impinging on the substrate from the value expected from the initial partial pressure of oxygen and the sputtering power level is the oxidation state of the target surface. In all cases prior to an actual deposition of a copper oxide film onto the substrate it was necessary to ensure that the target was in the steady-state condition, otherwise the film composition was not reproducible. That is, the oxidation rate and oxygen removal rate at the target surface had to be arranged to be equal. This steady-state condition at the target can be achieved by presputtering of the target at the same r.f. power (or current in the d.c. sputtering case) level and oxygen pressure as intended for use in film deposition. The precise procedure used for target presputtering depended on the nature of the previous deposition. For example if it was intended to perform a deposition at an oxygen partial pressure equal to or higher than the previous oxygen partial pressure used and at an r.f. power (or the current in the d.c. case) level equal to or lower than the r.f. power (or d.c. current) level previously used, then the target could be simply equilibrated by presputtering at the r.f. power (or the current in a d.c. sputtering case) and the oxygen pressure to be used during the actual deposition, provided the shutter covered the substrate. The same pocedure could be applied when the previous deposition was done at a slightly higher partial pressure of oxygen and the same or slightly lower r.f. power (or current in d.c. case) level than the intended one. However, when the previous partial pressure of oxygen was significantly higher or the sputtering power (or the current in d.c. case) level much lower than those intended to be used, then the target oxide coverage had to be reduced by large amount. It takes a much longer time to reduce the target oxide coverage than it does to build it up. This is due to a much lower

sputtering rate of copper oxide than of the metal copper. The recommended procedure in this case is to presputter the target in pure argon until the oxide layer completely disappears. Then one can utilize the first procedure, as described above.

Let us summarize these consideration for simplicity. One can denote by ψ the ratio of partial pressure of oxygen to the sputtering rate of copper:

$$\psi = \frac{P_o}{R_M} \tag{3.2}$$

Then the first procedure for target equilibration can be applied if $\psi_1 \lesssim \psi_2$, where ψ_1 and ψ_2 represents previous and intended deposition conditions respectively. In all cases when ψ_1 is significantly higher than ψ_2, the combination of pure argon presputtering followed by presputtering at intended condition ψ_2 is recommended. It is noteworthy that in all cases the presputtering, except the pure argon target preetch, has to be done at the same conditions as an intended deposition. The way to recognize whether the target was in a steady-state condition was different for d.c. and r.f. sputtering modes but in both cases the dependence of plasma impedance on the condition of the target surface was utilized. The discharge current (and thus also the plasma impedance) is a complex function of applied anode-cathode voltage, the total pressure in the sputtering chamber, the volume ionization coefficient, which depends on the sputtering gas, and the ion-electron emission coefficient under discharge conditions, which depends on the cathode material and sputtering gas [29]. If the target is not in a steady state condition, its coverage by oxide is changing with time. If $\psi_2 < \psi_1$, the target area covered by oxide reduces and results in an

increase in partial pressure of oxygen in the sputtering chamber. If $\psi_2 > \psi_1$, the target oxide coverage builds up, resulting in the trapping of oxygen by the target and in a decrease of oxygen partial pressure within the chamber. Thus in either of the above cases both the volume ionization coefficient and the ion-electron emission coefficient are affected by non-equilibrium condition at the target. In the d.c. sputtering case the nonequilibrium condition at the target is observed by discharge current instabilities and in the r.f. sputtering case by instabilities of reflected power resulting from the r.f. network mismatch .

In instances when the deposited films were intended for measurement of transmittance and room temperature resistivity, the substrates were supported directly by the water cooled substrate table. The actual copper oxide film deposition times were in this case limited to 2 minutes in order to prevent a significant rise in substrate temperature. (Note that the decomposition temperature for Cu_2O at the partial pressure of oxygen used for deposition of cuprous oxide is only a few hundred degrees celsius). When the substrate is just loosely supported by the substrate table the thermal conductance between the substrate and the substrate table is very limited. Therefore significant heating of the substrate by the plasma in this case is limited only by the thermal capacity of the substrate. In the cases when a longer deposition time was required, better thermal conductance between the substrate table had to be ensured. The problem was solved by placing a thin layer of Corning high vacuum silicone grease between the substrate and the custom-made substrate table (see Fig. 3.4.). When using silicon wafers as substrates these were contacted to the substrate table using gallium as a bonding material.

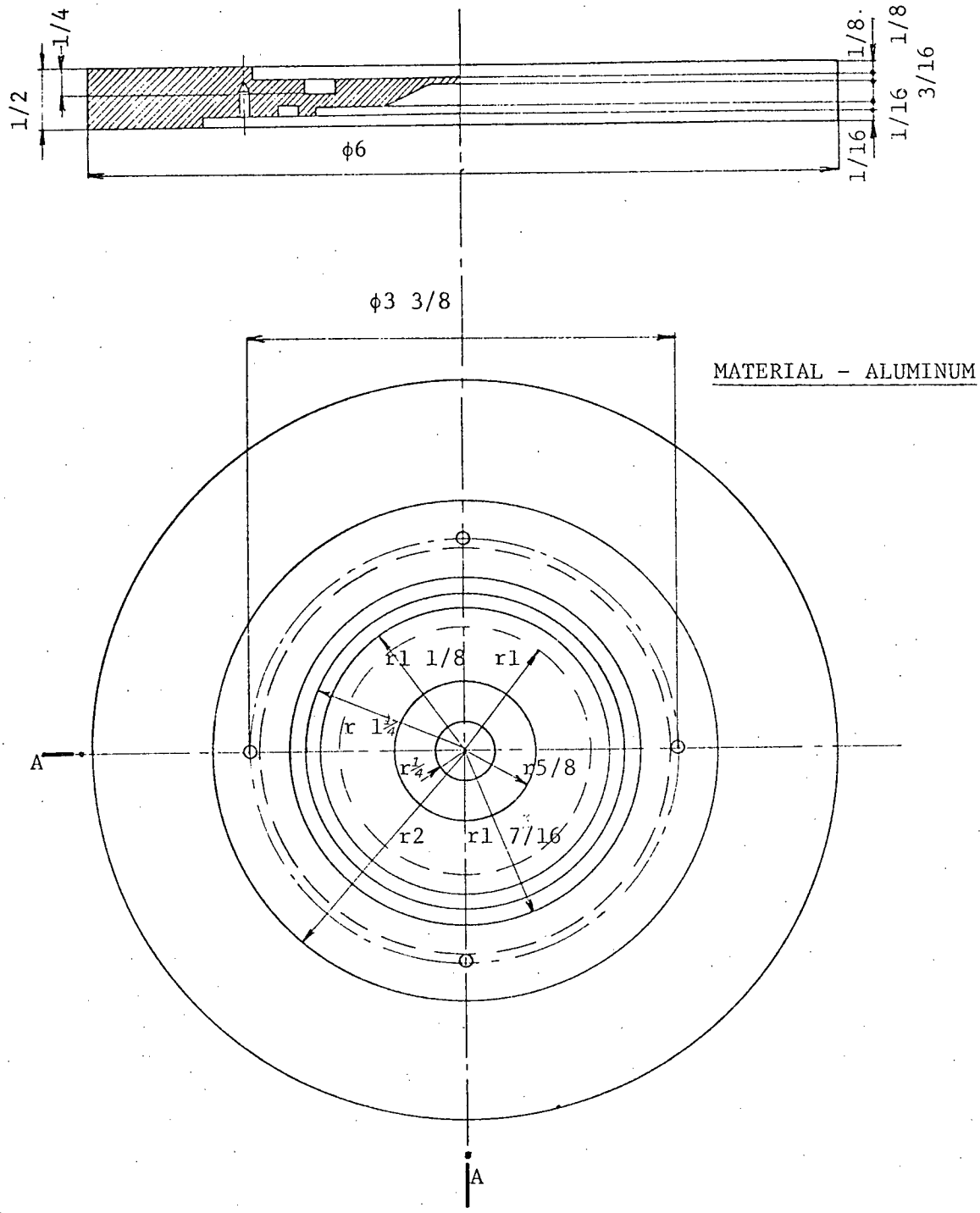

Fig. 3.4a Custom-made substrate table enabling efficient cooling of samples during their deposition. All dimensions are in inches.

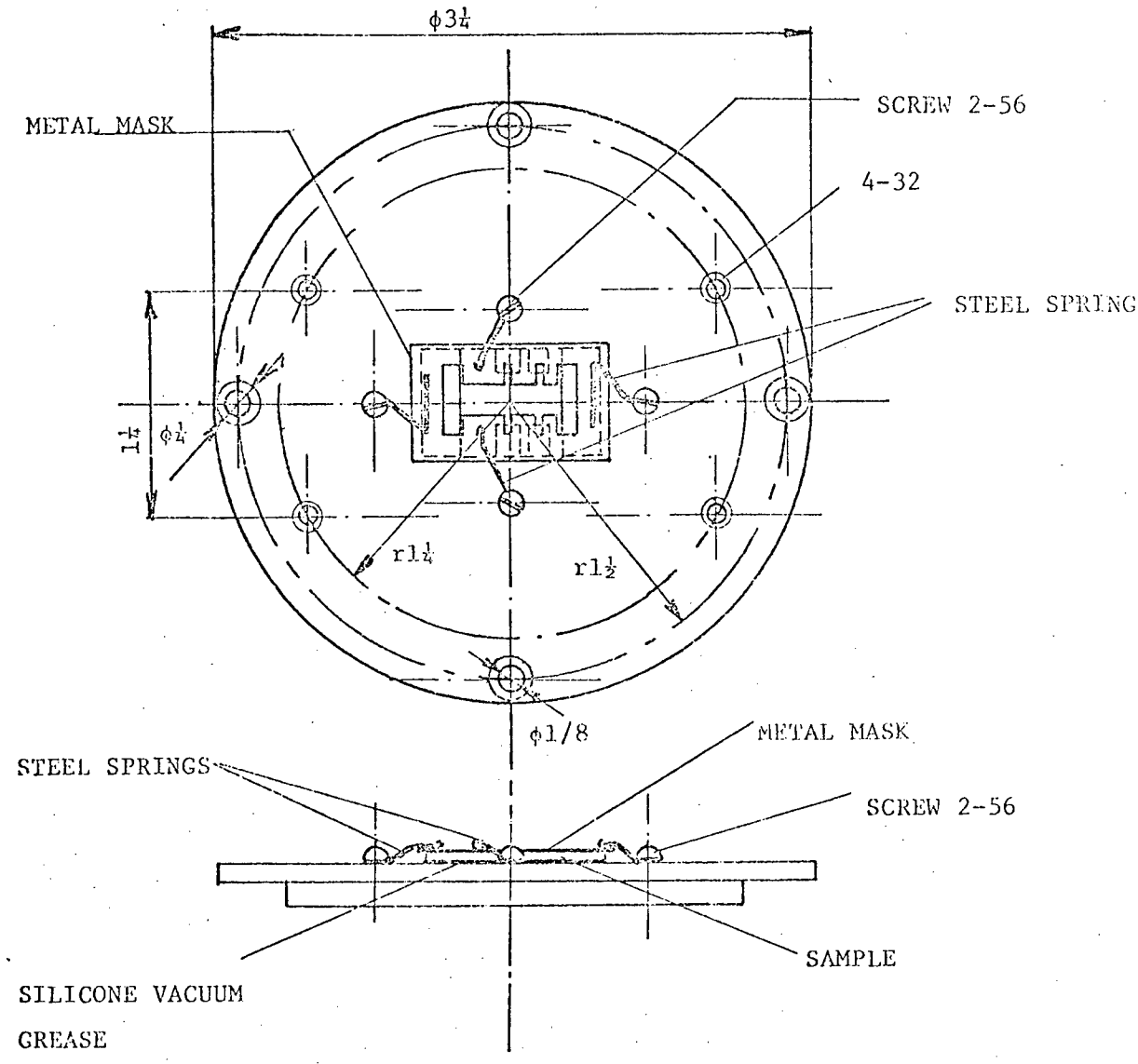

Fig. 3.4b Substrate table sample holder as used for deposition of samples for determination of thermal activation energies for conductivity.

The standard copper oxide film deposition procedure comprised the following steps:

i. Pumping down the bell jar to a base pressure of 5×10^{-7} Torr or less as indicated by the ionization gauge E (Fig. 3.1) coupled directly to the vacuum chamber.

ii. Throttling the diffusion pump by turning the throttle valve into its minimum conductance position, while watching the reading of the ionization gauge E. If the reading went up more than 20 - 30%, more pumping time had to be allowed. When the pressure stabilized at a value equal to, or lower than, 6×10^{-7} Torr with the throttle valve in its minimum conductance position, the next step could be followed.

iii. Switching the oxygen on-off valve in its "on" position and admitting the oxygen alone at such a rate that the desired partial pressure was reached. The leak rate was adjusted by means of the oxygen metering valve. Oxygen pressures below 2 mTorr were measured by the ionization gauge E and higher pressures were measured by the thermocouple gauge A.

iv. Admitting argon at such a rate as to build up the total pressure to 25 mTorr in the r.f. sputtering case, or 75 mTorr in the d.c. sputtering case.

v. r.f. sputtering: Turning the r.f. plasma on and adjusting the r.f. power level as desired. Then presputtering the target following the presputtering procedure as previously described with the shutter protecting the sample. After stabilization of the reflected power the actual deposition was initiated by removing the shutter from its substrate protecting position and fine tuning the forward power to the desired level and the reflected power to a minimum once again.

d.c. sputtering: Adjusting the discharge current to 70 mA and following the presputtering procedure as described above with the shutter protecting the sample until the discharge current stabilized. Then the shutter was removed, the discharge current was readjusted to the 70 mA level (i.e. an anode-cathode voltage of from 2.65 - 3.0 kV, depending on the oxygen partial pressure) and the deposition was initiated.

4. PROPERTIES OF COPPER OXIDE FILMS

4.1 FILM THICKNESS MEASUREMENT

The thickness of the copper oxide films was determined by the Fizeau fringes method on a Sloan M-100 Angstrometer. This method required the formation of an abrupt film step on the sample. Because of the diffusive nature of the transport of sputtered species at the pressures used for copper oxide film depositions (25 mTorr in r.f. and 75 mTorr in the d.c. sputtering case) a sharp enough step, enabling an accurate thickness measurement, could not be formed by the simple method of using a metal mask during a film deposition process. Therefore the edge was formed by an etching technique whereby a portion of the sample was briefly dipped into an etching solution and etched completely away. (The position of the film step on the sample was determined by the depth of immersion in the etching solution). The etching time was kept as short as necessary to just completely remove the portion of the film immersed in the etching solution and typically ranged from < 1 sec for Cu_2O + Cu films to $\sim$ 5 secs for CuO films. Thus the formation of a sharp film step was ensured. Etching solutions used were HNO_3 : H_2O in volume ratio 1:1 for the Cu_2O etch, and HNO_3 : HCl : H_2O in volume ratio 1 : 2 : 2 for the CuO and Cu_2O + CuO etches. In all cases the etching step was followed immediately by rinsing the sample in deionized water, subsequent rinsing in methanol and blowing dry in a stream of nitrogen. Then to ensure a good reflectivity from both surfaces of film and substrate respectively the sample was coated on the film side by approximately 2500 Å of copper (r.f. sputtered). It is noteworthy that d.c. sputtered copper films were not found to be reflecting enough to ensure a good resolution of fringes for the thickness measurements.

The thickness of thick (.3 - 3 μ) copper films (deposited for the purpose of estimating the copper sputtering rate) was determined from the mass difference between a glass slide with and without the copper film. Assuming the same density for sputtered and bulk copper, and knowing the area of the film, the thickness could be then calculated.

4.2 PHASE COMPOSITION

The fact that the reactively sputtered copper oxide films possessed a polycrystalline structure enabled use of transmission electron diffraction as the research tool for investigation of their compositional character. The electron diffraction (E.D.) measurements were performed on an Hitachi (110 A model) transmission electron microscope. The electron microscope was used in the transmission electron diffraction mode on the 75 kV range. With three acceleration voltage ranges available, namely 50, 75 and 100 kV, the 75 keV electrons were selected on the basis of the trade-off between the transparency of 200 - 1100 Å thick copper oxide films to high energy electrons and the physical size of the E.D. patterns. The typical thicknesses of films, for example deposited by r.f. reactive sputtering at 200 W of forward power for a 2 minute deposition , were $Cu_2O \sim 1000$ Å, $Cu_2O + CuO \sim 800$Å and $CuO \sim 225$Å. The films were deposited on thin amorphous carbon films (transparent for electrons) supported by a fine copper mesh. For details of substrate preparation see section 3.3. It is noteworthy that during a deposition the substrates had to be placed close to the centre of the substrate table. This requirement stems from the fact that the metal (copper) deposition rate decreases towards the outer regions of the substrate table resulting in a variation of film composition with the distance from the substrate table centre.

Note that in all cases the substrate table centre was used as the reference point, to which the measured properties of deposited films and the film deposition conditions were correlated.

All electron diffraction patterns were observed and their photographs taken at as low electron beam intensity as possible, thereby eliminating or at least minimizing the chance of decomposing the films. Interplanar spacings ("d - values") were obtained from the relation:

$$d_{(h_i k_i l_l)} = \lambda L / r_{(h_i k_i l_i)} \qquad (4.1)$$

where $r_{(h_i k_i l_i)}$ is the radius on the diffraction pattern of the ring representing a particular crystallographic plane $(h_i k_i l_i)$, λ the wavelength of electrons, and L the effective specimen - plate distance. The camera constant "λL" was determined by using the diffraction pattern from a gold film as the reference (Fig. 4.1e). The procedure was to measure the diameter of a particular diffraction ring, multiply this value by a corresponding interplanar spacing value from standard tables [30] (comparison of the intensity distribution of observed E.D. rings with the standard normalized intensities from tables helps to identify the plane corresponding to a particular observed E.D. ring) and so obtain the camera constant. Better accuracy was achieved by repeating the above procedure for the first 4 - 6 rings of the gold electron diffraction pattern and calculating the average from Eq.(4.2)

$$\overset{\sim}{\lambda L} = \frac{\Sigma_i (\lambda L)_i}{i} \qquad [\text{Å cm}] \qquad (4.2)$$

The camera constant so determined was then taken as the reference in all measurements, and its validity was ensured by keeping the current settings of the objective, intermediate and projection lenses the same in all measurements.

The phase composition of the deposited copper oxide films was determined by first measuring the diameter of diffraction rings from a particular sample, then calculating the interplanar spacings from Eq.(4.1), and comparing these numbers and the relative intensities of diffraction rings with tabulated lists of "d"-values for known structures (Cu, CuO and Cu_2O), until an identification was made.

Typical electron diffraction patterns for films corresponding to each of the four oxide phases observed are shown in Fig. 4.1 a-d, and the results of their identification are summarized in Table 4.1 a-d. In Fig. 4.1a the fourth ring from the center reveals the presence of metallic copper. This is the second most intense copper ring. The strongest copper ring (111) is masked somewhat by the (200) cuprous oxide ring. In Fig. 4.1c the presence of CuO is revealed principally by the strong third diffraction ring from the (111) and (200) CuO planes. The other strong cupric oxide diffraction rings, (002) and $(\bar{1}11)$ are masked by the (111) diffraction ring from cuprous oxide. Cuprous oxide is unequivocally identified in Fig. 4.1c by the first diffraction ring (110) (note its absence from Fig. 4. 1d). Each of the compositions represented by Fig. 4.1 a-d could be obtained with either d.c. or r.f. plasma excitation. In both instances the trend in film composition with increasing oxygen partial pressure was found to be:

$$Cu \rightarrow Cu + Cu_2O \rightarrow Cu_2O \rightarrow Cu_2O + CuO \rightarrow CuO$$

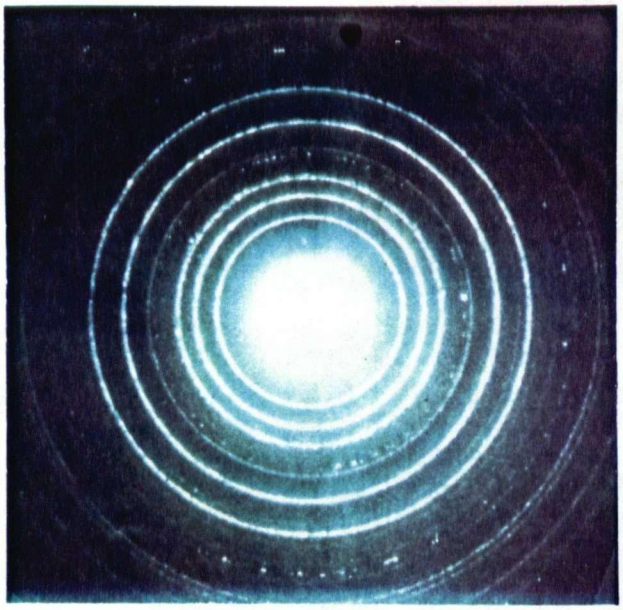

(a)

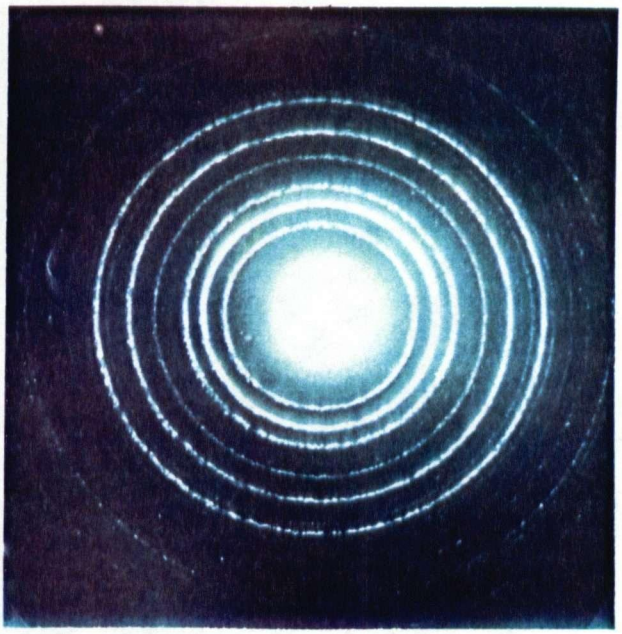

(b)

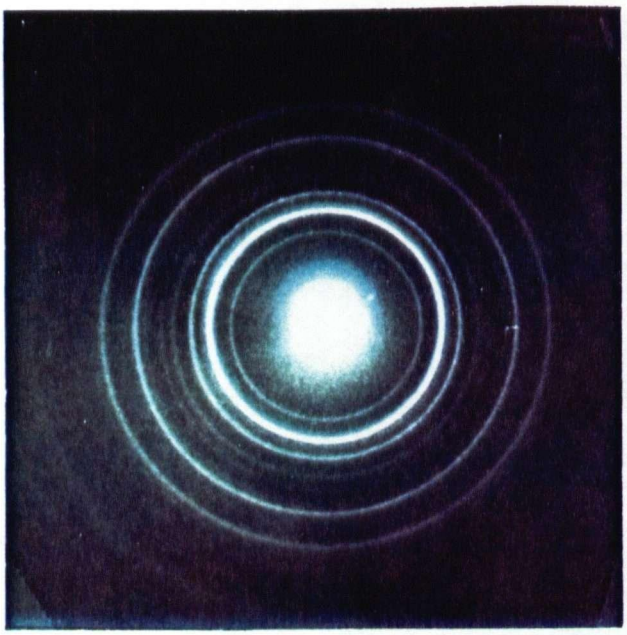

(c)

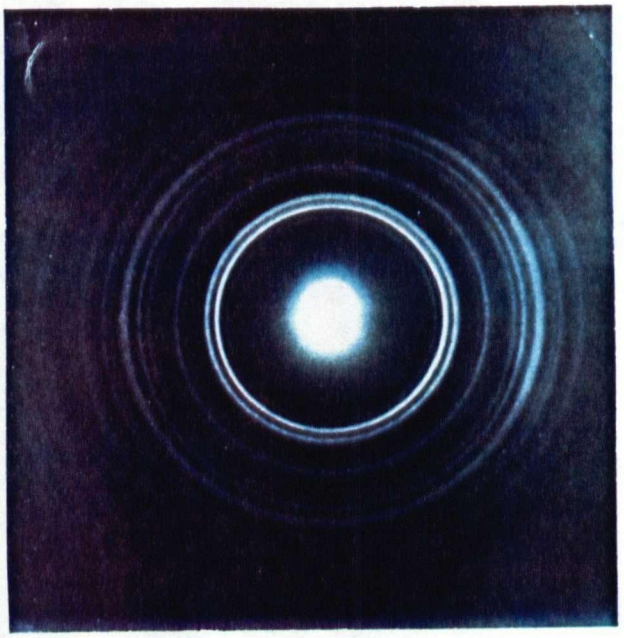

(d)

Fig. 4.1 Electron diffraction patterns for copper oxide films.

a. $Cu_2O + Cu$

b. Cu_2O

c. $Cu_2O + CuO$

d. CuO

Table 4.1 Identification of the diffraction rings in Fig. 4.1

	Ring No.*	Cu_2O	CuO	Cu
1a	1	110		
	2	111		
	3	200		111
	4			200
	5	211		
	6	220		
	7	311		
	8			
	9			
1c	1	110		
	2	111	002, $\bar{1}11$	
	3		111, 200	
	4	200		
	5		$\bar{2}02$	
	6		202	
	7	220	$\bar{1}13$	
	8	311		
	9			

	Ring No.*	Cu_2O	CuO
1b	1	110	
	2	111	
	3	200	
	4	211	
	5	220	
	6	311	
	7		
	8		
	9		
1d	1		110
	2		$\bar{1}11$, 002
	3		111, 200
	4		$\bar{1}12$
	5		$\bar{2}02$
	6		202
	7		$\bar{1}13$
	8		$\bar{3}11$, 310
	9		

* Starting at the innermost ring.

Table 4.2 Oxygen partial pressure ranges required for various compositional structures.

Phase observed by E.D.	Oxygen partial pressure range [m Torr]	
	R.F. Sputtering P = 200 W	D.C. Sputtering I = 70 mA
Cu_2O + Cu	< .3	< .26
Cu_2O	.34 - .52	.33 - .51
Cu_2O + CuO	.57 - .92	.62 - .89
CuO	>1.0	>1.06

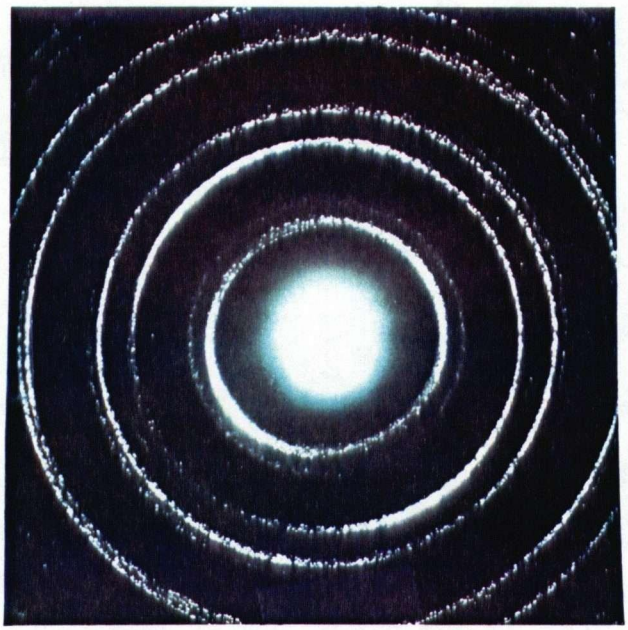

Fig. 4.1e Electron diffraction pattern taken from gold film.

The same trend could be observed, at constant oxygen partial pressure, by decreasing the copper deposition rate. The partial pressures of oxygen required to obtain the various compositions for given excitation conditions are summarized in Table 4.2.

4.3 OPTICAL TRANSMITTANCE

Substrate preparation was as described in section 3.3 and films intended for optical transmittance determination were usually deposited at the same time as films to be used for electron diffraction analysis. Thus a good correlation between the compositional character and optical properties of film was assured. The measurement of optical density of films utilized a Cary 14 double beam spectrophotometer. In all cases the sample was placed in the sample beam compartment and the reference beam remained unchanged (no neutral density filters were used in this case). Optical density (O.D.) is related to the intensity of light incident on the sample I_o and the intensity of light leaving the sample I_T by

$$O.D. = \log \frac{I_o}{I_T} \tag{4.3}$$

The transmission coefficient T is defined as the ratio of transmitted to incident light intensity

$$T = \frac{I_T}{I_o} \tag{4.4}$$

Then from Eqns. (4.3 and 4.4)

$$T = 10^{-O.D.} \tag{4.5}$$

When using the double beam spectrophotometer I_o is equal to the reference beam intensity if the spectrophotometer is zero-balanced with the sample withdrawn from the sample beam.

In all cases, when calculation of transmittances from optical density data were required, the optical density curves were digitized on an Instronics Gradicon digitizer. Transmittances were then calculated on an IBM 370/168 computer and plotted as a function of wavelength on a Calcomp plotter.

The optical transmittance data taken from films deposited at various oxygen pressures in an r.f. discharge at 200 W are shown in Fig. 4.2. Films deposited using a d.c. discharge at 70 mA of discharge current showed very similar features. The pure cuprous oxide phase (curve 3 on Fig. 4.2) is characterized by a steep absorption edge, as would be expected from a direct band gap semiconductor material [31]. The band gap of Cu_2O is 2.04 eV which corresponds to a wavelength of 607 nm. As the oxygen partial pressure is reduced below that required to form pure Cu_2O (curves 2-1) the free copper content of the film increases, leading to a decrease in transmittance. On increasing the oxygen partial pressure above that required for pure cuprous oxide formation the nature of the absorption curve changes, and tends towards a shallow absorption characteristic (curve 5), which is presumably typical of sputtered CuO. Similarly shaped transmittance curves for 880Å thick thermally grown CuO films have been observed by Weider and Czanderna [46]. Optical transmittance alone (optical constants were determined using both reflectance and transmittance data, see chapter 5) was utilized as a supplemental research tool in investigating the compositional character of deposited copper oxide films. Here the fact that Cu_2O is characterized by a steep absorption edge around 600 nm wavelength, CuO by a shallow absorption curve

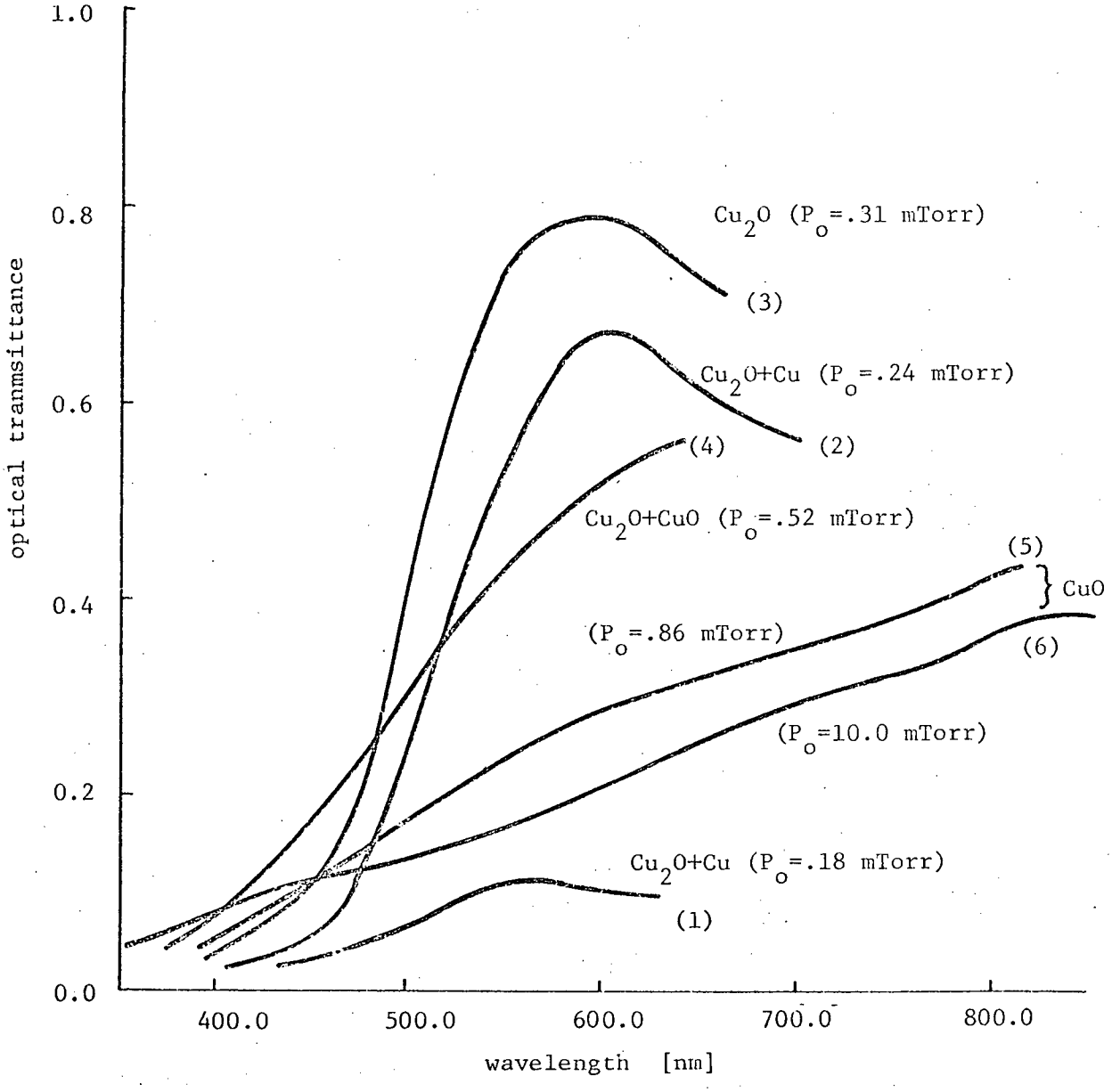

Fig. 4.2 Optical transmittance data for copper oxide films deposited by r.f. sputtering at 200W of forward power and total pressure of 25 mTorr. All data normalized to represent results for 1000 Å thick films.

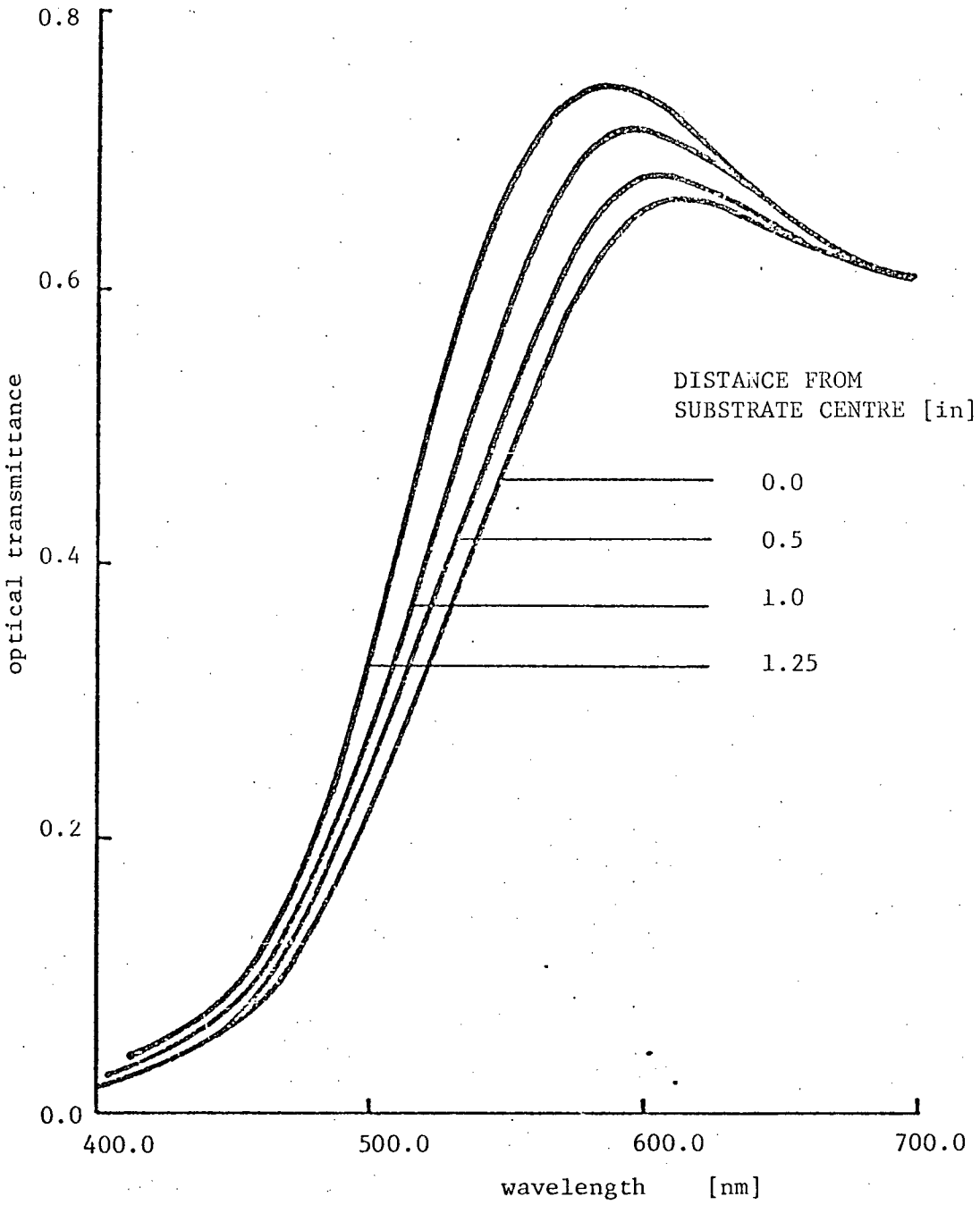

Fig. 4.3 Variation of optical transmittance with radial distance along copper oxide film (sample #234, see Fig.4.5). Film thickness = 950Å. Compare data with that of Fig. 4.2 and note the reduction in Cu content on moving away from the centre of the substrate.

and that an increased free copper content in a copper oxide film causes significant decrease in transmittance between 500 - 600 nm was utilized. As a particular example optical transmittance data was used in seeking an explanation of the variation of film resitivity across a deposited copper oxide film (see section 4.6). It was found that due to the nonuniform metal deposition rate with distance from the substrate table centre (deposition rate decreasing with distance from the centre of the substrate table), a nonuniform composition of film across the sample resulted, thus obviously affecting the film resistivity (see section 4.6 for more details). The theory on reactive sputtering described in chapter 2 thus predicts an increasing composition ratio ([O]/[Cu] with an increasing distance from the substrate table centre. It was suggested that the variation in resistivity across the sample was due to the above effect and this was confirmed by transmittance measurements. Fig. 4.3 represents typical transmittance curves taken from a Cu_2O film that was nearly stochiometric at the centre point of the substrate and substrate table. A decrease in free copper content in the film on moving away from the centre of the substrate table can be seen (compare Figs. 4.2 and 4.3).

Measurement of optical transmittance was also utilized for determination of optical constants of copper oxide films, and this is discussed in chapter 5.

4.4 RESISTIVITY

The resistivity measurements were done on the same samples as used for transmittance measurements. Here great care was taken to have an observation of phase composition (by TEM) and a measurement of resistivity on

samples prepared during the same deposition run, in order to have a direct correlation between the resistivities and the phases observed.

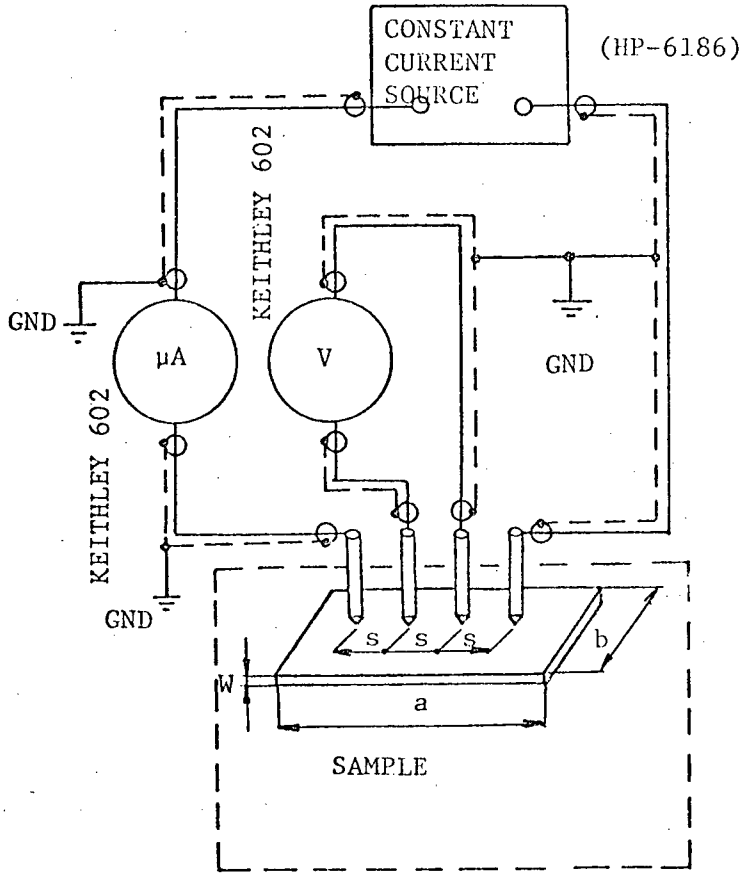

Fig. 4.4 Circuit diagram of the four-point probe set-up used for resistivity measurements.

The four-point probe technique was chosen as the measurement method for resistivity because of its simplicity and speed. For an infinite film sheet with thickness much smaller than the probe spacing the resistivity of a film can be calculated from the following current - voltage relationship [49]

$$\rho = \frac{\pi}{\ln 2} \frac{V}{I} W \qquad (4.6)$$

where ρ is the film resistivity, I is the current flowing through the outer probes, V is the voltage measured between two inner probes and W is the film thickness.

Fig. 4.4 shows the circuit diagram of the four-point probe set-up as used in resistivity measurements. The outer probe current was supplied by the constant current source HP 6186. Both the voltage and the current were measured by electrometers (Keithley model 602) because of their high input resistance and low current measurement capabilities. The four-point probe used was a Kulicke & Soffa instrument, model number 3007. The resistivity was measured in the central portion ($\sim$ 1") of each film. The measurement of thickness utilized a Sloan M-100 Angstrometer, as described in section 4.1.

Each film composition exhibited a characteristic range of resistivities as can be seen from Fig. 4.5 for r.f.-and Fig. 4.6 for d.c.-reactively sputtered films. Note the similar trends in variation of copper oxide film resistivity with the oxygen partial pressure used during deposition for d.c. and r.f. sputtered films. This suggests that a common mechanism of copper oxide film formation in both an r.f. and a d.c. reactive sputtering environment exists. However, on comparing the absolute values of resistivities of films with the same composition it can be seen that d.c. sputtered copper oxide films possessed resistivities higher than those of r.f. sputtered films. This can be attributed to differences in both radiation damage (caused by high energy electron bombardment of the film and the substrate) and impurity effects. For example, let us compare some aspects of r.f. and d.c. sputtering where the sputtering conditions are such that in both cases approximately equal sputtering rates are obtained. Cases in point would be:- for d.c. sputtering at 75 mTorr of total Ar + O_2 pressure

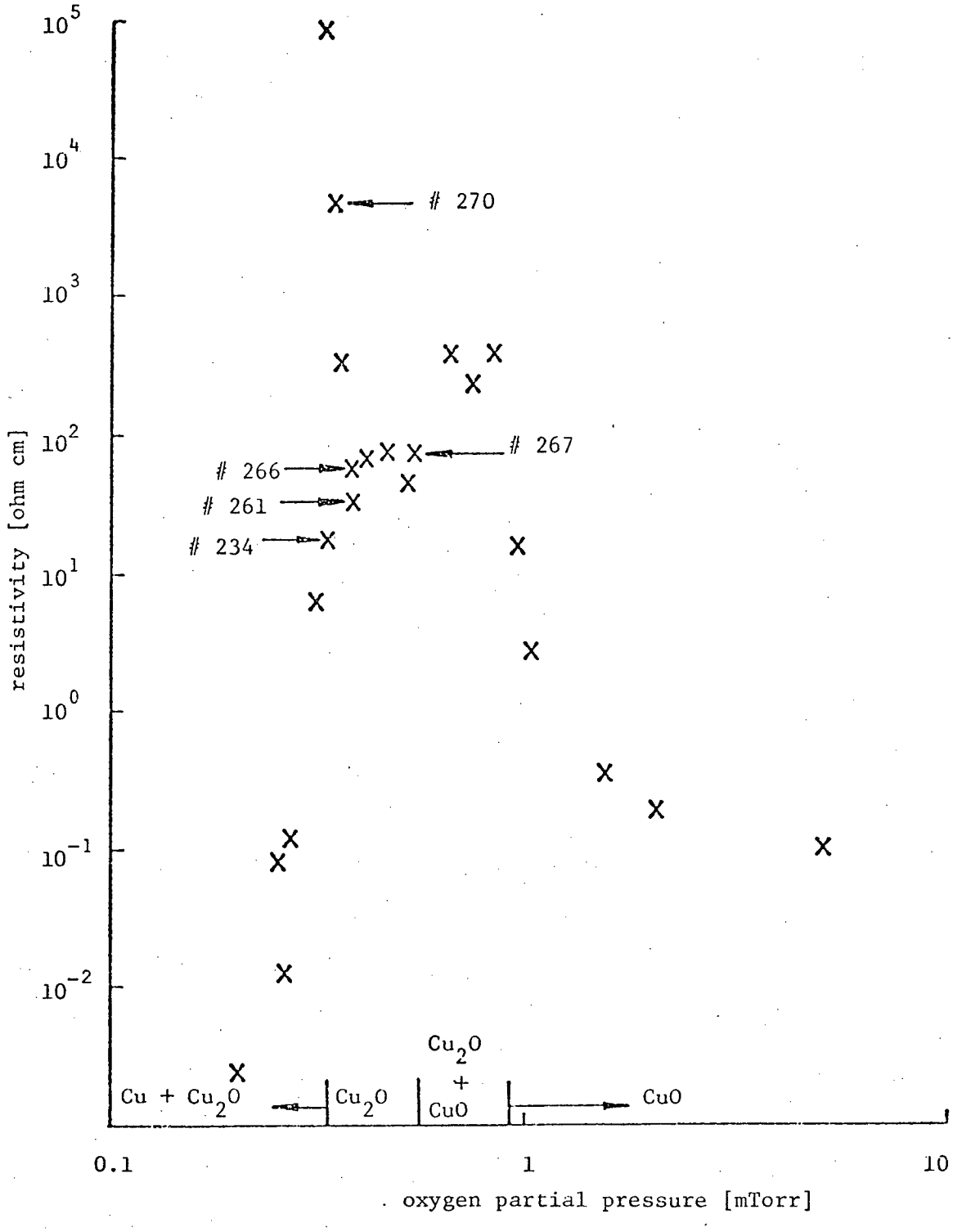

Fig. 4.5 Resistivity data for films deposited by r.f. sputtering at 200W and total pressure of 25 mTorr. The partial pressure boundaries for the various film compositions are from Table 4.2. The sample numbers shown identify the samples used to produce Figs. 4.3 and 4.13.

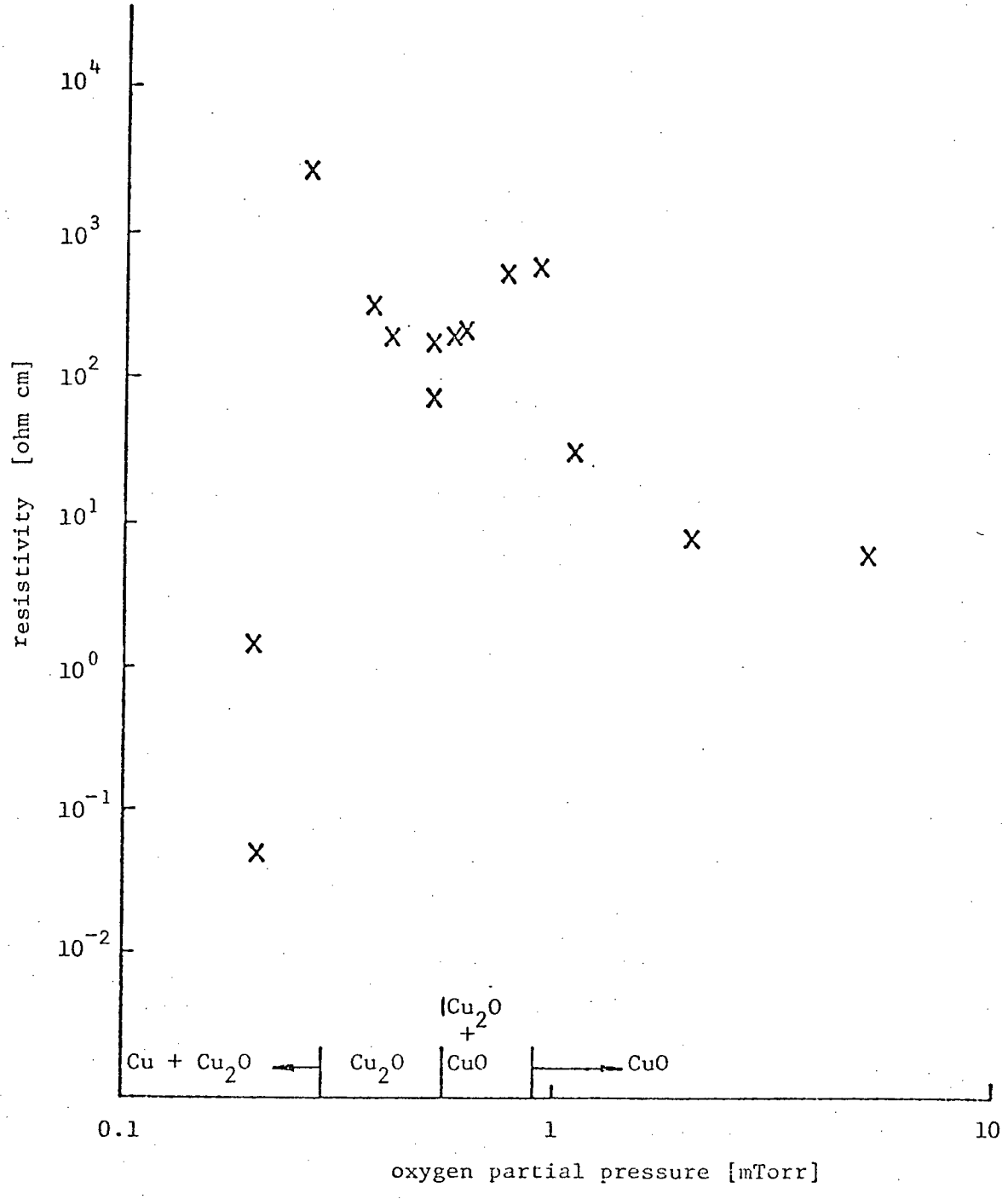

Fig. 4.6 Resistivity data for films deposited by d.c. sputtering at 70 mA and total pressure of 75 mTorr. The partial pressure boundaries for the various film compositions are from Table 4.2.

and 70 mA of discharge current:- for r.f. sputtering at 25 mTorr of total pressure and 200 W of r.f. power. Then if the d.c. case is compared with the r.f. case, it follows that:- (i). the anode-cathode voltage is ∿ 900 V in the r.f. case and ∿ 3kV in a d.c. case. Thus the d.c. sputtering will result in more serious radiation damage to the film caused by high energy electron bombardment; (ii). more energetic electrons will result in a higher rate of emission of impurity gases from the bell jar walls and fixtures. Thus it will result in higher concentrations of impurities in the sputtering chamber; (iii). the higher total pressure at the same pumping rate requires a higher Ar leak rate. Thus,if the concentration of impurities in the argon gas makes a significant contribution to the impurity species concentration in the sputtering chamber, then the d.c. case will be characterized by a higher concentration of impurities in the sputtering chamber; (iv). the higher total pressure used in the d.c. case also results in a higher thermal conductance of the sputtering gas and plasma, thus resulting in a higher heat transfer from the cathode to the bell jar walls and inside fixtures. This again could result in greater emission of impurity gases.

The partial pressure boundaries (Figs. 4.5 and 4.6) for various film compositions were determined by analysis of electron diffraction data. The procedure was described in section 4.2. At low oxygen partial pressures the large free copper content in the films produces metallic-like conduction. Increasing the oxygen partial pressure leads to a peak in resistivity which is thought to be associated with the formation of stochiometric cuprous oxide. This conclusion stems from the excellent correspondence between the occurrence of this peak and the onset of the Cu_2O phase. Further increases in oxygen pressure result in a lowering of the resistivity by doping of the film with excess oxygen. It is well known that cuprous oxide is doped by excess oxygen resulting in the formation of copper ion vacancies [48].

The doping process is described by the following equation:

$$1/2\ \ O_2 + 2\ Cu_2O \rightleftharpoons 3\ Cu_2O + 2[V_{Cu}^{-}] + 2h \qquad (4.7)$$

where $[V_{Cu}^{-}]$ denotes a copper ion vacancy and "h" is a conduction hole. Doping of this type therefore results in an enhanced p-type conduction. Attainment of resistivity values of 20-100 ohm-cm in Cu_2O is encouraging in view of the fact that other preparation methods (e.g. thermal oxidation of copper [3-6, 32], electrodeposition [35]) have not been able to yield stable cuprous oxide material of resistivity less than several thousand ohm-cm. On further increasing the oxygen partial pressure, the concentration of defects reaches a certain critical value at which a change in valency at some local defects occurs and thus the nucleation of cupric oxide begins. The formation of these electrically neutral defects in turn reduces the amount of electrically active copper ion vacancies, thus reducing the conductivity of the semiconducting oxide. The cuprous oxide-cupric oxide mixture produces a semiconducting material of characteristic resistivity around 500 ohm-cm. At even higher partial pressures of oxygen the CuO phase is deposited, with resitivity first decreasing with increasing partial pressure of oxygen and then, above a certain value of oxygen pressure, saturating in the range 0.1 - 1.0 ohm-cm (see Figs. 4.5 and 4.6). This result is surprising, because CuO is known to be an insulator when grown by the thermal oxidation of copper. The fact that the CuO films were semiconducting p-type (determined by thermoelectric probe measurement) suggests that excess oxygen in CuO films could provide a doping effect. However, on the other hand, Purdes et al. [24] have found that CuO films deposited by reactive sputtering are oxygen deficient and that the composition ratio of CuO saturates at a value of 0.86 at oxygen pressures of 6.25×10^{-4} Torr.

4.5 THERMAL ACTIVATION ENGERGIES FOR CONDUCTIVITY

In semiconductors in which donors and acceptors are not fully ionized in the temperature range explored, the bulk condctivity depends, in general, exponentially on 1/T with a unique activation energy as described in

$$\sigma = \sigma_o \exp(-\varepsilon_a / kT) \tag{4.7}$$

where σ is the sample conductivity, σ_o the constant of proportionality, k Boltzmann's constant, T the sample temperature. The activation energy ε_a can be found by measuring the conductivity dependence on temperature and its value is given by the slope of the $\ln\sigma$ versus 1/T plot i.e. from

$$\varepsilon_a = k \frac{\ln \sigma_2 - \ln \sigma_1}{\frac{1}{T_1} - \frac{1}{T_2}} \tag{4.8}$$

where σ_1 and σ_2 are the conductivities at temperatures T_1 and T_2 respectively.

In some semiconductors, of which cuprous oxide is an example, multiple activation energies can be found. Thus over some temperature ranges more than one activation energy affects the thermal dependence of conductivity. Thus without proper care a false value of activation energy can be determined. Also the temperature dependence of hole mobility can contribute to an error in determining the activation energy. To avoid the influence of both the above mentioned effects, only linear parts of $\ln\sigma$ versus 1/T plots should be considered.

Activation energy measurements were made on Hall effect-shaped, r.f. sputtered samples as described in section 3.4 (Fig. 3.3). Sample

shapes were defined by sputter deposition of copper oxide films through a thin metal mask (Fig. 4.7). The mask was made of stainless steel (100 μm thick) or brass (70 μm thick) foil. The desired pattern was formed by the combination of photolithographic masking techniques and subsequent spray etching of the pattern in 50 ^{o}C commercial ferric chloride ($FeCl_3$) solution.

In order to achieve a sufficiently high current (minimum 0.2 μA)for I-V measurements that could be carried by the sample without applying a high bias voltage across the sample, the films used here were much thicker than those used for optical and resistivity measurements. The minimum current used for activation energy measurements was determined by the signal to noise ratio and also by the limited ability of the constant current source HP 6186 to control at very low currents. The maximum sample bias voltage ($\sim$40 V) was limited by the maximum voltage range of the Keithley 602 electrometer (10 V), which was used to measure the voltage V_σ proportional to sample resistivity. The Keithley 602 was used for voltage measurement because it offers a high input impedance capability (10^{14} ohms). No back-off voltage was used to extend the measured voltage range because it introduced inconveniences in further data processing.

To obtain samples with the desired film thickness of 5,000 - 10000 Å, deposition times of 10-20 minutes (at 200 W of r.f. power) were required. Such long deposition times required good sample cooling during the film deposition process, otherwise a significant rise in the substrate temperature resulted. A good thermal conductance between the substrate and the substrate table was ensured by employing silicon vacuum grease (see section 3.4, Fig. 3.4). An excessive shadowing at the edges of the metal mask, which is typical for r.f. diode sputtering at the pressure used (25 mTorr)

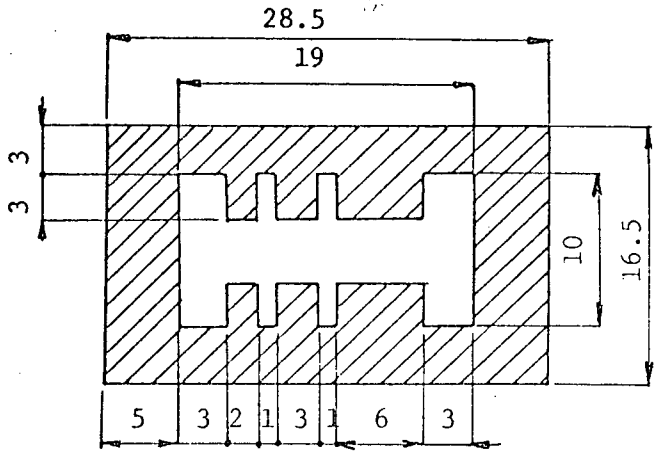

Fig. 4.7 Metal mask for deposition of samples used for measurement of thermal activation energies for conductivity. All dimensions are in millimetres.

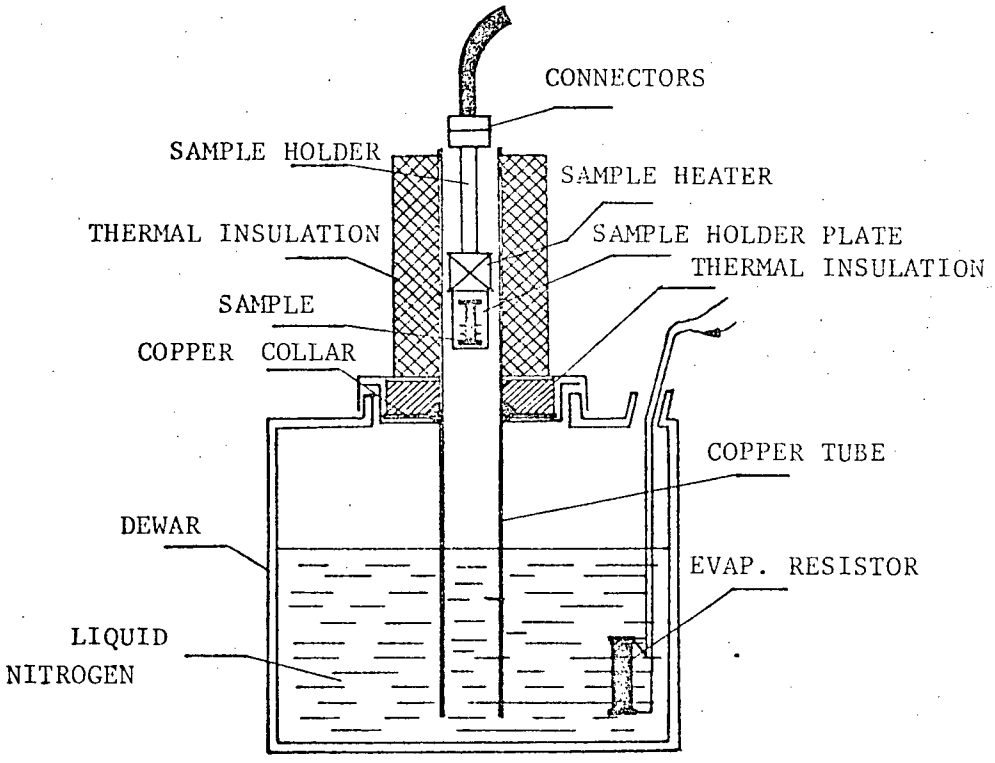

Fig. 4.8 Cryostat used for measurement of thermal activation energies for conductivity.

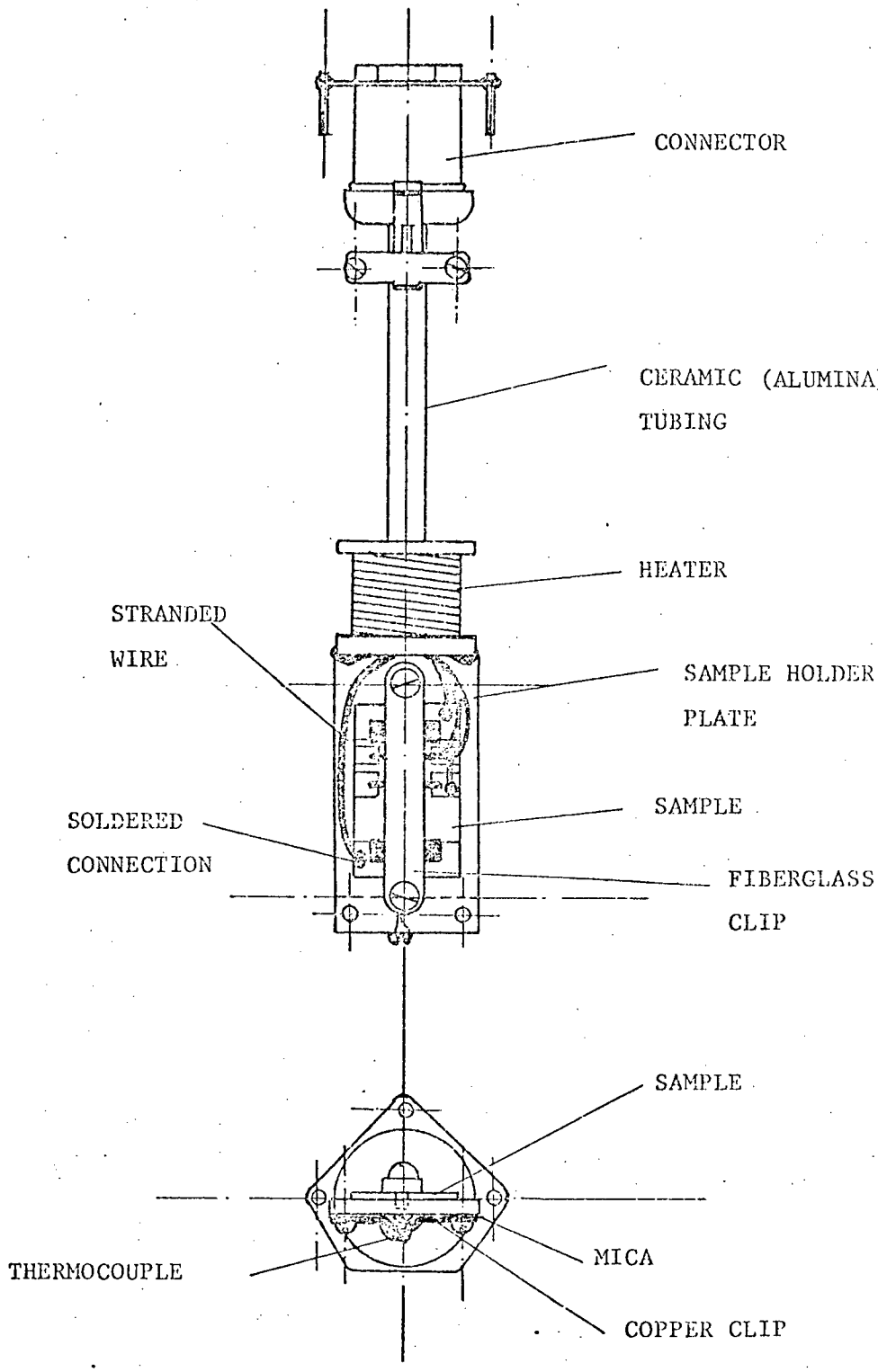

Fig. 4.9 Sample holder

[26], was avoided by contact mounting the mask on the substrate using four steel springs, as shown in Fig. 3.4.

Measurement of the temperature dependence of conductivity over the range 90-400 K was performed in the simple cryostat shown in Fig. 4.8. Heat developed by the resistor immersed in liquid nitrogen caused evaporation of nitrogen from the flask through the 1" I.D., 1/8" thick copper tubing also immersed in liquid nitrogen. The entire copper pipe, being a good thermal conductor, was thus held at a temperature very close to 77 K. Cooling of the sample holder and sample was provided by the action of the nitrogen gas passing through the copper tubing. The effectiveness of the cooling action was directly proportional to the evaporation rate of nitrogen. This arrangement of a continuous flow of nitrogen also prevented water condensation on the sample surface. When a sample temperature rise above room temperature was desired, the evaporator resistor power was switched-off and the heater coil (part of the sample holder assembly) power was switched-on. The desired rate of temperature rise was adjusted by the level of the power supplied to the heater coil. Good thermal conductance between the sample and the substrate plate was ensured by applying a thin layer of thermal compound (Wakerfield 120-2) and by pressing down the sample by the fiber-glass clip , see Fig. 4.9. All electrical connections to a sample were achieved by a standard PbSn solder. The sample temperature was measured using a copper-constantan thermocouple fastened between two mica plates by a copper clip to the substrate plate. The reference junction was kept at $0^{o}C$ in a water-ice mixture.

Data was recorded on an X-Y plotter (model HP 7044). Sample temperature, in the form of the thermocouple output voltage, was displayed on the X channel and sample resistivity, in the form of the voltage V_{σ} between sample terminals a,b (see Fig. 4.10), was displayed on the Y-channel.

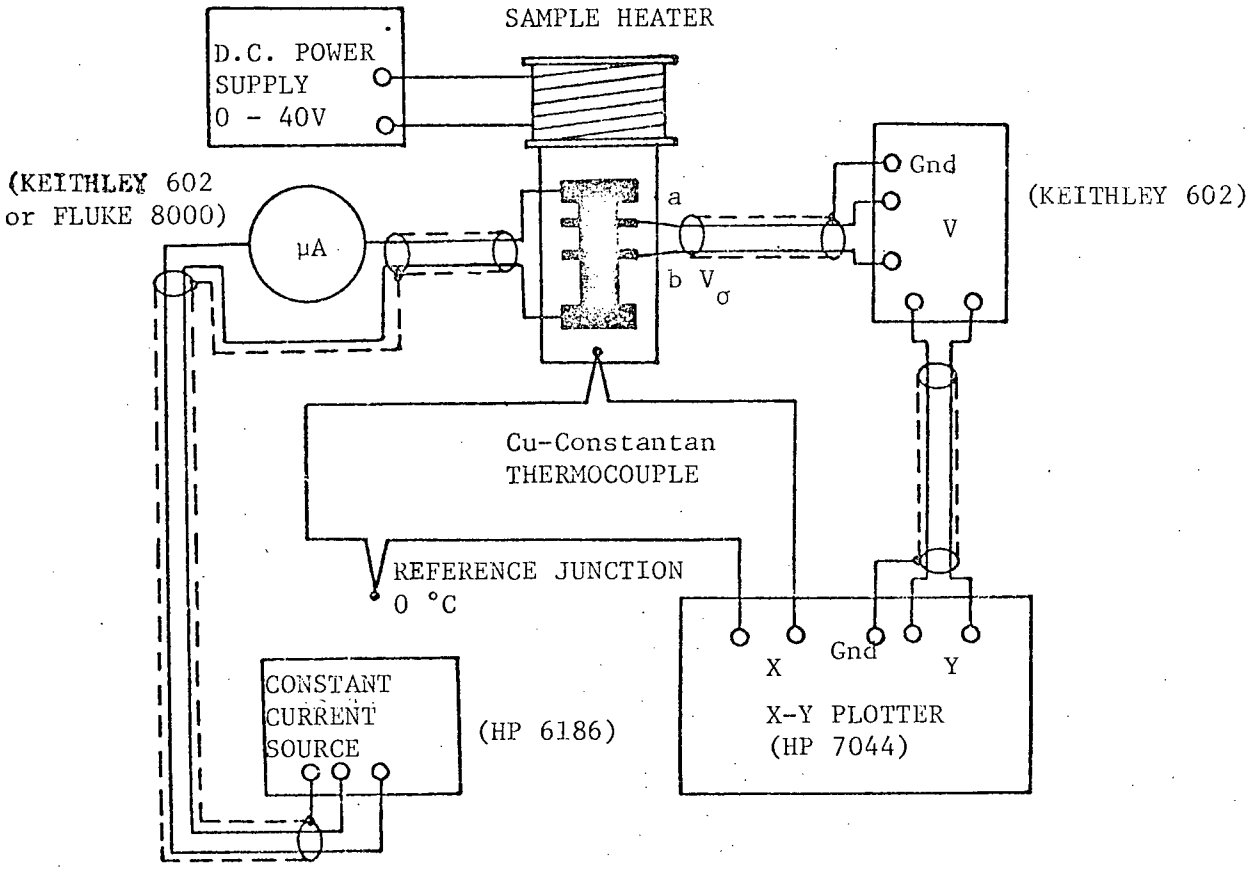

Fig. 4.10 Schematic diagram of the setup for measurement of thermal activation energy for conductivity.

Because the input impedance of the X-Y plotter was so low ($\sim$ 10 Mohm) and might cause significant loading of the sample voltage V_σ, especially at lower temperatures and for the higher resistivity samples, the input of the Y-channel was interfaced with the sample through a Keithley 602 electrometer. The sample current was measured either by a Keithley 602 electrometer or by a Fluke 8000 multimeter.

Evaluation of results for ε_a required the plotting of $\ln\sigma$ versus 1/T, selection of linear parts of this curve and then calculation of activation energies by using Eq. (4.8). The entire evaluation process for activation energy calculation was mechanized as follows. All graphs from the X-Y plotter were first digitized on an Instronics Gradicon digitizer and transferred to IBM cards for further processing on an IBM 370/168 computer. The computer program allowed for the calculation of temperature from thermocouple voltages by using a spline function interpolation. A thermocouple voltage-temperature data set for 100 points between -200 to + 250 °C was stored on a file, to which the program had access.

Data output was in a print-out form for 1/T, σ and $\ln\sigma$ as well as a graphical form, which yielded a plot of $\ln\sigma$ versus 1/T. From these plots one could then select visually the linear parts of the slope giving particular activation energy values. The data in print-out form from the selected temperature ranges were then used in Eq. (4.8) to calculate the values of activation energies.

The calculated values of activation energies for conductivity, corresponding to a particular oxide phase and temperature range, are summarized in Table 4.3. For samples deposited at the lowest partial pressures of oxygen, where the Cu_2O + Cu phase is formed, the resistivity was found to be almost independent of temperature in the range from 77-400 K. Thus no activation

TABLE 4.3

Thermal activation energies for conductivity of copper oxide films deposited by reactive sputtering.

Oxide Phase	Temperature Range [°C]	Activation Energy [eV]
Cu_2O	-60 - -4	0.09
	-30 - + 60	0.19
	+ 50 - + 116	0.23
Cu_2O + CuO	-90 - - 56	0.14
	+ 2 - + 47	0.19
	+ 56 - + 76	0.23
CuO	-150 - + 20	0.11
	-150 - + 20	0.14

energy for this cermet-like material in this temperature region was determined. Pure reactively sputtered cuprous oxide is characterized by three thermal activation energies, namely 0.09, 0.19 and 0.23 eV. Therefore the electrical conduction of reactively sputtered cuprous oxide cannot be explained in terms of a simple energy level diagram. In addition the fact that films are polycrystalline makes interpretation of these results even more difficult. Comparison of the above results with results obtained for thermally grown Cu_2O is not easy, because activation energies for thermally grown cuprous oxide depend strongly on the thermal history of the measured samples and have been found to have values between 0.1 and 1 eV [47]. For samples of composition Cu_2O + CuO two activation energy levels with the same values as for Cu_2O films were found. This indicates a similarity in the mechanism responsible for conduction processes in both Cu_2O and Cu_2O + CuO films. However, the fact that a significant portion of electrically neutral defects (nucleation of CuO) replaces electrically active defects (copper ion vacancies) on increasing the oxygen partial pressure results in a lowering of the conductivity and disappearing of the 0.09 eV level. The new level (0.14 eV) that appears is presumably associated with formation of CuO.

4.6 COMPARISON OF REACTIVE SPUTTERING THEORY WITH EXPERIMENTAL DATA.

To illustrate the validity of the theory proposed in chapter 2, the ratio of P_o/R_M^* required for formation of near-stochiometric cuprous oxide films was found experimentally for various r.f. power levels and then compared with theoretical values calculated from Eq. (2.36). The deposition rate R_M of copper sputtered from a pure copper target in pure argon was measured at various r.f. power levels. The standard procedure was to deposit copper for a period of one hour at the desired power level, and then to estimate the

thickness of the deposited film by the weighing method described in section 4.1. The results obtained are graphically presented in Fig. 4.11 and as described in section 2.2, can be taken as a measure of the dependence of R_M^* on r.f. power. Then the required values of P_o to produce near-stochiometric Cu_2O films at each r.f. power level were determined. This necessitated many depositions at each r.f. power level, each time slightly varying P_o and then studying the electron diffraction data for each deposition until the occurrence of pure Cu_2O films was indicated. Stochiometric, undoped cuprous oxide is an insulator at room temperature and it is believed that the sharp peak in the resistivity data shown in Figs. 4.5 and 4.6 is indicative of formation of this material. Clearly, exact attainment of the required P_o at each power level (therefore sputtering rate R_M) would require a considerable number of film preparations. The procedure adopted was to prepare 10-15 samples at each r.f. power level and record the highest value of P_o at which the electron diffraction pattern of Cu + Cu_2O was observed and the lowest value of P_o at which Cu_2O + CuO was detected. The results are plotted in Fig. 4.12. Taking the data at 200 W as references (see also Fig. 4.5 for the precise extreme values of P_o needed to produce Cu_2O) the variation in R_M with power level (Fig. 4.11) was used to predict the extreme values of P_o for formation of Cu_2O at r.f. power levels other than 200 W using Eq. (2.36). These results are shown as the solid lines on Fig. 4.12 while the experimentally determined P_o values are represented by the dots.

Note that in the above experiments and calculations R_M rather than R_M^* was used because if was easy to determine R_M at any r.f. power level (using the above discussed method), while the determination of R_M^* required knowledge of the compositon, thickness and density of the deposited films. Obviously the composition and density of the film are properties which are

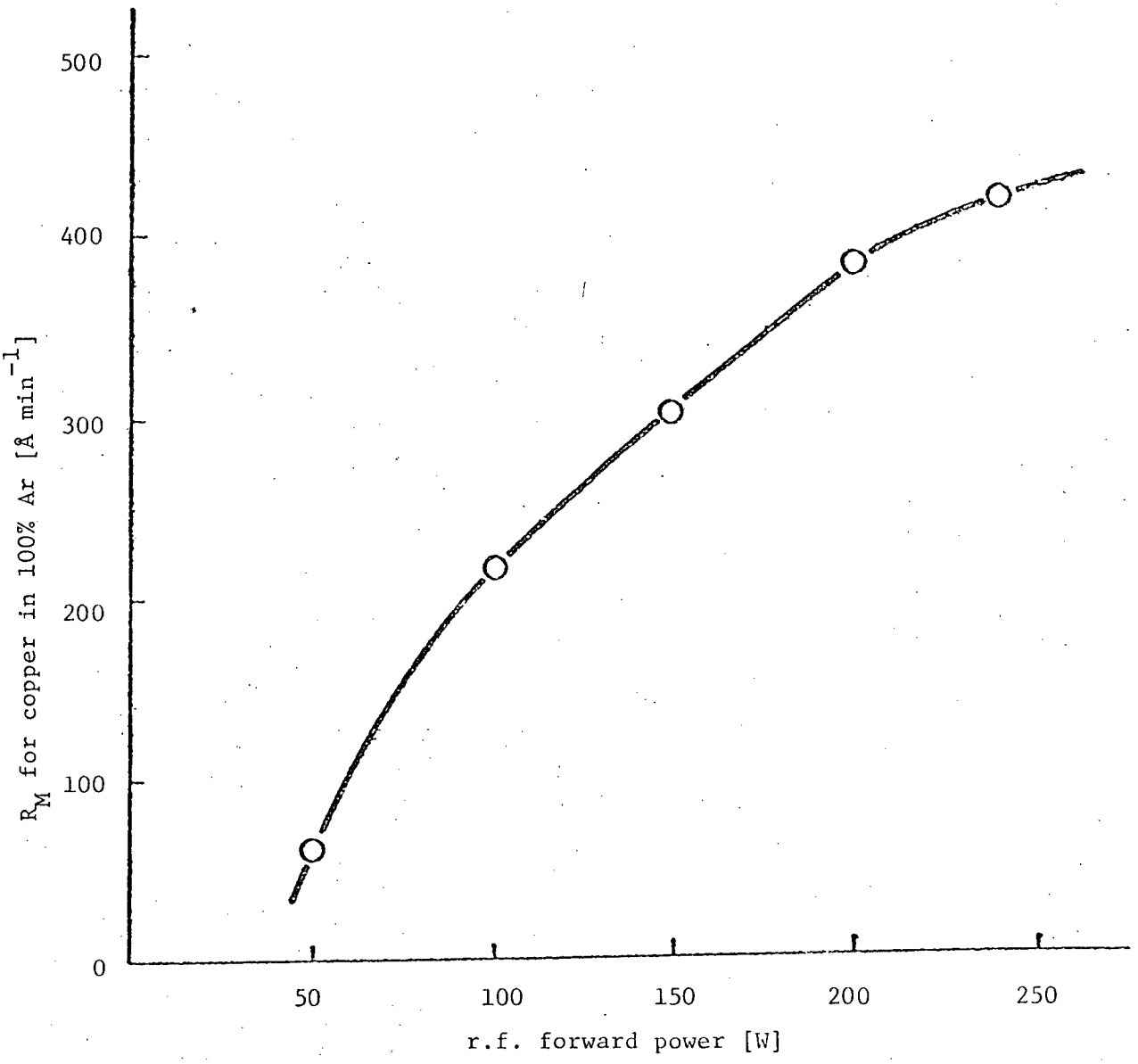

Fig. 4.11 Deposition rate of pure copper (measured at the center of substrate table) for various r.f. power levels and the total pressure of 25 mTorr.

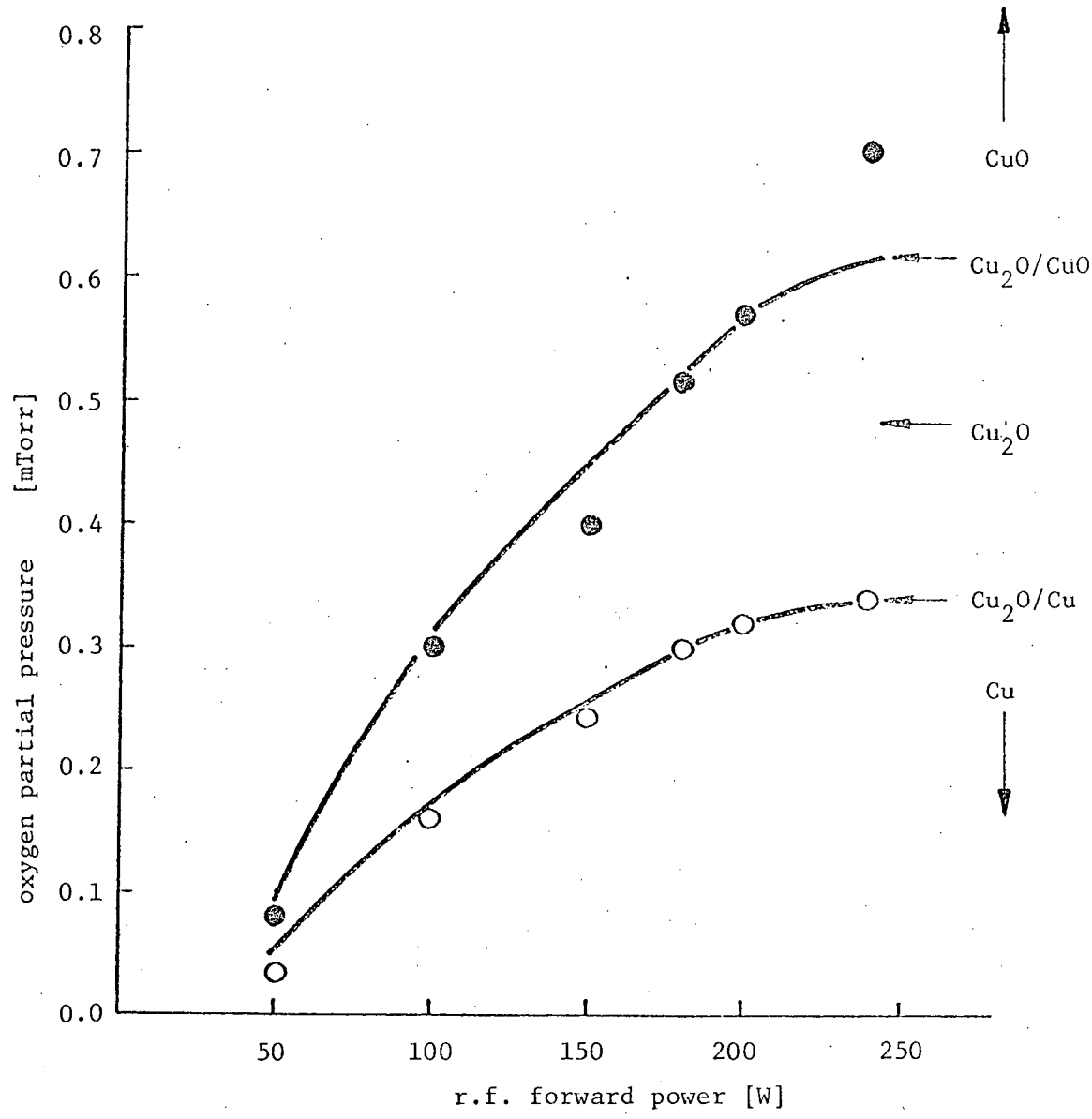

Fig. 4.12 Comparison of theoretical and experimental data regarding the oxygen partial pressure required to form particular copper oxide films at various r.f. power levels. ● = experimental data indicating lowest observed partial pressures for producing Cu_2O+CuO; ○ = experimental data indicating highest observed partial pressures for producing Cu_2O+Cu; solid lines based on constant values of P_o/R_M, with R_M being taken from Fig. 4.11 and reference values of P_o at 200W taken from Table 4.2.

much more difficult to measure than the thickness and mass of copper film necessary for determination of R_M. The validity of using R_M instead of R_M^* in the above calculations was discussed in chapter 2.

Let us now discuss some factors in the denominator of Eq. (2.36) which can influence the above experiments.

$$C = \frac{P_o}{R_M^*}\left[\frac{1}{\frac{N_s \alpha_M^* \Delta_M}{N_e \alpha_o r(T)} + \frac{A_s kT}{S}}\right] \qquad (2.36)$$

The value of N_s/N_e for a given composition ratio C remains constant, regardless of the deposition conditions used to obtain this composition. Generally, the temperature of the sputtering gas can be affected by the r.f. power level. However, in a dynamic sputtering system (continuously pumped system with a constant leak rate of the sputtering gas, see section 3.1) having a constant supply of a fresh sputtering gas, the influence of the r.f. power level (over the range used here) on the sputtering gas temperature can be assumed to be negligible. Thus the terms r (T) and $A_s kT/S$ remain constant provided, in the latter case, that the throttled pumping speed S remains unchanged in all experiments. Therefore neither r(T), $A_s kT/S$ nor N_s/N_e, for a given film composition ratio, have an effect on the value of the square bracketed term of Eq. (2.36). The value of Δ_M may slightly increase with increasing r.f. power level due to the fact that atoms ejected from the target with higher energies are thermally equilibrated with the sputtering gas at a shorter distance from the substrate than those having lower energies However, if the target-substrate table distance is much smaller than the target diameter, then, particularly near the centre of the substrate table,

this effect can be neglected. The temperature of the target and the substrate depends on the sputtering power level. This affects the values of α_o and α_o^T, the sticking coefficients for oxygen at the substrate and the target respectively. Values of α_o and α_o^T decrease with increasing temperature and, thus, also with the r.f. power level used for sputtering. Thus an increase of r.f. power level can result in an increase in the value of the denominator in the square bracketed term of Eq. (2.36). At the target a decrease in α_o^T will result in a lowering of the target coverage by oxygen (see Eq.(2.31)) and thus enhanced R_M^*, see also Eq. (2.32). The effect of the temperature dependence of α_o and α_o^T on the composition ratio thus depends on the experimental conditions. In particular if the efficiency of the cooling systems for the target and the substrate is poor then there will be a tendency for the composition ratio at a given P_o/R_M ratio to decrease with increasing sputtering power level. Thus at a higher r.f. power level a higher P_o/R_M ratio may be required than at a lower power level, to obtain the same composition ratio in both cases. Therefore, considering the effect of α_o and α_o^T on the composition ratio and that a limited number of experiments were done, especially in the Cu_2O + CuO region, the fit of theoretically predicted values and experimental data shown in Fig. 4.12 is very good.

The proposed theory also provides a basis for explaining the variations in film resistivity that were observed on taking measurements at different positions (with respect to the centre of the substrate table) on the deposited films. Data for films deposited at various oxygen partial pressures are shown in Fig. 4.13. This effect is not due to a variation in film thickness as this has been allowed for in the data presented in Fig. 4.13. The correction procedure was as follows: the spatial dependence of the thickness of a pure copper film (deposited in 100% argon) was estimated from a thickness measurement of the central part of the film and resistance data taken at 1/4"

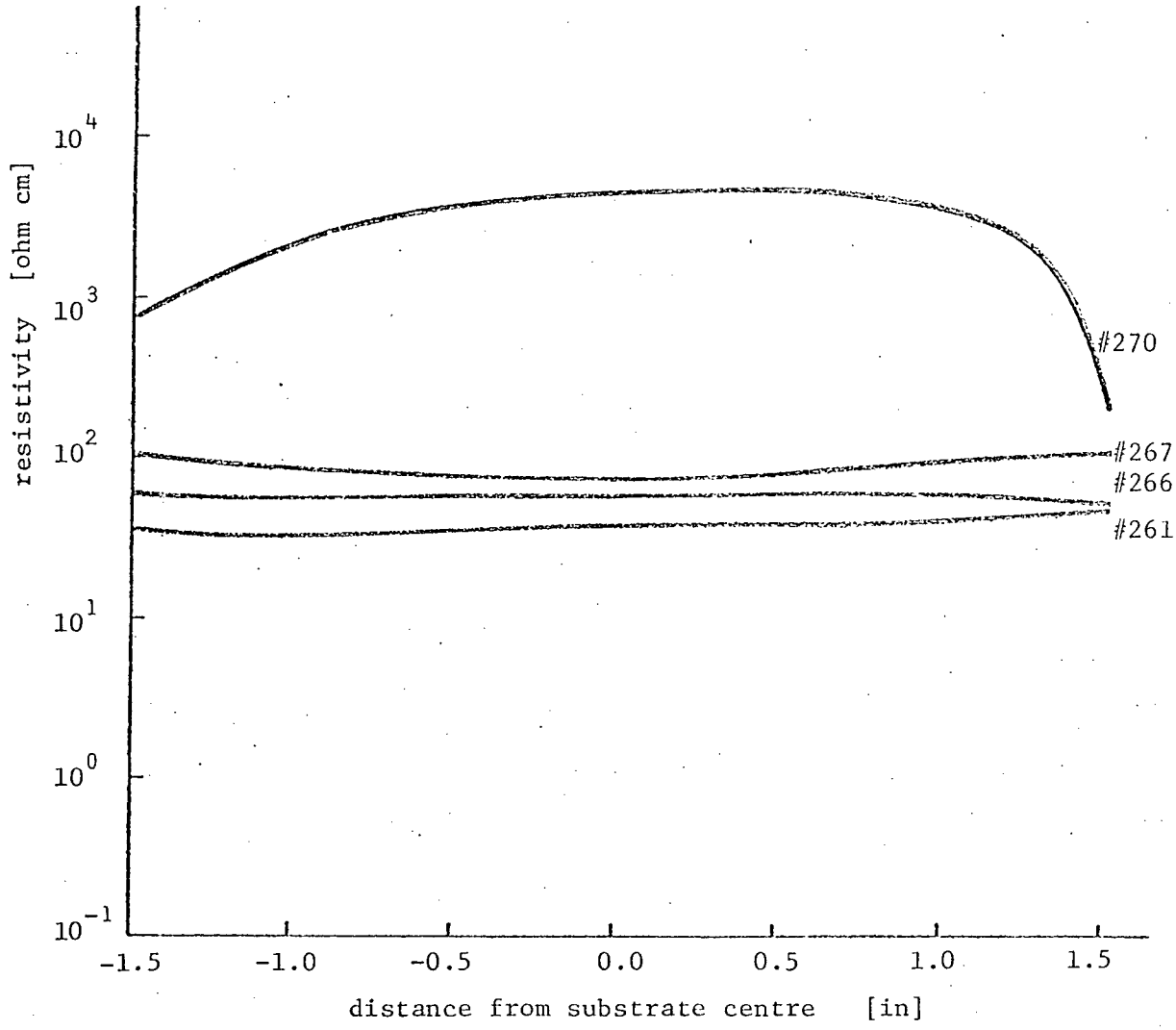

Fig. 4.13 Variation of resistivity with radial distance along copper oxide films. The sample numbers refer to those marked on Fig. 4.5.

intervals along the film (a constant value of film resistivity was assumed), see Fig. 4.14. Resistance data were obtained by the four-point probe technique. Each film deposited at each partial pressure of oxygen (Fig. 4.13) was then assumed to exhibit the same thickness variation (on a percentage basis) as the pure copper film, and the reference thickness for each film was determined by an Angstronmeter measurement on the central portion of each film. The slight asymmetry around the centre point of the substrate table exhibited by the curves in Figs. 4.13 and 4.14 is related to the plasma disturbance caused by the shutter fixture. The significance of the curves in Fig. 4.13 is that they suggest a variation of film composition across the substrate. With reference to Figs. 4.5 and 4.13, large changes in resistivity will result across the substrate slide at P_o values suitable for preparation of nearly stochiometric cuprous oxide at the centre of the slide (sample #270); also the resistivity of the outer regions of the film will become greater than that at the centre for films prepared at P_o values approaching the value appropriate to $Cu_2O + CuO$ formation (sample #267).

The observed nonuniformity (across the substrate table) in deposition rate of copper is caused by the diffusive nature of the mechanism of transport of copper species towards the substrate, resulting from the fact that $\Delta_M(x)$ is a function of the distance x from the centre of the substrate table. Thus the decrease of $\Delta_M(x)$ towards the outer regions of the substrate table (equivalent to a decrease in the flux of copper species) results in an increasing compositional ratio with the distance from the substrate table center. An increasing composition ratio with the distance from the substrate table center was observed by measurement of the spacial dependence of film resistivies and was confirmed by spectrophotometer measurements taken at various positions along the film, see Fig. 4.3 and compare with Fig. 4.2. This is

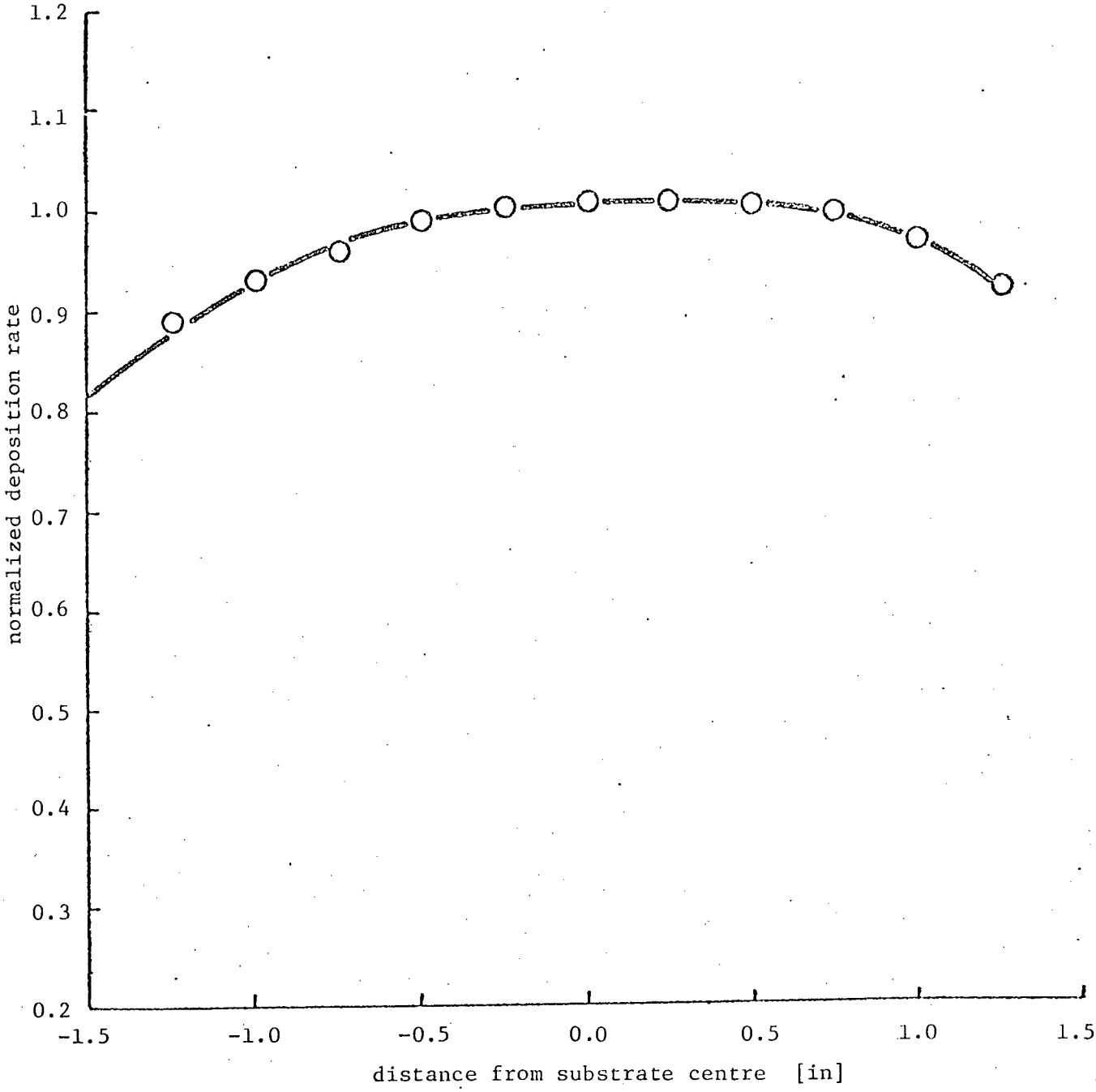

Fig. 4.14 Deposition rate of pure copper r.f. sputtered in 100% Ar, normalized with respect to the deposition rate at the centre of the substrate table. (Total pressure = 25 mTorr).

further direct evidence of the validity of the above proposed theory embodied in Eq. (2.36), namely that the film compositional ratio is directly proportional to the relative magnitudes of the fluxes of metal and oxygen species at the substrate.

A further way to show the validity of the reactive sputtering theory proposed in chapter 2 is to compare the r.f. and d.c. P_o/R_M^* ratios required to obtain near-stochiometric Cu_2O, where the composition is precisely known (C = 0.5). From electron diffraction data (section 4.2) and resistivity data (section 4.4) the partial pressures of oxygen required for formation of near-stochiometric Cu_2O films could be very precisely determined. Let us concentrate on two cases where similar sputtering rates for r.f. and d.c. deposition were obtained, namely r.f. sputtering at 200 W of forward power which required a P_o of 0.0427 Pa (0.32 mTorr) for near-stochiometric cuprous oxide formation, and d.c. sputtering at 70 mA of discharge current, where a P_o of 0.0347 Pa (0.26 mTorr) was required to form the near-stochiometric Cu_2O phase. In both cases deposition times of 2 minutes were used, which produced films of thickness 1080 Å and 870 Å for the cases of r.f. and a d.c. sputtering respectively. From the known Cu_2O deposition rate D [cm sec^{-1}], Cu_2O density(s = 6.2 g cm^{-3}), Cu_2O molecular weight (M = 143 g $mole^{-1}$) and Avogadro's number (N_A = 6.023x10^{23} molecules $mole^{-1}$) one can calculate, assuming $\Delta_M \simeq 1$ (this approximation can be allowed near the centre of the substrate table), the effective copper sputtering rate R_M^* as

$$R_M^* = \frac{D\ s\ N_A}{M} N_M \qquad [at.cm^{-2}sec^{-1}] \qquad (4.9)$$

where multiplication by N_M(=2) arises from the fact that one molecule of Cu_2O has two copper atoms. Applying Eq. (4.9) to the above r.f. and d.c.

cases one can show that in the r.f. sputtering case

$$R_M^* = 4.7 \times 10^{19} \text{ at } m^{-2}sec^{-1}; \text{ and } \frac{P_o}{R_M^*} = 9.08 \times 10^{-22} \text{ Pa } m^2 \text{ sec;}$$

and in the d.c. sputtering case

$$R_M^* = 3.79 \times 10^{19} \text{ at } m^{-2}sec^{-1}; \text{ and } \frac{P_o}{R_M^*} = 9.15 \times 10^{-22} \text{ Pa } m^2 sec.$$

Here, if one takes into consideration that two different plasma energizing methods were used and that the total pressure and anode-cathode voltage were both about 3 times larger in the d.c. case than in the r.f. sputtering case (possibly leading to a different α_o and α_o^T) the agreement between the d.c. and r.f. values of P_o/R_M^* is excellent. Eq. (2.37) is useful in allowing comparison of theory and experimental data, but its main function is as a starting point from which the experimental conditions required to form a film of given composition ratio could be determined. To use Eq. (2.37) in this fashion requires a knowledge of the system constants, namely γ, ω and ε, (defined in chapter 2, Eq. (2.27)). Determination of ω required knowledge of the throttled pumping speed S. The following procedure was used to determine the pumping speed S. First the sputtering system was pumped down to a vacuum better than 10^{-6} Torr. Then the throttling valve was turned into its minimum conductance (sputtering) position and oxygen was admitted to the system at such a rate that a pressure of 4×10^{-4} Torr was reached (the pressure reading was taken according to the ionization gauge E, see Fig. 3.1). After the pressure stablilized, the oxygen on-off valve was closed, the setting of the oxygen metering valve was unchanged and the system was allowed to pump down to a base pressure of approximately 10^{-6} Torr again. Then the high vacuum valve was closed and the oxygen on-off valve opened. Thus the pressure in the bell jar started to increase and the time required to

increment the total pressure by 60 mTorr was measured. This procedure was repeated 5 times and the average time Δt was calculated. The pressure reading was given by the thermocouple gauge B. In order to avoid any error caused by incorrect zeroing and nonlinearity of the gauge, the pressure increments were taken in different pressure regions, for example between 1-61 mTorr, 20-80 mTorr, etc. The average time Δt required to increment the pressure by ΔP = 60 m Torr was 67 seconds. Knowing the total volume of the enclosure $V(2.23\times10^{-2}\ m^3)$, the leak rate of oxygen could be calculated from the relation

$$L = \frac{\Delta P \quad V}{\Delta t} \tag{4.10}$$

$$= \frac{60\times10^{-3}\times0.023}{67} = 2.027\times10^{-5} \quad m^3 Torr\ sec^{-1}$$

The throttled pumping speed S can be then be calculated from the relation

$$S = \frac{L}{P} = \frac{2.027\times10^{-5}}{4\times10^{-4}} = 5.07\times10^{-2}\ m^3\ sec^{-1}$$

Then, knowing the target area ($0.0182\ m^2$) and assuming T = 300 K

$$\omega = \frac{0.0507 \quad 0.0507}{0.0182 \times 1.38\times10^{-23}\times 300} = 6.7\times10^{20}\ N^{-1}m^{-1}$$

The constant β was determined from (Eq.2.37) and from the values of P_o and R_M^* required to obtain near-stochiometric Cu_2O of which the compositional ratio is known (C=0.5). Using the data from r.f. deposition at 200 W where the near-stochiometric cuprous oxide was formed, namely P_o = 0.0427 Pa and $R_M^* = 4.7\times10^{19}\ m^{-2}\ sec^{-1}$, β equal to 0.1148 was obtained. Assuming again $\Delta_M \simeq 1$ and also

$\alpha_M \simeq 1$ then $\beta \simeq \alpha_o = 0.1148$, which appears to be a reasonable value for the sticking coefficient of oxygen on copper, especially taking into consideration that the substrate is exposed to bombardment by high energy electrons. As the factors ω, β (hence ε) and S can be maintained constant over a wide range of sputtering conditions, the numbers calculated above can be used in Eq. (2.37) to predict the required values of R_M^* and P_o needed to produce a copper oxide film of given composition ratio. It remains only to estimate R_M^* from observable parameters.

Calculation of R_M^* from Eq. (2.32) requires R_{ox}, R_M and F to be known. The sputtering rates R_{ox} and R_M have to be determined experimentally for each deposition power, but F, which is independent of sputtering power, providing good cooling of the target is ensured, can be determined once for a given target-reactive gas system. The coefficient F was determined from Eq. (2.32) using data from sputter deposition at 200 W and $P_o = 0.0427$ Pa, where near stochiometric Cu_2O ($C = 0.5$) was deposited. The sputtering rates R_M and R_{ox} were determined from the deposition rate of copper in 100% argon and the deposition rate of CuO in 100% oxygen atmosphere respectively, using the same calculation method as used previously to determine R_M^* (Eq. 4.9). Thus from:

$$R_M^* = 4.7 \times 10^{19} \ m^{-2} sec^{-1} \qquad P_o = 4.27 \times 10^{-2} P_a$$

$$R_M = 5.42 \times 10^{19} \ m^{-2} sec^{-1} \qquad C = 0.5$$

$$R_{ox} = 8.55 \times 10^{18} m^{-2} sec^{-1}$$

one obtains $\underline{F = 2.73 \times 10^{-3}}$

A convenient check on the usefulness of the above values for the system constants is to use them to compute the composition ratio in a range of pressure and power values which experimentally are known to produce a well-defined phase, e.g. CuO for which C=1. This was done for oxygen partial pressures of 1 mTorr and 10 mTorr and the resulting values of C, computed using the above values of constants in the simplified version of Eqn. (2.27) i.e. Eqn.(2.37), were 0.987 and 0.995 respectively.

5. OPTICAL CONSTANTS OF COPPER OXIDE THIN FILMS

5.1 POSSIBLE MEASUREMENT METHODS

The optical constants of thin films can be determined either from intensity measurements (photometric) or from polarization measurements (polarimetric). Photometric measurements can be performed either at normal or non-normal incidence, while polarometric at non-normal only. Only photometric methods were considered for the determination of the optical constants of the various copper oxide films prepared in this work, and all measurements were done at normal incidence of light. There are many experimental advantages to be gained by making measurements at normal incidence. The angle of incidence does not need to be known accurately, measurements are insensitive to the convergence angle of light on the sample and polarization effects are unimportant [36]. Also surface nonuniformities in flatness and contamination often do not greatly influence the result [37]. Because all the present experiments were performed on absorbing films, a determination of both the refractive index n and the extinction coefficient k was necessary, where the total complex index of refraction is $\tilde{n} = n - ik$.

Generally, when a number N of optical constants are to be determined, N independent measurements must be made. Then N independent equations for the measured quantities written in terms of the N unknown optical parameters have to be solved. Considering photometric methods only, reflectance R of light from the film side, reflectance R' from the substrate side and transmittance T are the measured quantities. The analytical expressions for the dependencies of R, R' and T on the refractive index and extinction coefficient, the wavelength of the light λ, the film thickness d and the refractive index and thickness of the substrate n_s and d_s are very

complicated. Inverting of functions analytically to obtain "n" and "k" in terms of the measured quantities R and T is virtually impossible. The solutions used to be obtained in the past through approximate formulas and/or graphical methods. Reviews of such methods have appeared elsewhere [38-40, 45]. The method used in the present work for determining the optical constants of thin films takes advantage of powerful numerical iteration methods for solving simultaneous nonlinear equations and the availability of fast powerful computers. This allows attention to be concentrated on accuracy instead of the former simplicity of evaluation. There are a number of independent measurement combinations. Considering only perpendicular incidence, n,k and d can be obtained from a combination of T-R-R'. Because in our case d was determined independently by a Sloan M-100 Angstrometer, we can concentrate on determination of n and k only. In that case two independent measured quantities which can be expressed in terms of n and k (to be determined), have to be obtained. The most common choice is to use R and T measurements [36,37, 41-44]. Usually R' measurements are not used, because they often contain systematic errors [36]. In some cases, however, the ratio R/R' can be used, and thus the measurement of absolute reflectivity can be avoided. In the cases when the measurement of reflectivity is not available, a combination of two transmittance measurements for similar films of two different thickness can be used.

Speaking of accuracy in the optical constants determination, one would like to know how the error in some of the measured quantities affects the accuracy of the calculation of optical constants. This is very difficult to generalize because the accuracy depends on the selection of measured quantities, the wavelength and the range of values of optical constants to be determined. Let us consider the cases of measurements involving R-T and

$T(d_1) - T(d_2)$. The expressions for the dependence of R and T on n, n_s the refractive indeces of the film and the substrate respectively, k the extinction coefficient of the film, d, d_s the thicknesses of the film and the substrate respectively and the light wavelength λ have the following form [36]:

$$R = \frac{a_1 \exp(4\pi dk/\lambda) + b_1 \cos(4\pi dn/\lambda) + c_1 \sin(4\pi nk/\lambda) + f_1 \exp(-4\pi dk/\lambda)}{a_2 \exp(4\pi dk/\lambda) + b_2 \cos(4\pi dn/\lambda) + c_2 \sin(4\pi dn/\lambda) + f_2 \exp(-4\pi dk/\lambda)} \tag{5.1}$$

$$T = \frac{a}{a_2 \exp(4\pi dk/\lambda) + b_2 \cos(4\pi dn/\lambda) + c_2 \sin(4\pi dn/\lambda) + f_2 \exp(-4\pi dk/\lambda)} \tag{5.2}$$

where

$$a_1 = [(n-1)^2 + k^2][(n_s^2 + 1)(n^2 + k^2 + n_s^2) + 4nn_s^2],$$

$$a_2 = [(n+1)^2 + k^2][(n_s^2 + 1)(n^2 + k^2 + n_s^2) + 4nn_s^2],$$

$$b_1 = -2[(n_s^2 + 1)(n^2 + k^2 - 1)(n^2 + k^2 - n_s^2) + 8k^2 n_s^2],$$

$$b_2 = -2[(n_s^2 + 1)(n^2 + k^2 - 1)(n^2 + k^2 - n_s^2) - 8k^2 n_s^2],$$

$$c_1 = 4k[-(n_s^2 + 1)(n^2 + k^2 - n_s^2) + 2n_s^2(n^2 + k^2 - 1)],$$

$$c_2 = 4k[(n_s^2 + 1)(n^2 + k^2 - n_s^2) + 2n_s^2(n^2 + k^2 - 1)],$$

$$f_1 = [(n+1)^2 + k^2][(n_s^2 + 1)(n^2 + k^2 + n_s^2) - 4nn_s^2],$$

$$f_2 = [(n-1)^2 + k^2][(n_s^2 + 1)(n^2 + k^2 + n_s^2) - 4nn_s^2], \quad \text{and}$$

$$a = 32\, n_s^2(n^2 + k^2).$$

To illustrate graphically the correlation between the error in measurement of reflectance and transmittance and accuracy of optical constants determination, the contours of constant R and T were plotted in the n-k plane for a region of n and k values where the optical constants of Cu_2O were expected to lie. The refractive index n for thermally grown Cu_2O as a function of wavelength over the visible region of light has been determined by Pastrnak [98] to have values near 2.7. From values of absorption coefficient $\alpha(\lambda)$ for bulk Cu_2O determined by Pastrnyak [99] it could be inferred that the maximum value of extinction coefficient k should have a value less than unity in the wavelength region of interest (4000Å - 8000Å). Multiple solutions for n and k may exist at given values of reflectance and transmittance. In order to gain some information about the location of solutions other than the correct one and having refractive indices of lower values than expected for Cu_2O films, the contours of constant R and T were plotted for the range of n-values from 0.5 to 3.0 and of k-values from 0.0 to 1.0. The proximity of the multiple solutions and manner in which the measured quantities intersect in the n-k plane were used to judge the suitability of a given method for determination of the optical constants of copper oxide films at a given wavelength.

Let us consider the two transmittances method, where a measurement of absolute specular reflectance can be avoided. As the first example the transmittance data for films with thicknesses of 1080Å and 540Å were considered, see Fig. 5.1. Transmittances in this case intersect at very small angles leading to a large inaccuracy in determining the optical constants, especially the refractive index n. This is especially critical in the region of $n > 1.5$ and $k > 0.3$, where Cu_2O optical constants at 4000Å are expected to fall. Moreover, n and k are multiple-valued functions of the transmittances

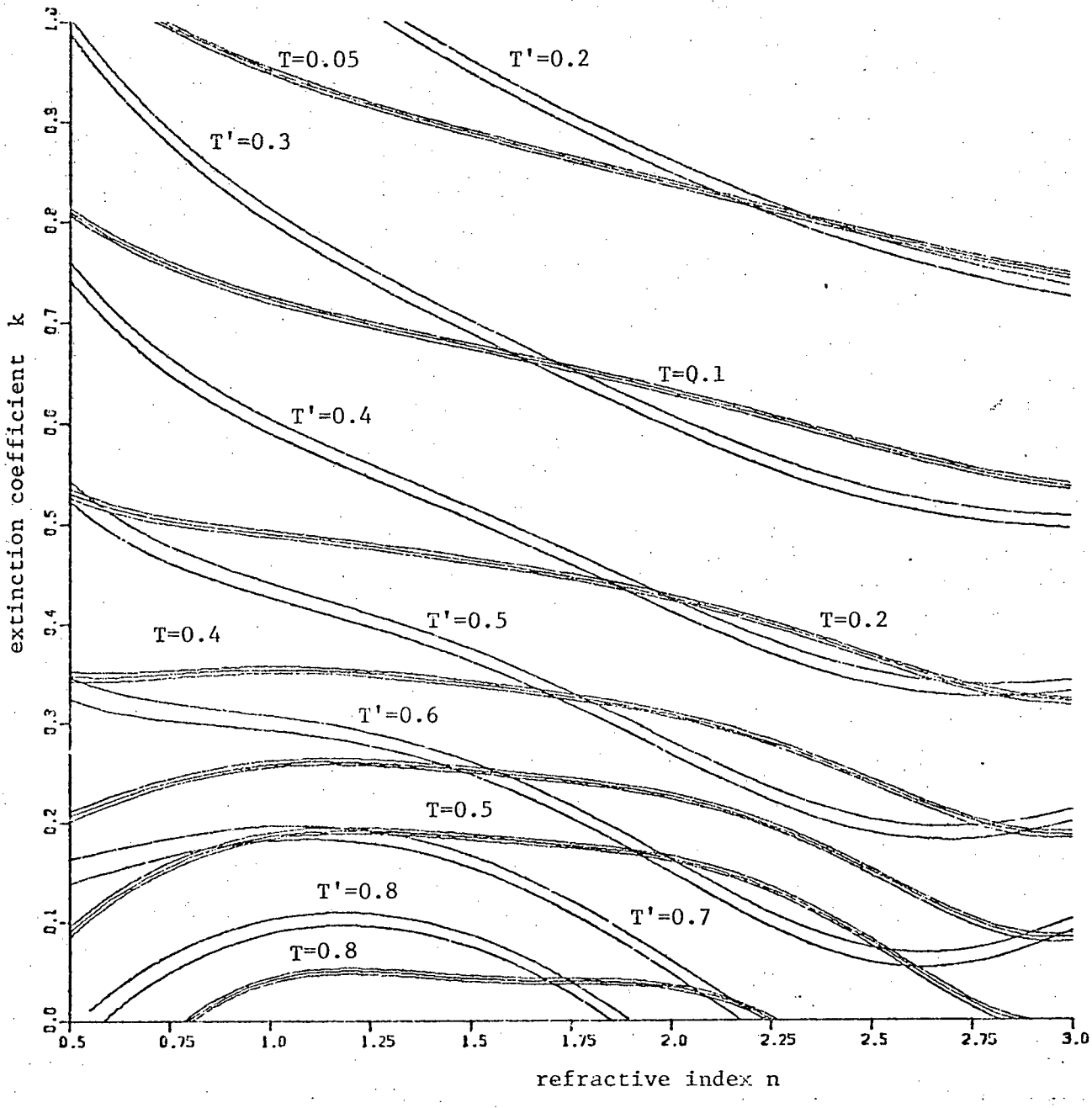

Fig. 5.1 Transmittance curves for two samples of different thickness as a function of refractive indices of the film. The width of the countours indicates an experimental error in transmittance measurement of ±1% of the nominal transmittance value. The double line represents a sample with film thickness = 540Å (T') and the triple line a sample with thickness = 1080Å (T). Curves are computed for n_s = 1.5 and λ = 4000Å.

in the region of n > 1.5. Thus if errors in measurement of transmittances are large (> 1%), the uncertainity in n and k determination can be so large that this method is not able to offer reliable results. Significant improvement in the reliability and accuracy of the two transmittances method can be achieved by increasing the difference between the thicknesses of the samples used. This is shown in Figs. 5.2 and 5.3 where the transmittances from films of thicknesses 1080Å and 360Å are given. Note that n and k are in this case single-valued functions of R and T over the plotted n-region. However, one has to be aware when using this method that in some cases two films with very different thicknesses may not have identical physical properties and this may yield an additional inaccuracy in the determination of optical constants.

Turning now to the R-T method Fig. 5.4 displays transmittance and reflectance curves, in the n-k plane, computed for a 1080Å thick film. Here all R and T curves intersect at very large angles, except for films with $n \approx n_s = 1.5$ and thus a high accuracy of n and k determination using this method for films with $n \neq n_s$ can be achieved. The fact that n and k are multiple-valued functions of R and T does not seem to be a drawback of this method, because individual solutions are far apart and by careful consideration an acceptable solution can be easily determined. If one follows the behaviour of n and k over the measured wavelength region, and n-values for some wavelength points are known either from the literature or from independent measurements, it is not very likely that an erroneous solution can be obtained. Considering the theoretical accuracy of the R and T method this method was selected for determination of the optical constants of copper oxide films. The technique used in their determination and the results obtained are discussed in the next section of this chapter.

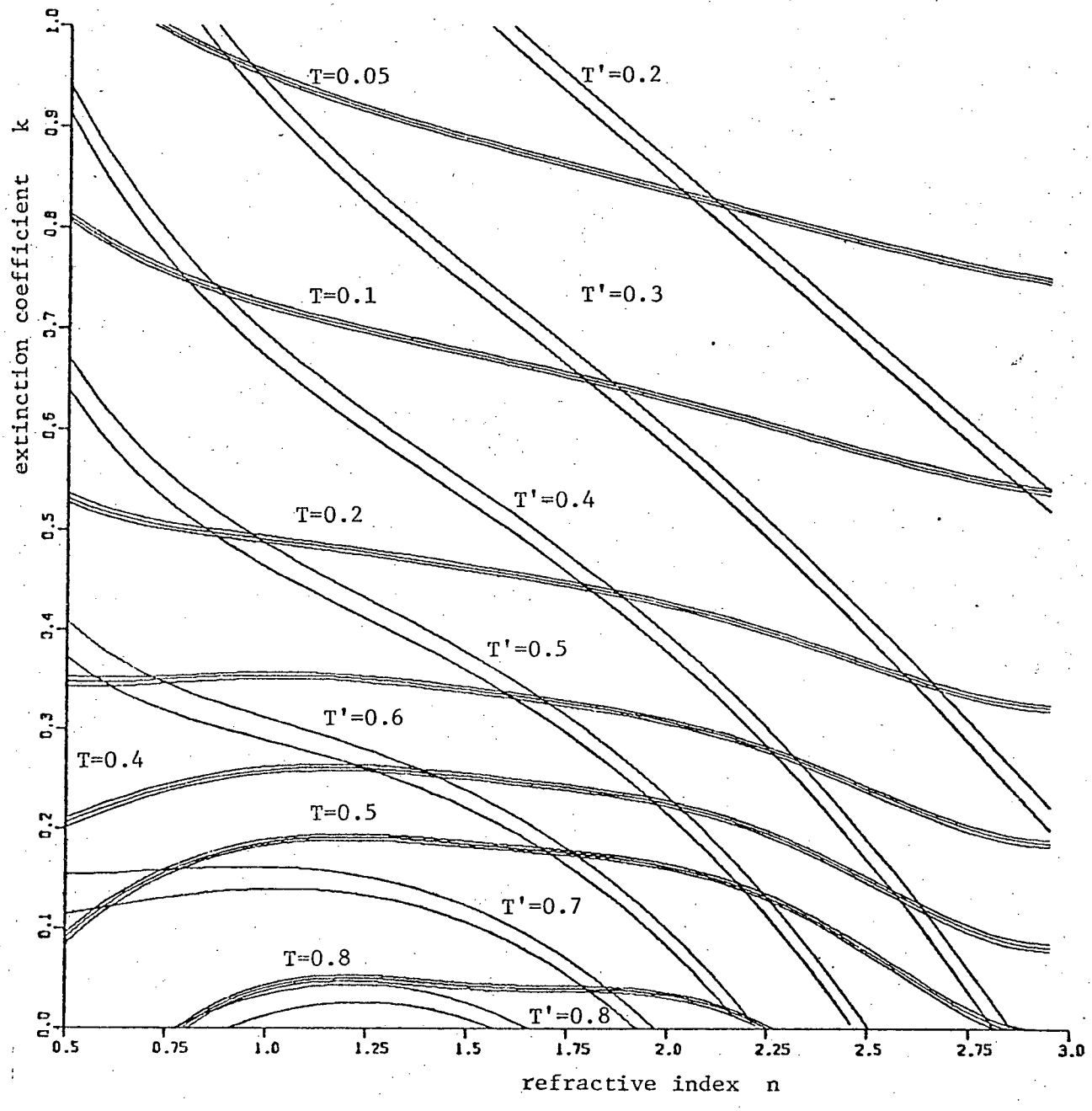

Fig. 5.2 Transmittance curves for two samples of the same material with thicknesses of 1080Å (triple line (T)) and 360Å (double line (T')). The width of the countours represents an experimental error in transmittance measurements of ±1% of their nominal values. Curves were computed for $n_s = 1.5$ and $\lambda = 4000$Å.

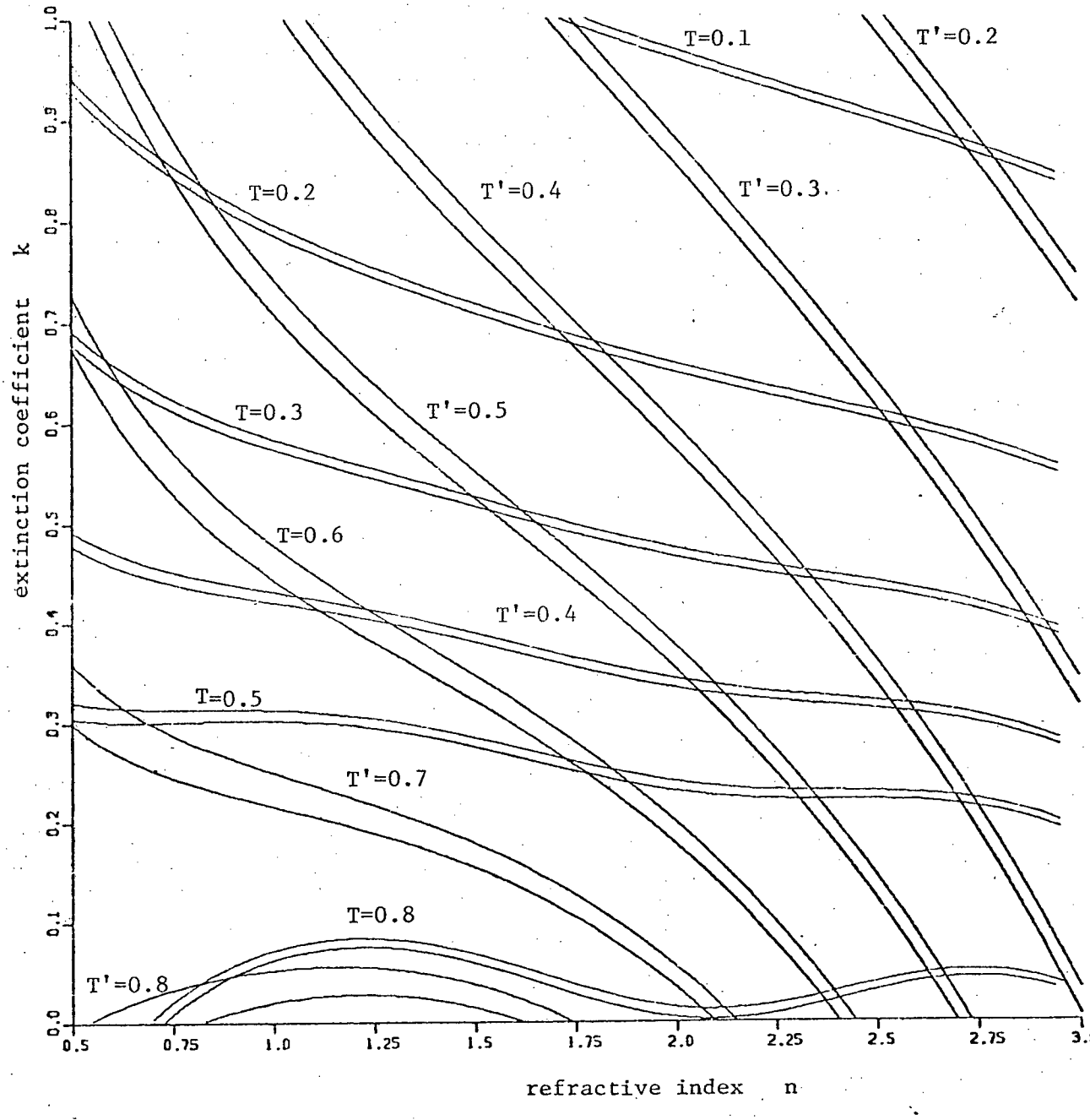

Fig. 5.3 Transmittance curves for a sample with thickness of 1080Å (T) and for a sample with thickness of 360Å (T'). The width of the countours represents an experimental error in transmittance measurements of ±1% of their nominal values. Curves were computed for n_s = 1.5 and λ = 6000Å.

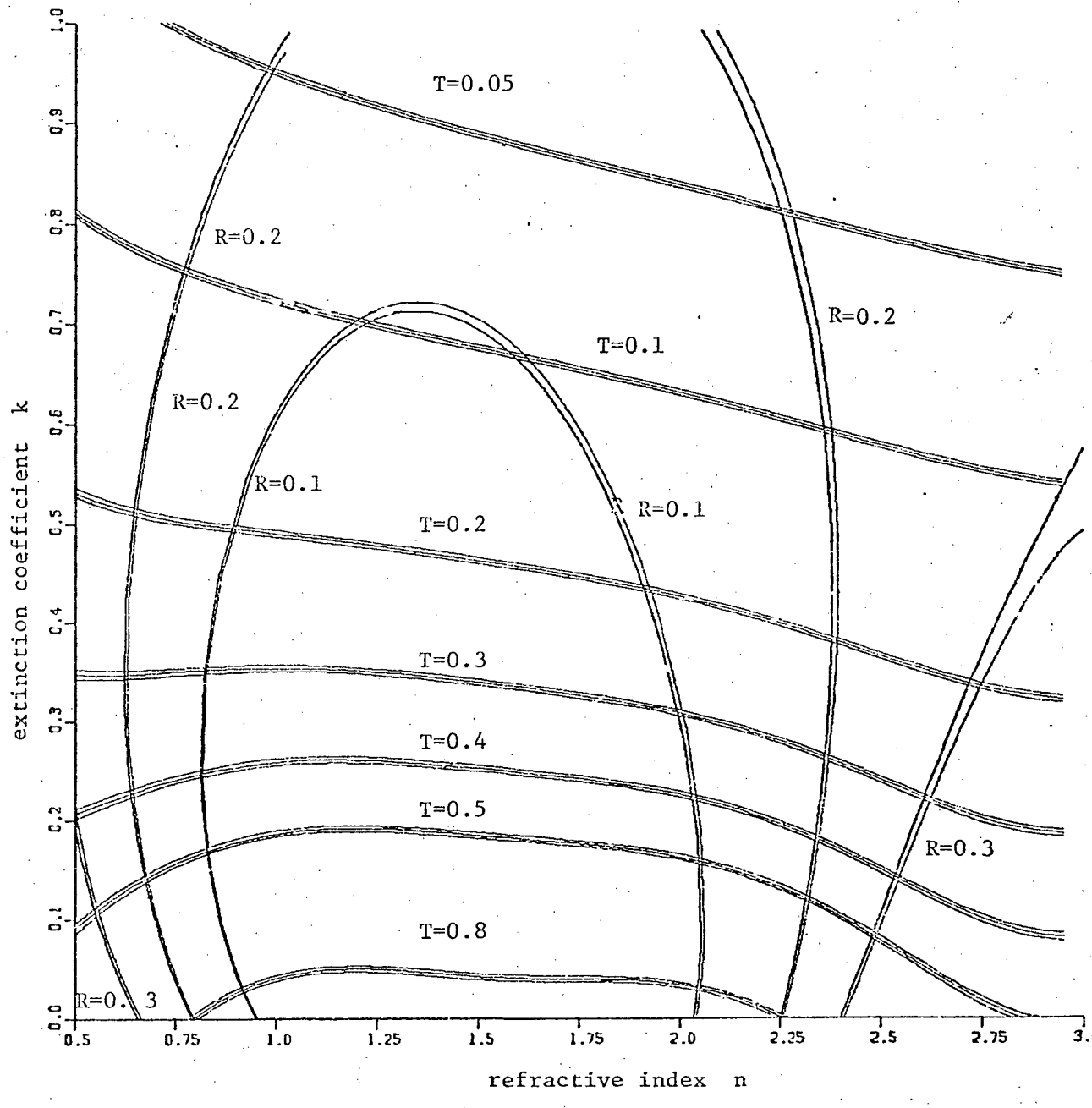

Fig. 5.4 Transmittance and reflectance curves for film with thickness of 1080Å. The countours width indicates an error in transmittance and reflectance measurements ±1% of their nominal values. Curves were computed for n_s = 1.5 and λ = 4000Å.

5.2 TECHNIQUE USED FOR OPTICAL CONSTANTS DETERMINATION

The transmittance T and absolute specular reflectance R from the film side of the copper oxide coated substrates were measured at perpendicular incidence of light using a Cary 14R spectrophotometer* and plotted as a function of wavelength. The data output for reflectance and transmittance were in the form of optical densities, namely

$$T.O.D. = \log I_r/I_T \tag{5.3}$$

$$R.O.D. = \log I_{RO}/I_R \tag{5.4}$$

where T.O.D. was the optical density corresponding to transmittance, R.O.D. the optical density corresponding to the reflectance, I_r the intensity of the light beam incident upon the sample during measurement of transmittance (equal to the intensity of the reference beam), I_T the intensity of the transmitted beam, I_{RO} the intensity of light reflected from a reference aluminium mirror and I_R the intensity of light reflected from the film side of the sample. The transmittance was then calculated from the following relation

$$T = 10^{-T.O.D.} \tag{5.5}$$

and similarly the reflectance was computed from

$$R = RO(\lambda) \times 10^{-R.O.D.} \tag{5.6}$$

where $RO(\lambda)$ was the reflectance of the reference aluminium mirror derived from data supplied by the National Bureau of Standards.

For further data processing the curves obtained from the spectrophotometer measurements were digitized and stored on file. Measurements of film thickness were performed using the M-100 Sloan Angstrometer, as described in chapter 4.1.

Footnote: * These R and T measurements were performed at RCA Labs, Princeton, N.J. by Dr. P. Zanzucchi.

The computation of the optical constants n, k for given R,T,λ values was based on the secant iteration method and utilized the NDINVT routine [103] available from the UBC computing centre. Eqns. (5.1) and (5.2), which give the relationship between n,k, and R,T were used in implicit form. Because n,k are multiple-valued functions of R,T,λ, the particular solution obtained depended on a guess n,k vector requested by the iteration routine. The refractive index n is expected to be a smooth function of wavelength and thus an erroneous solution could often be easily recognized by any discontinuities in n values near some wavelength point. All n,k computations were performed using a conversational terminal, which enabled direct operator control over the selection of a particular solution. The program allowed computation of n,k either continuously for the whole range of wavelength (0.38 - 0.8μm) where R,T was determined, or only for a selected region of this range which could be, when requested, a given single wavelength point. In the case when continuous computation over the whole or a particular region of wavelength was requested, the initial n,k guess vector supplied by the operator was assumed for the first wavelength point only . For the next wavelength point the n,k solution determined for the previous wavelength point was assumed as the n,k guess vector. In the single point run mode an n,k guess vector had to be supplied for each point by the operator.

The following procedure was adopted in the calculation of n,k using the above mentioned program. First for a given n,k guess vector, the values of optical constants were determined for the whole measured wavelength range. If a discontinuity in n occured at a certain wavelength point, the calculation was repeated using a new n,k vector, until all discontinuities were removed. It could also happen that for some wavelength point no solution or at least no physically acceptable solution could be obtained. This could be caused by

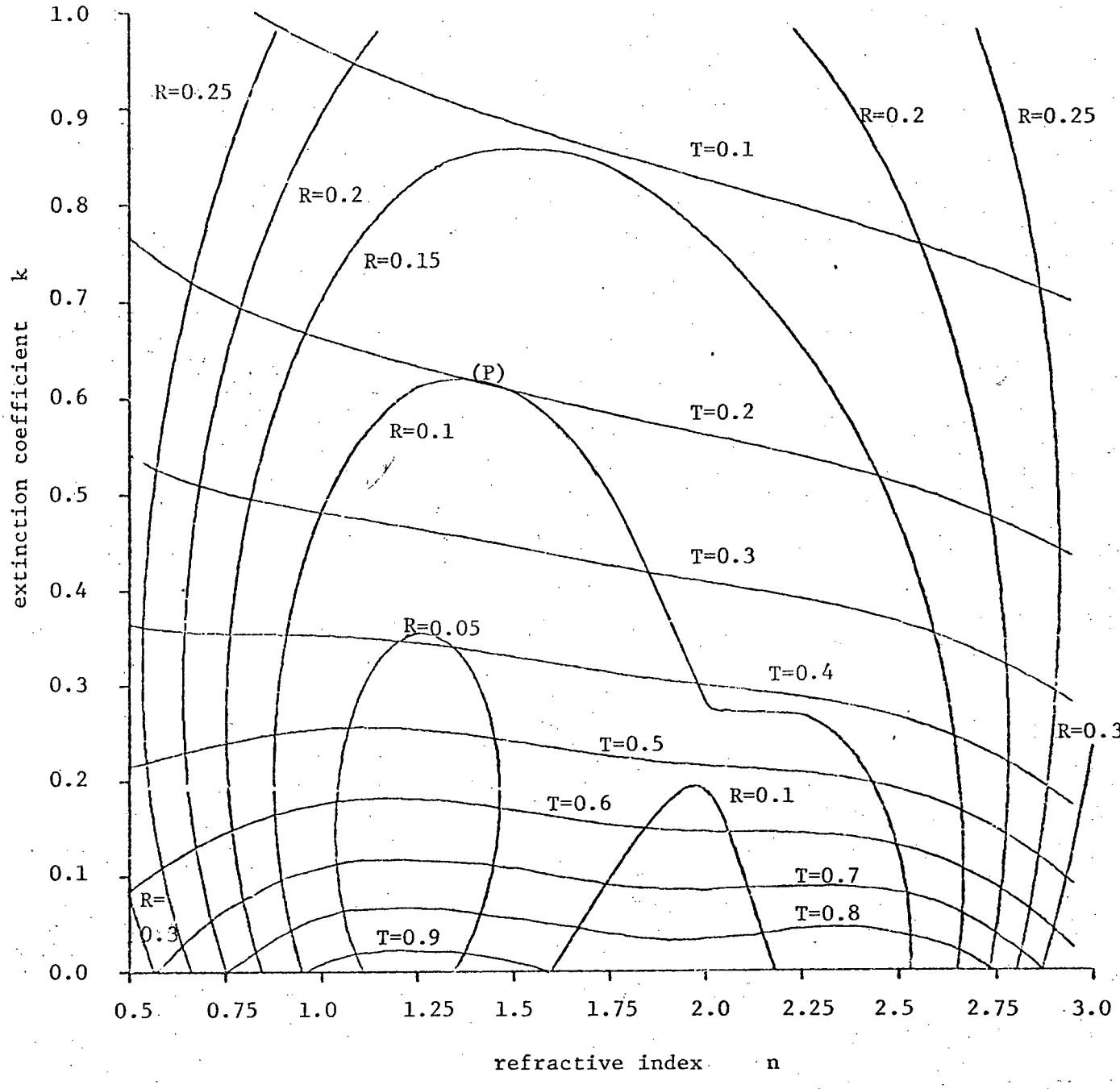

Fig. 5.5 Transmittance and reflectance curves for film with thickness of 1000Å at λ = 5000Å and n_s = 1.5. Note, that in this particular case four different solutions for n,k can be obtained for example, for combination of R = 0.1 and T = 0.6 - 0.8.

a small experimental error in the R,T measurements for which the solution was most probably close to one of the branch points, see for example point P(R = 0.1, T = 0.2) in Fig. 5.5. In such cases a small error in R,T measurements may cause the R,T curves not to intersect and thus no solution for that given R,T combination can be found. Any such points were either removed from the data, or n,k were determined for two neighboring wavelength regions, omitting the point in question. Note that the single point run mode was used to determine n,k for such critical points in order to firmly establish whether a solution for such a point could be found. The program listing including its description is given in Appendix B.

5.3 RESULTS

The absolute R,T data calculated from the measured optical densities and the optical constants determined from this data for various copper oxide films are reported in Figs. 5.6 - 5.13. The descriptions of the experimental conditions at which the particular films were deposited, including some of their related properties are included in their respective captions. All curves were computer-generated and plotted by a Calcomp plotter. Values of absorption coefficient α were calculated from the following relation:

$$\alpha = \frac{4\pi k}{\lambda} \tag{5.7}$$

By comparing Figs. 5.6 (a-b) - 5.11 (a-b), the variation of optical properties with the film compositional character can be clearly seen. The characteristic transmittances for each film phase have been discussed earlier (section 4.3). It can now be appreciated that the reduction in transmittance on going from near-stochiometric Cu_2O films to Cu_2O + Cu films (compare e.g. Figs. 5.6a and 5.9a) is not due to large changes in reflectance but more to an increase in absorptance. Extinction and absorption coefficient values for

Cu_2O + Cu films are thus significantly larger than in Cu_2O films, whereas the real part of the refractive indices are similar (Figs. 5.6b, c and 5.9b, c). There is little change in absorptance as the stochiometry of Cu_2O on the side of copper deficiency is changed (compare Figs. 5.7c, 5.8c and 5.9c) until the nucleation of CuO starts to occur, whereupon the absorptance increases. The optical properties for Cu_2O + CuO films are thus, as expected, intermediate between those of pure Cu_2O and pure CuO (Figs. 5.7, 5.10 and 5.11). The large increase in CuO n-value with increasing wavelength (Fig. 5.11b) has also been reported in thermally-prepared CuO films [46]. Values of n and k for the latter films and the reactively-sputtered CuO films prepared in the present work are very similar.

Published data on optical properties of copper oxide films is very meagre. Wieder and Czanderna [46] have made some measurements on CuO (quoted above) and on thermally-prepared $CuO_{0.67}$ which is a gross defect structure of Cu_2O. Values of k reported for the $CuO_{0.67}$ films are similar to those found to obtain in the present reactively-sputtered Cu_2O + CuO films. As regards other work on copper oxides Pastrnak [98] has given n-values for bulk Cu_2O material out to a wavelength of 12μm, but the detail in the range of interest in the present work (0.4 - 0.8μm) is only sufficient to say that n is about 2.7 for bulk Cu_2O material [46]. This value is approached in the present films towards the higher wavelength end of the range covered. Around 0.48μm a peak in n-value ($n \approx 3.36$) was observed which appears to be characteristic of the presence of Cu_2O irrespective of whether Cu, CuO or copper ion vacancies are also present (Figs. 5.7b, 5.8b and 5.9b). Values of α for bulk Cu_2O have been reported by Pastrnyak [99] and from these k values have been deduced [46]. The reported data bear little resemblence to the present results, as is perhaps to be expected [91] from the fact that one set of data is for bulk

material and one for very thin films. Nevertheless the absorption coefficient data for the present films indicates a band gap value (see Fig. 5.13) which falls within the range of values of 1.94 - 2.14 generally accepted for bulk Cu_2O [35, 74, 99]. The appearance of exciton peaks in the absorption spectrum, which is apparently common in bulk samples [99, 100, 101], was not observed with the present film samples at room temperature. For unspecified "Cu_2O films" Wieder and Czanderna [46] were also not able to identify definite exciton peaks. There is however some structure at long wavelengths in the values of absorption coefficient for the three Cu_2O films shown in Fig. 5.13. The correspondence between increased absorption and conductivity suggests the presence of either free carrier absorption or significant absorption by copper ion vacancies. The latter has been postulated [46] as responsible for the high k values in the $CuO_{0.67}$ material discussed above. In the present case it would appear that the broad dispersion shown by the high conductivity samples can be attributed to the free carrier absorption. However in the case of the near-stochiometric Cu_2O sample of resistivity 892 ohm cm (for which the free carrier absorption would certainly be less than in the other two samples) there is evidence (Figs. 5.9c and 5.13) of an additional absorption "shoulder" close to the absorption edge. The threshold energy for this shoulder is lower than the bandgap by about 0.2 eV, suggesting the possibility of a transition between an ionized acceptor level (copper ion vacancy) and the conduction band. This value of ionization energy correlates well with the range of thermal activation energies for conductivity as reported in section 4.5.

(a) Wavelength dependence of the transmittance and reflectance.

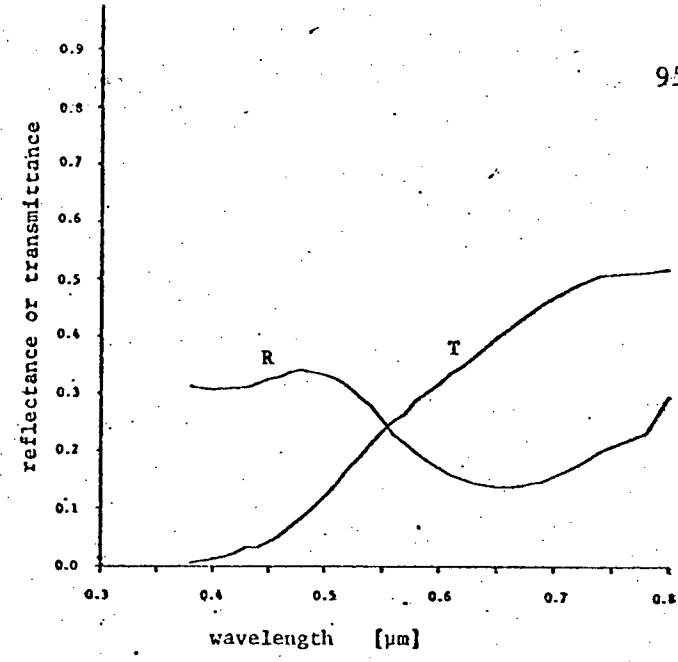

(b) Wavelength dependence of the refractive index n and the extinction coefficient k.

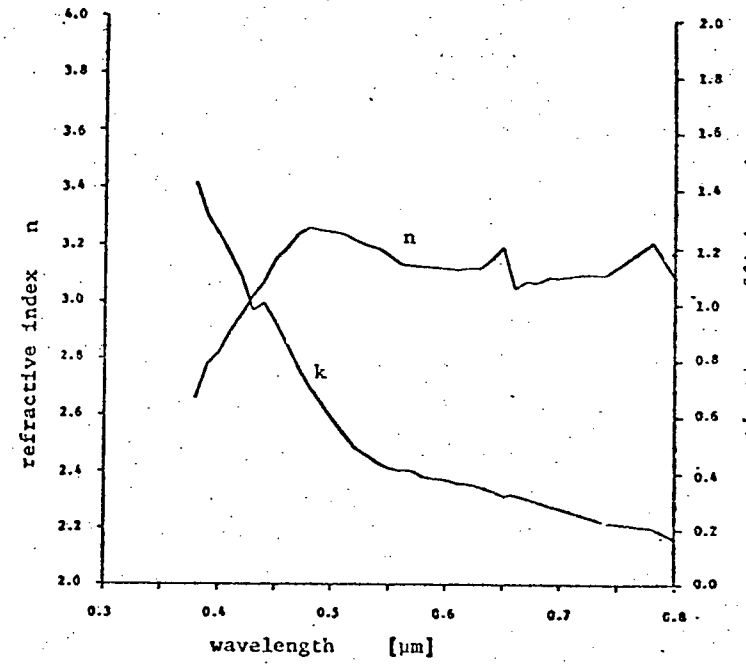

(c) Depenedence of the absorption coefficient α on the incident photon energy.

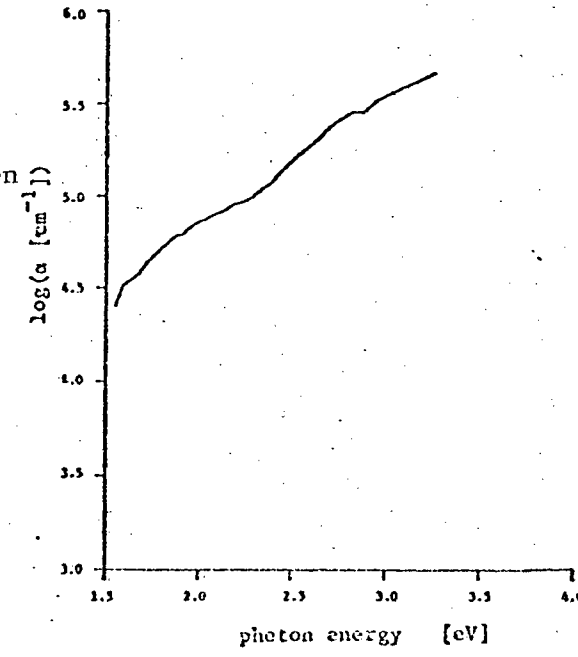

Fig. 5.6 Optical properties of Cu_2O+Cu 1030Å thick film deposited on Suprasil 2 substrate at 200W of r.f. power and .32 mTorr of oxygen.

(a) Wavelength dependence of the transmittance and reflectance.

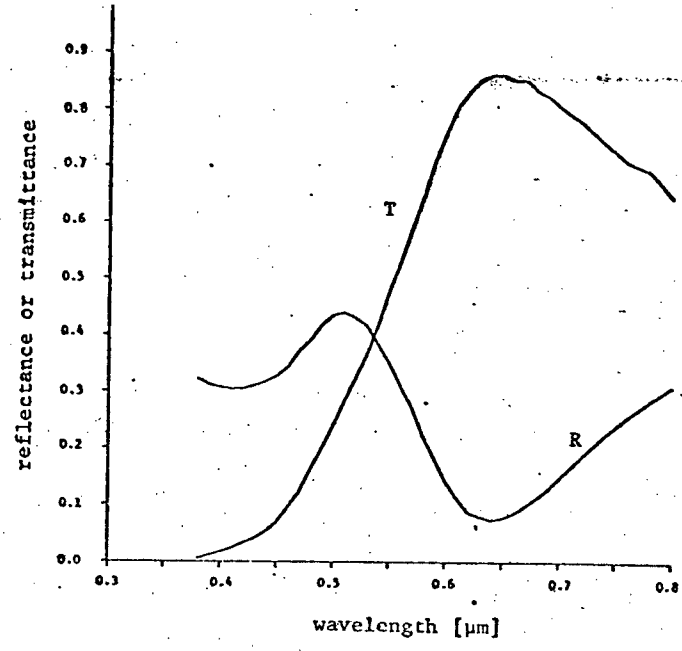

(b) Wavelength dependence of the refractive index n and the extinction coefficient k.

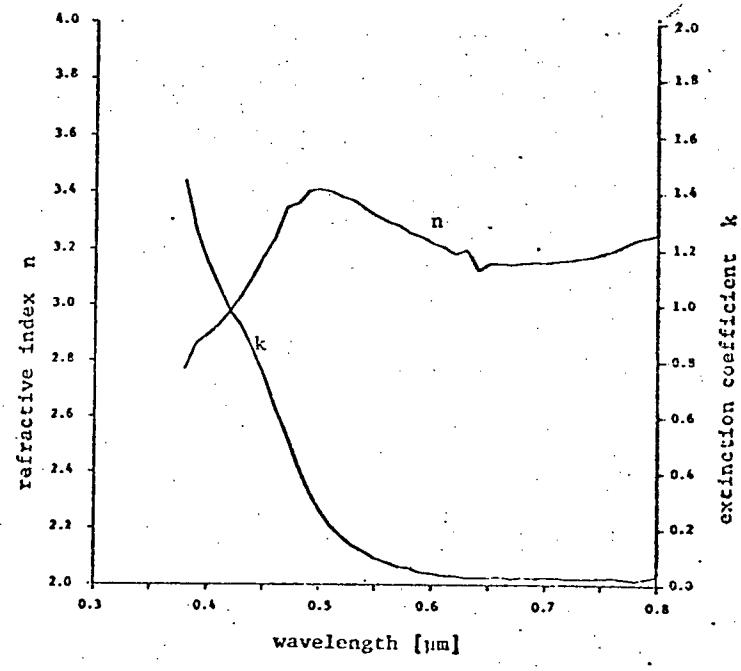

(c) Dependence of the absorption coefficient α on the photon energy of incident light.

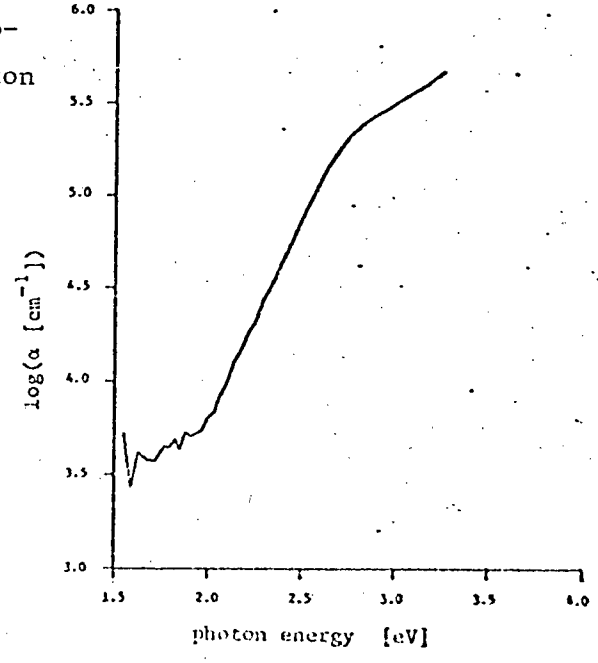

Fig.5.7 Optical properties of the Cu_2O 1010Å thick film deposited on Suprasil 2 substrate at 200W of r.f. power and .36 mTorr of oxygen. The film resistivity ρ = 91 ohm cm.

(a) Wavelength dependence of the transmittance and reflectance.

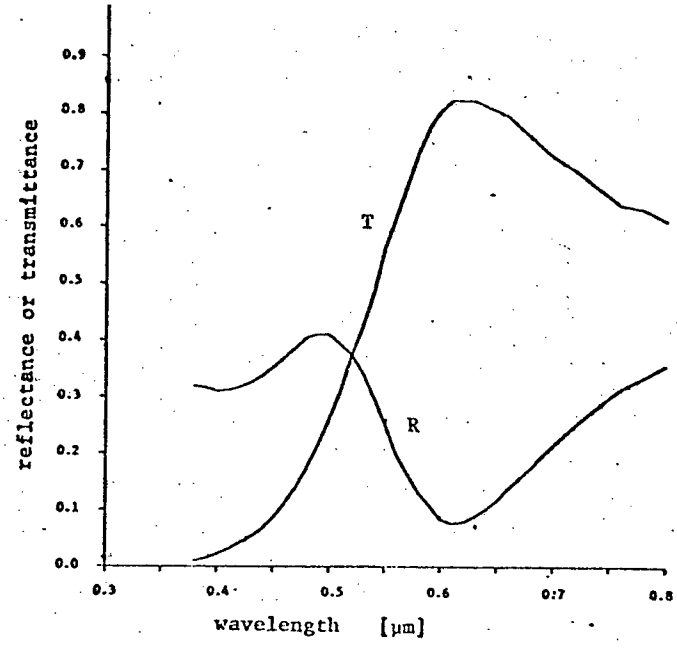

(b) Wavelength dependence of the refractive index n and the extinction coefficient k.

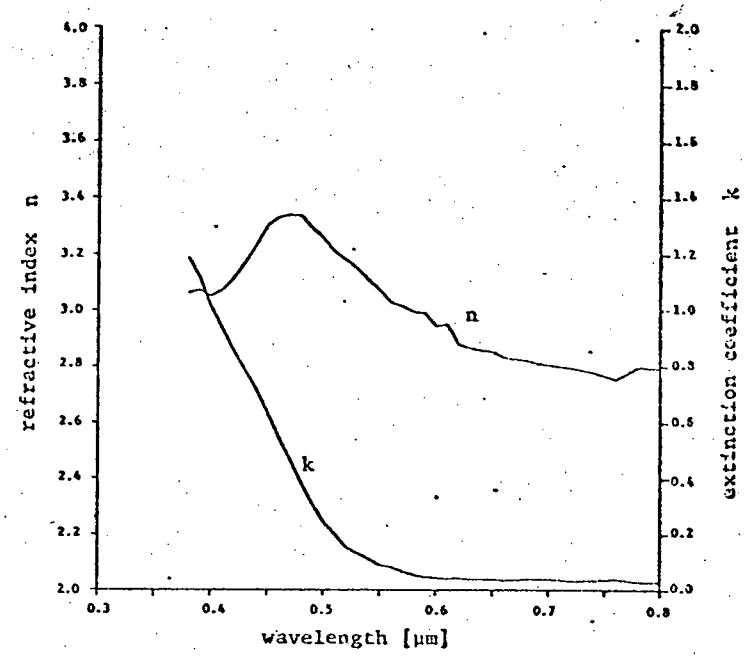

(c) Dependence of the absorption coefficient α on the photon energy of incident light.

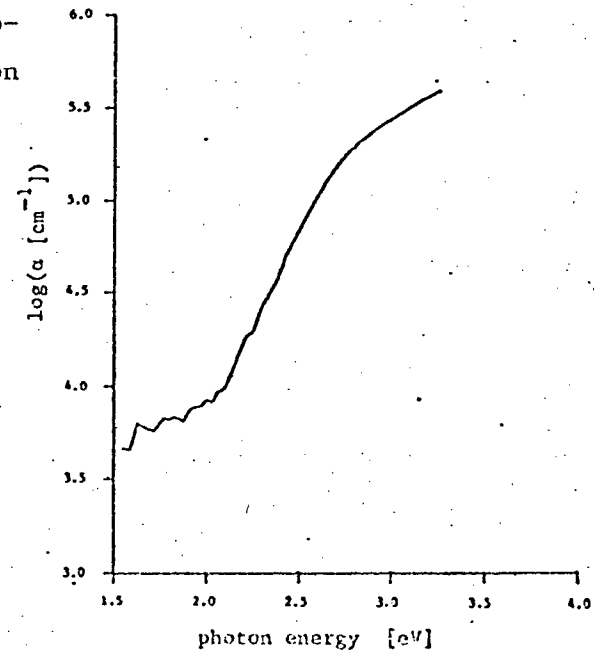

Fig.5.8 Optical properties of the Cu_2O 1050Å thick film deposited on the Suprasil 2 substrate at 200W of r.f. power and .4 mTorr of oxygen. The film resistivity ρ = 48 ohm cm.

(a) Wavelength dependence of the transmittance and reflectance.

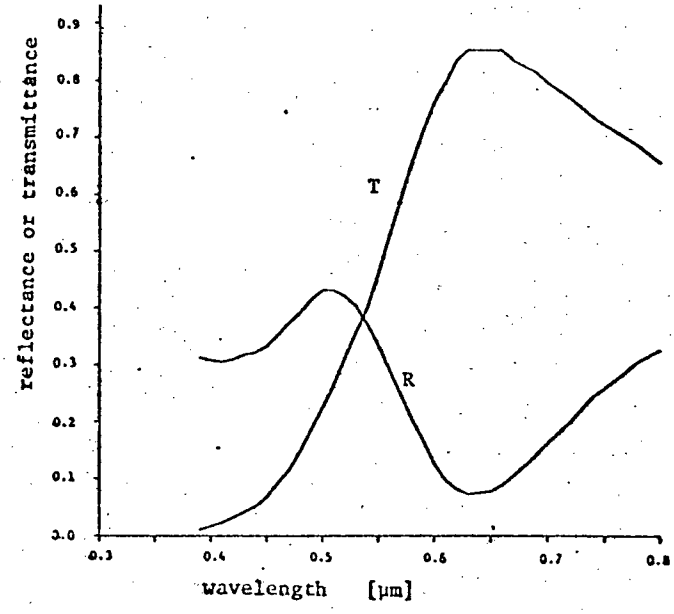

(b) Wavelength dependence of the refractive index n and the extinction coefficient k.

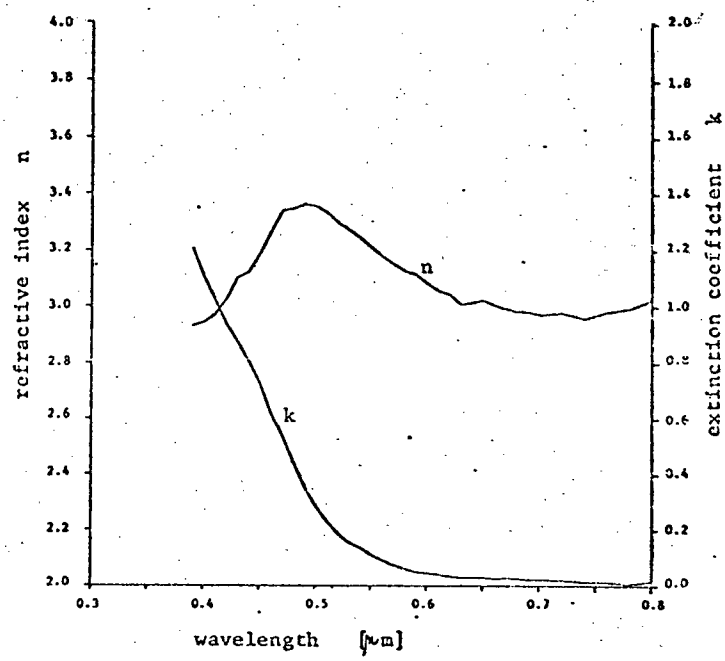

(c) Dependence of the absorption coefficient α on the photon energy of incident light.

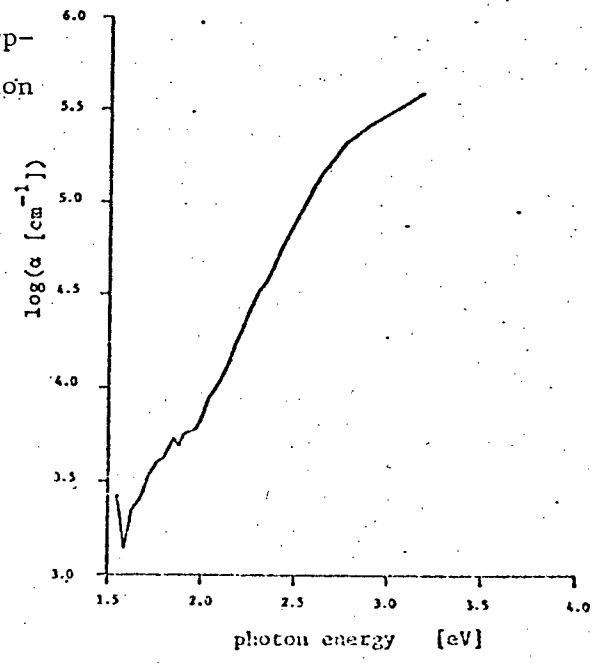

Fig. 5.9 Optical properties of the Cu_2O 1050Å thick film deposited on the Suprasil 2 substrate at 200W of r.f. power and .35 mTorr of oxygen. The film resistivity ρ = 892 ohm cm.

(a) Wavelength dependence of the transmittance and reflectance.

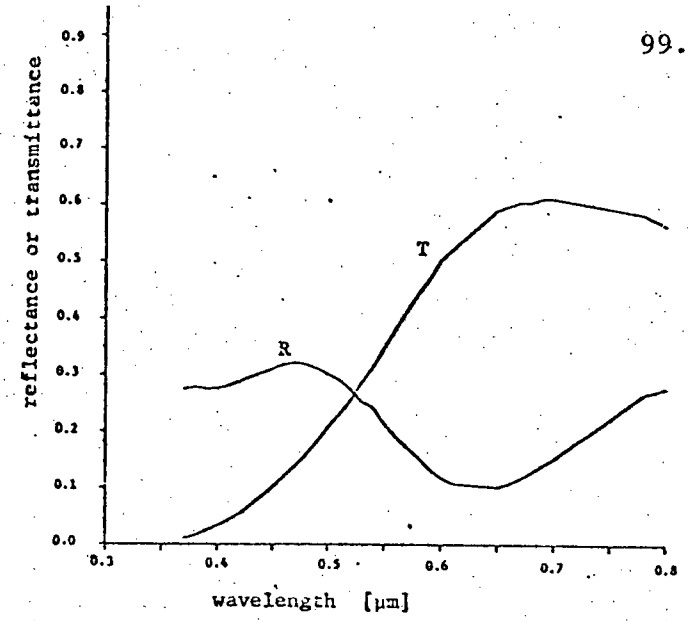

(b) Wavelength dependence of the refractive index n and the extinction coefficient k.

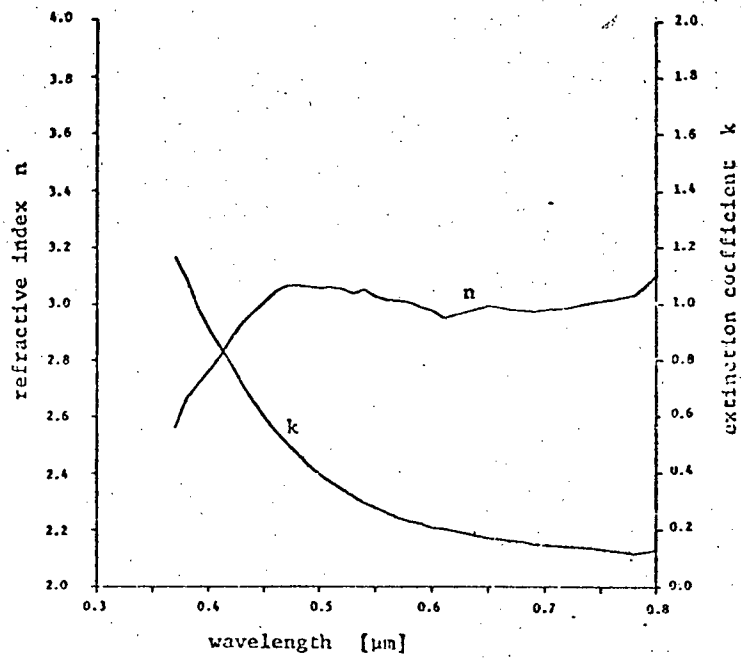

(c) Dependence of the absorption coefficient α on the photon energy of incident light.

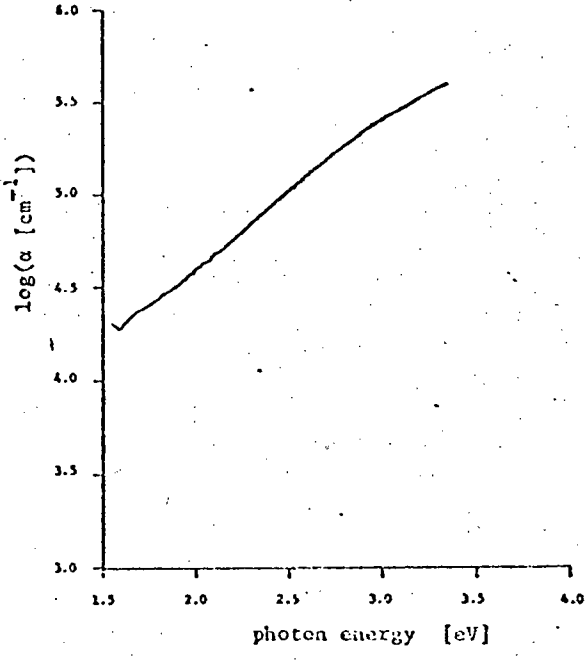

Fig. 5.10 Optical properties of Cu_2O+CuO 1050Å thick film deposited on the Suprasil 2 substrate at 200W of r.f. power and .7 mTorr of oxygen.

(a) Wavelength dependence of the transmittance and reflectance.

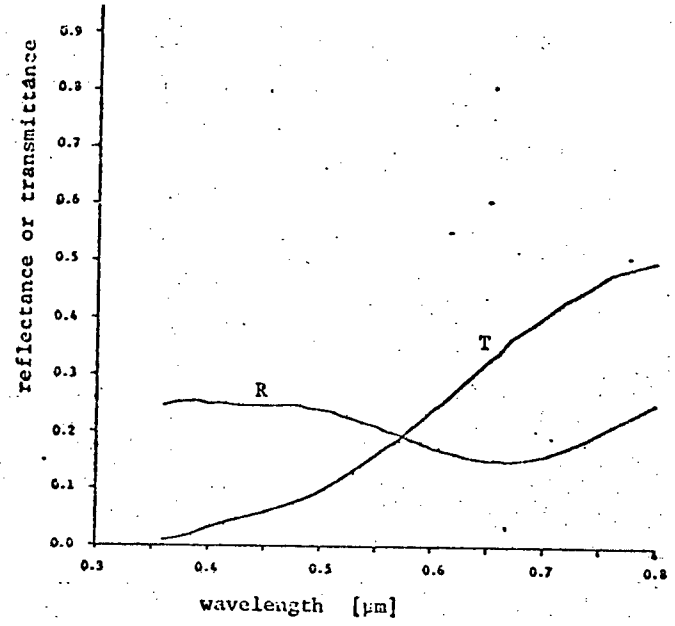

(b) Wavelength dependence of refractive index n and extinction coefficient k.

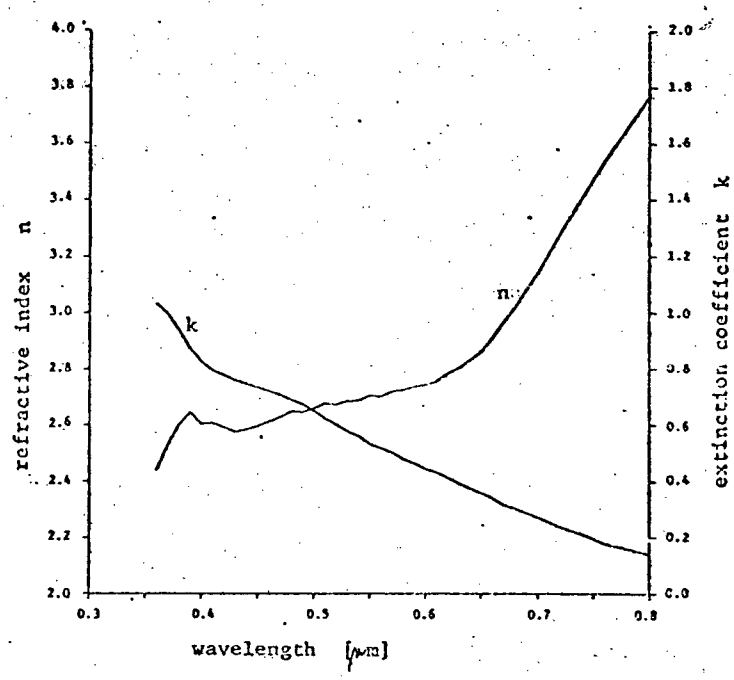

(c) Dependence of the absorption coefficient α on the incident photon energy.

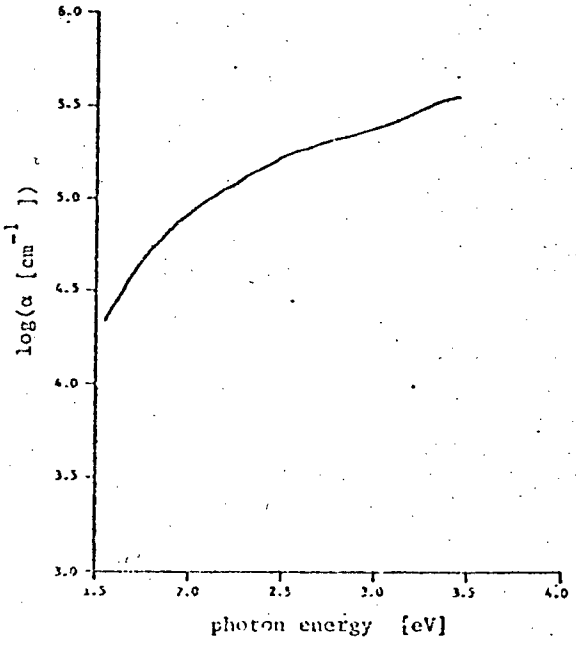

Fig. 5.11 Optical properties of CuO 1200Å thick film deposited at 200W of r.f. power and 6. mTorr of oxygen.

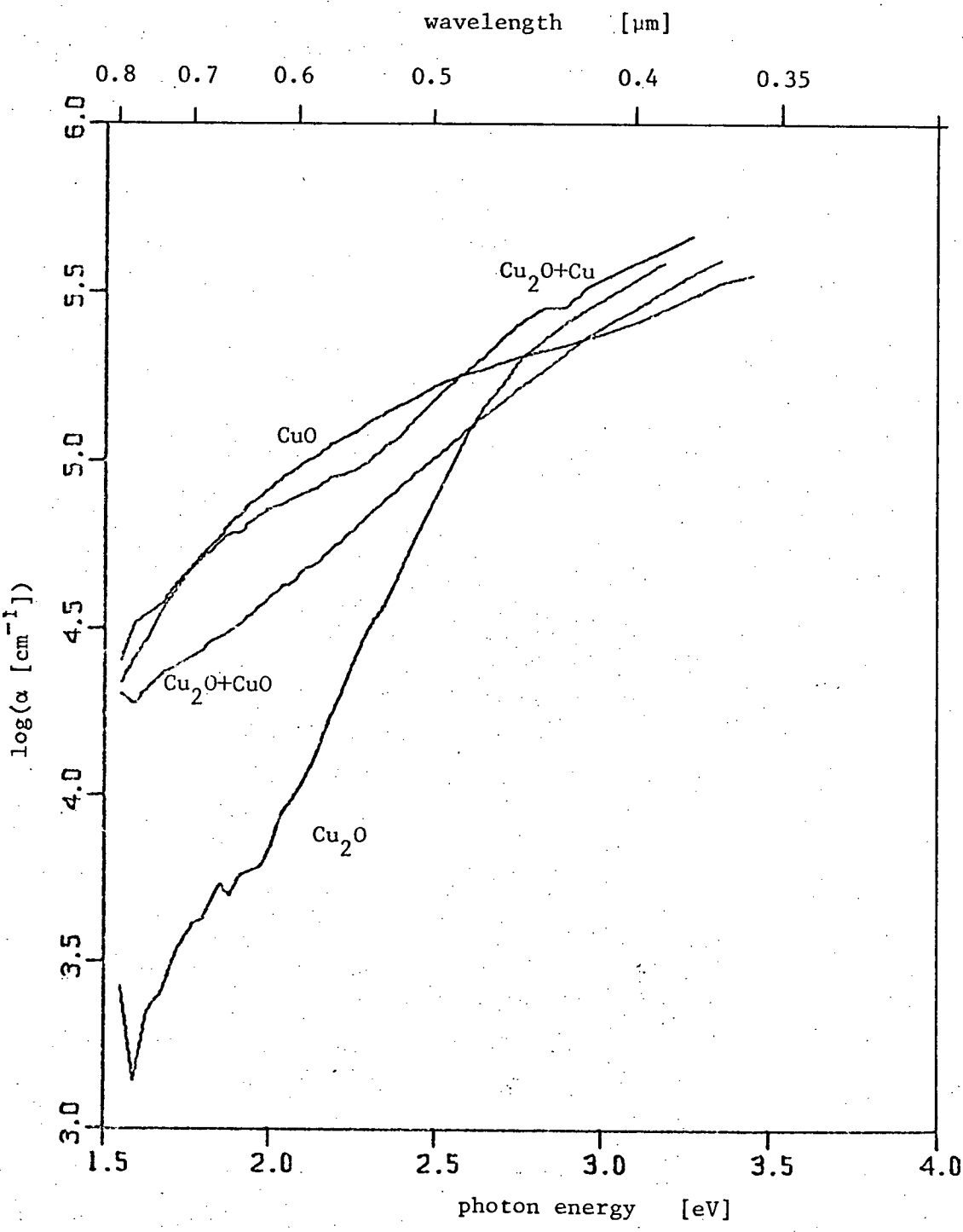

Fig. 5.12 Dependence of the absorption coefficient α on the incident photon energy for various copper oxide films.

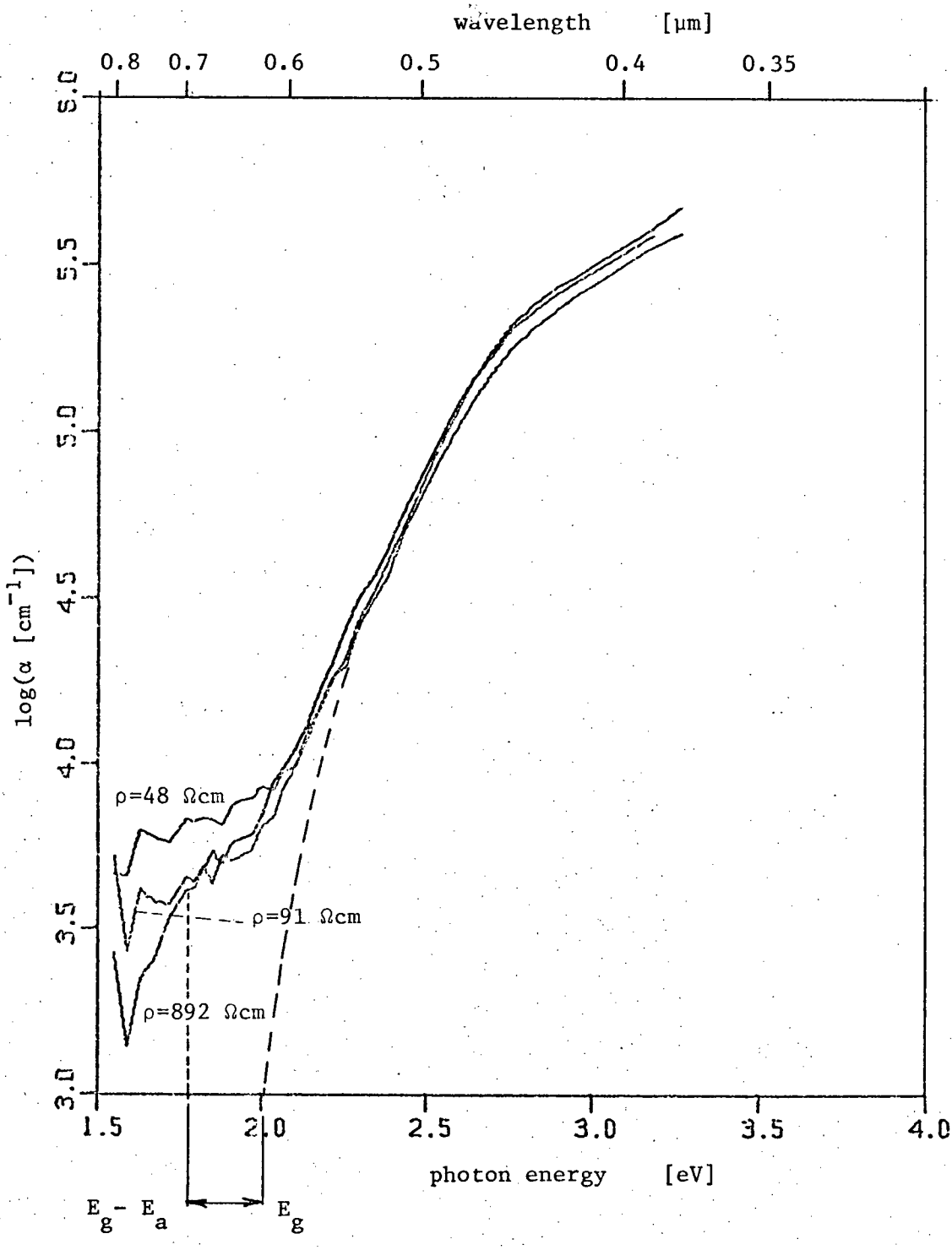

Fig. 5.13 Dependence of the absorption coefficient α on the photon energy of incident light for cuprous oxide films of different resistivities.

6. COPPER OXIDE/SILICON HETEROJUNCTION DIODES

6.1 INTRODUCTION

As mentioned in chapter 1, one of the attractions of copper oxide films is their potential suitability to large, thin film photovoltaic converters. As a first investigation of this possibility a fabrication procedure for Cu_2O/Si solar cells was developed and the photovoltaic properties of these diodes were investigated. This work is described later in this chapter, following a brief review of heterojunction solar cells based on silicon.

Heterojunction solar cells have very interesting optical, electrical and technological properties, which make these cells attractive for possible use in terrestrial photovoltaic power generation. In some cases heterojunction cells can be superior to classical homojunction cells. In a conventional homojunction solar cell photons, with an energy equal to or only slightly higher than the bandgap energy of the solar cell semiconductor, are mostly absorbed deeply within the semiconductor, especially if the semiconductor has an indirect bandgap. Electron-hole pairs created deeply within the semiconductor (therefore far from the collecting junction) have a large chance of recombining before they can be separated by a p-n junction. Photons with energy much higher than the bandgap energy of the semiconductor are absorbed very close to the surface of the solar cell, especially in the cases when the semiconductor has a direct bandgap nature. If the surface recombination velocity at the surface is very high, most of these

photogenerated electron-hole pairs will recombine, rather than diffuse towards the p-n junction, where they could be otherwise collected. This results in collection losses. By employment of a heterojunction cell structure, providing the semiconductor facing the radiation has a larger bandgap than the base semiconductor and that the heterojunction-interface recombination velocity is sufficiently low, this problem can be efficiently overcome. The higher energy bandgap semiconductor (the "window") clearly needs to have a lower absorption coefficient than the base semiconductor. As a result, in the heterojunction cell, high energy photons are absorbed at a larger distance from the surface of the cell than in the comparable p-n homojunction cell. Electron-hole pairs contributed from high energy photons thus have, in the heterojunction cell, less chance to recombine at the surface than in a comparable p-n homojunction cell. This can result in an improved short wavelength response of a heterojunction cell, compared to a homojunction cell [33,34].

The cost of forming a homojunction by diffusion or epitaxial processes forms a substantial portion of the solar cell fabrication cost. On the other hand a heterojunction can often be formed by employing low cost processing, such as sputtering, evaporation, pyrolitic spraying, etc., and this is another motivation for investigating heterojunction solar cell technology. There are also cases where the formation of a heterojunction is essential, because nowadays, when looking for low cost solar cell semiconductors, many of them are available in only one type of conductivity, so making formation of a p-n homojunction in this case impossible. There are four basic groups of heterojunction solar cells, namely

1. Abrupt heterojunction cells
2. Heteroface solar cells

3. Graded bandgap solar cells
4. Metal-Semiconductor (MS) and Metal-Insulator-Semiconductor (MIS) solar cells

In an abrupt heterojunction solar cell the rectifying junction is formed between the window semiconductor and a base semiconductor of, usually, opposite conductivity type from the window semiconductor. The heteroface solar cell [50] is basically a p-n homojunction cell having a layer of a larger bandgap semiconductor on its top, and it is usually arranged that the two top semiconductors have the same type of conductivity. The graded bandgap cell [51] is similar to the abrupt solar cell, except that the window semiconductor has a band gap which increases towards the surface of the solar cell. Such a built-in field helps in the collection of carriers photogenerated in the larger band gap semiconductor. In an MS solar cell [52] a suitable semitransparent metal film, usually deposited on top of the semiconductor by vacuum evaporation, forms a barrier (so called Schottky barrier) with rectifying properties. The induced energy band bending at the surface of the semiconductor results in a built-in field which separates majority and minority carriers. The MIS structure differs from the MS structure in that a thin interfacial insulating layer is grown, either naturally or deliberately, between the metal and the semiconductor. This interfacial layer, if optimally designed, can greatly improve performance of the cell [53].

Because in heterojunction(HJ)solar cells most of the photons are absorbed in the smaller bandgap material, the latter should have a bandgap in the range from 1.1 - 1.9 eV [54] to achieve a high efficiency solar cell. The larger bandgap semiconductor should have an energy bandgap as large as possible, so that it absorbs a minimum number of photons. The lattice

constants and the thermal expansion coefficients of both heterojunction partners should be nearly equal and the electron affinities compatible, so that resulting discontinuities in energy bands will have a minimal effect on the collection efficiency of a cell. The window semiconductor should have a low resistivity and an optical refractive index in a suitable range, so as to serve as an antireflection coating for the lower bandgap semiconductor.

It has been found recently that certain oxide semiconductors, namely SnO_2 [55], In_2O_3[56], their mixture ITO [57-59] and Cd_2SnO_4 [60] show promise as suitable window semiconductor materials for heterojunction or heteroface solar cells using Si as the base material. Interest in these materials arose because of their combination of low resistivity, high AM1 solar transmittivity and high thermal infrared reflectance [61]. The refractive indices of these oxides are in the range of 1.9 - 2.0 [11], and thus are able to perform as an antireflection coating on Si [57,58,62], or other semiconductors. The highest oxide semiconductor-semiconductor (OSO) solar cell efficiencies that have been reported to the present date are 9.9% for SnO_2/nSi cells [55], where the SnO_2 was deposited on Si by electron beam evaporation, 12% from an ITO/pSi cell [57], where the ITO was deposited on Si by neutral beam sputtering, and 10% for ITO/nSi [58], where ITO was deposited on Si by a pyrolitic spraying method. All highly conductive SnO_2, In_2O_3 and ITO materials are degenerate semiconductors and thus OSO solar cells employing any of the above oxide semiconductors cannot be unequivocally classified in any of the four groups as defined at the beginning of this chapter. Recently, Schewchun, DuBow, Myszkowski and Singh [102] proposed to describe the properties of the above-mentioned heterojunction structures in terms of a degenerate semiconductor-insulator-semiconductor structure (SIS),

which, in principle, is very similar to the MIS configuration. They have shown that the maximum efficiency of ITO/pSi calls could reach 19.9% under AMI illumination.

Turning now to the relevance of Cu_2O to solar cells it is noted that the bandgap of Cu_2O is 2.04 eV and is direct, thus suggesting use of Cu_2O either as a window material in a heterojunction structure with lower bandgap semiconductor partners, or as an absorbing semiconductor component for thin film solar cells. Even in the latter case the formation of a heterojunction structure is necessary, because Cu_2O at the present time is available only with p-type conductivity. Cells based on Cu_2O as the absorbing component have been fabricated from thermally-grown Cu_2O and have utilized the rectifying nature of the Cu/Cu_2O contact to obtain weak photovoltaic performance (η = 1% [3,4,6,9]). However it seems clear that to fully implement a suitable heterojunction technology a deposition method, rather than a "grown-method" is required. A deposition technique able to produce Cu_2O with properties potentially acceptable from the standpoint of photovoltaic application [27,90] has been developed based on the reactive sputtering procedures and theory described elsewhere in this thesis. Cu_2O produced by this technique exhibits desirably low resistivities (20-60 ohm-cm) and potentially suitable optical absorption properties (chapter 5). There is however little known about other Cu_2O properties which can affect heterojunction performance, namely electron affinity, thermal expansion coefficient and lattice match with other heterojunction partners. In the present work Si was used as the partner semiconductor with Cu_2O, mainly for the reason that Si is a well defined, abundant material, with desirable low bandgap and well-established processing technology. In the next section experiments and results obtained with the Cu_2O/Si structure are presented.

6.2 WAFER PREPARATION

The silicon substrates used were polished on the front side and were either n-type ([111], 2 ohm-cm) or p-type ([100], 2-8 ohm-cm). In all cases the preparation process was as follows:

i. PREFURNACE CLEANING

1. Immerse the sample for 10 minutes in a freshly prepared solution of H_2O : H_2O_2 : NH_4OH in the ratio of 5: 1: 1 : by volume held at 75-85°C. The solution was prepared by adding NH_4OH and H_2O_2 to boiling deionized water.
2. Rinse in a deionized water cascade, 2 minutes (first bath) and 8 minutes (second bath)
3. Dip in solution of D.I. H_2O : HF in the ratio of 9: 1 by volume for 30 sec.
4. Repeat step 2 rinses.
5. Immerse for 10 minutes in a freshly prepared solution of D.I. H_2O : H_2O_2 : HCl in the ratios of 6 : 1 : 1 by volume held at 75-85°C. The solution was prepared by adding HCl and H_2O_2 into boiling D.I. water.
6. Repeat step 2.
7. Dip in isopropyl or methyl alcohol for 5 minutes.
8. Dry in freon vapor for 2-3 minutes.

ii. WAFER OXIDATION

After cleaning, the Si wafer was oxidized at 1100 °C using a wet oxidation process to obtain a layer of SiO_2 of thickness approximately 6000 Å.

The following oxidation cycle was used:

1. 5 minutes in O_2 (1.0 l/min)
2. 2 hours in H_2 (1.6 l/min) + O_2 (1.0 l/min)
3. 30 minutes in N_2 (1.0 l/min)

iii. BACK SIDE OXIDE STRIPPING

The purpose of this step was to prepare the wafer for the back contact doping procedure and it included:

1. Application of Waycoat Positive LSI photoresist at 4500 rpm on the front side of the wafer, followed by a 1 minute dip in Waycoat Positive LSI developer, a 60 sec. rinse in D.I. water and then blowing dry in nitrogen.
2. Baking the sample in a convection oven for 30 minutes at 120°C.
3. Removal of the back side oxide in a 6:1 solution by volume of NH_4F stock and HF. The NH_4F stock was a 40% by weight solution of NH_4F in D.I. water.
4. Removal of the photoresist in boiling acetone. This procedure was repeated twice, always with new acetone.

iv. PREFURNACE CLEANING

(Same procedure as described in step i).

v. PREDEPOSITION

Here it is necessary to distinguish between the processes used for p-type and n-type wafers.

N^+ predeposition for back side ohmic contact to n-type wafers

(Furnace temperature = 965°C)

1. Predoping of the predeposition tube and the predoposition boat for 20 minutes in N_2 (2.0 l/min) + O_2 (60 cc/min) + $POCl_3$ (15°C) driven by N_2 (60 cc/min).

v. PREDEPOSITION (cont'd)

2. Inserting the samples into the predeposition tube.

3. 10 minute cycle in N_2 (2.0 1/min) + O_2 (60 cc. min)

4. 55 minutes exposure to the same gas flow rates as in step 1.

5. 5 minute exposure to the same gas flow rates as in step 3.

$\underline{P}^+$ predeposition for back side ohmic contact to p-type wafers (Furnace temperature = 1090°C)

1. 10 minutes in N_2 (2.0 1/min)

2. 5 minutes in N_2 (2.0 1/min) + dopant (B_2O_3 in methanol and some HCl kept at 15°C) driven by N_2 (60 cc/min).

3. 15 minutes in N_2 (2.0 1/min)

vi. DEGLAZING

$\underline{N}^+$ - 1 minute etch in a 10 : 1 solution of D.I. H_2O and HF, followed by D.I. water rinsing and blowing dry in nitrogen.

$\underline{P}^+$ - 20 sec. etch in a 1: 1 solution of D. I H_2O and HF, followed by D.I. water rinsing and blowing dry in nitrogen.

vii. DIFFUSION

$\underline{N}^+$ - Furnace temperature was 1090°C and the timing used was as follows:

1. 5 minutes in O_2 (1.5 1/min)

2. 50 minutes in O_2 (1.5 1/min) + H_2 (2.4 1/min)

3. 5 minutes in O_2 (1.5 1/min)

$\underline{P}^+$ - Furnace temperature was 1090°C and timing used was as follows:

1. 5 minutes in O_2 (1.5 1/min)

2. 2 hours in O_2 + HCl (60 cc/min)

DIFFUSION (cont'd)

3. 30 minutes in O_2 + HCl + H_2 (2.4 l/min)
4. 5 minutes in O_2

viii. OPENING THE DIODE WINDOWS ON THE WAFER FRONT SIDE

In this step the oxide was stripped from the back side of the wafer and, simultaneously, windows of 4.7 mm diameter were opened photolithographically in the oxide covering the front Si surface. The following steps were necessary:

1. Application of Waycoat Positive LSI 295 photoresist at 4500 rpm.
2. Prebaking the samples at 90°C for 30 minutes.
3. Exposure by an ultraviolet light source for 2 minutes through the mask shown in Fig. 6.5.
4. Developing in Waycoat Positive LSI Developer, diluted 1 : 1 with D.I. water, for 90 seconds, followed by D.I. water rinse for 60 sec. and blowing dry in nitrogen.
5. Postbaking the samples at 120°C for 30 minutes
6. Removal of unmasked Si_2O in solution of 6 :1 by volume NH_4F stock and HF.
7. 2 and 8 minutes D.I. water cascade rinses.
8. Blowing dry in nitrogen.
9. Removing the photoresist in boiling acetone.
10. Deposition of a $\sim$ 2000 Å thick gold film on the back side of the wafer by vacuum evaporation.
11. Alloying the contact at 500°C for 20 minutes in a nitrogen atmosphere.
12. Scribing and breaking the wafers into quarters.

The above procedure produced samples with an ohmic back contact and a front side comprising eight 4.7 mm diameter circles of exposed Si, isolated from each other by $\sim$ 6000 Å of SiO_2. Cu_2O deposition and subsequent diode fabrication is described in the next section.

6.3 Cu_2O/Si HETEROJUNCTION PREPARATION.

Prior to Cu_2O deposition each sample (silicon wafer quarter) was immersed in 10% HF for 10 seconds, rinsed thoroughly in deionized water (2 minute and 8 minute D.I. water cascade rinses), blown dry in nitrogen and then contacted to the substrate table sample holder (see Fig. 6.1) using gallium as a bonding material. The sample bonding was a very straightforward procedure. The substrate table sample holder was removed from the substrate table (Fig. 3.4) and heated by a plate heater to a temperature of approximately $50^{o}C$. Then the wafer was placed in the inlay of the substrate table sample holder which was filled with gallium. Areas for Cu_2O deposition (6.5 mm diameter, centred on the oxide windows) were defined by a metal mask (Fig. 6.3) which was pressed down on the sample by three steel spring clips, (see Fig. 6.2). Thus an intimate contact of the mask and the sample was ensured, avoiding excess shadowing at the mask edges. The substrate table sample holder was then inserted into the substrate table and the sputtering chamber was evacuated to a vacuum of better than $5x10^{-7}$ Torr. Then sputtering at the desired r.f. power level was carried out such as to produce Cu_2O films $\sim$ 1500 Å thick and of resistivity $\sim$ 50 ohm cm. This combination of Cu_2O and Si exhibited a black appearance, suggesting that this particular structure had good anti-reflection properties. Finally, in another vacuum system, gold was evaporated through another metal mask (Fig. 6.4) to produce either a 4-finger,

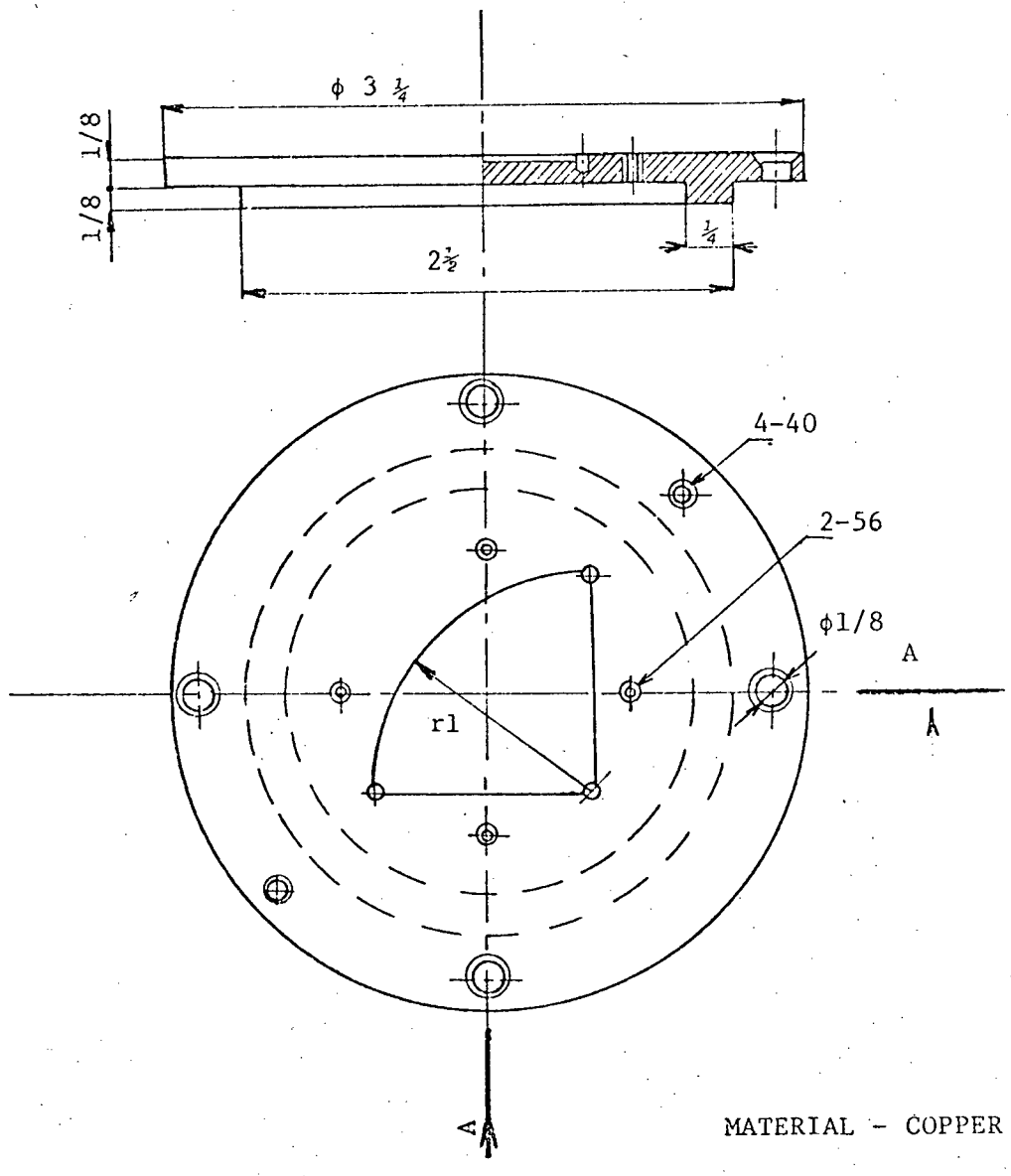

Fig. 6.1 Substrate table sample holder

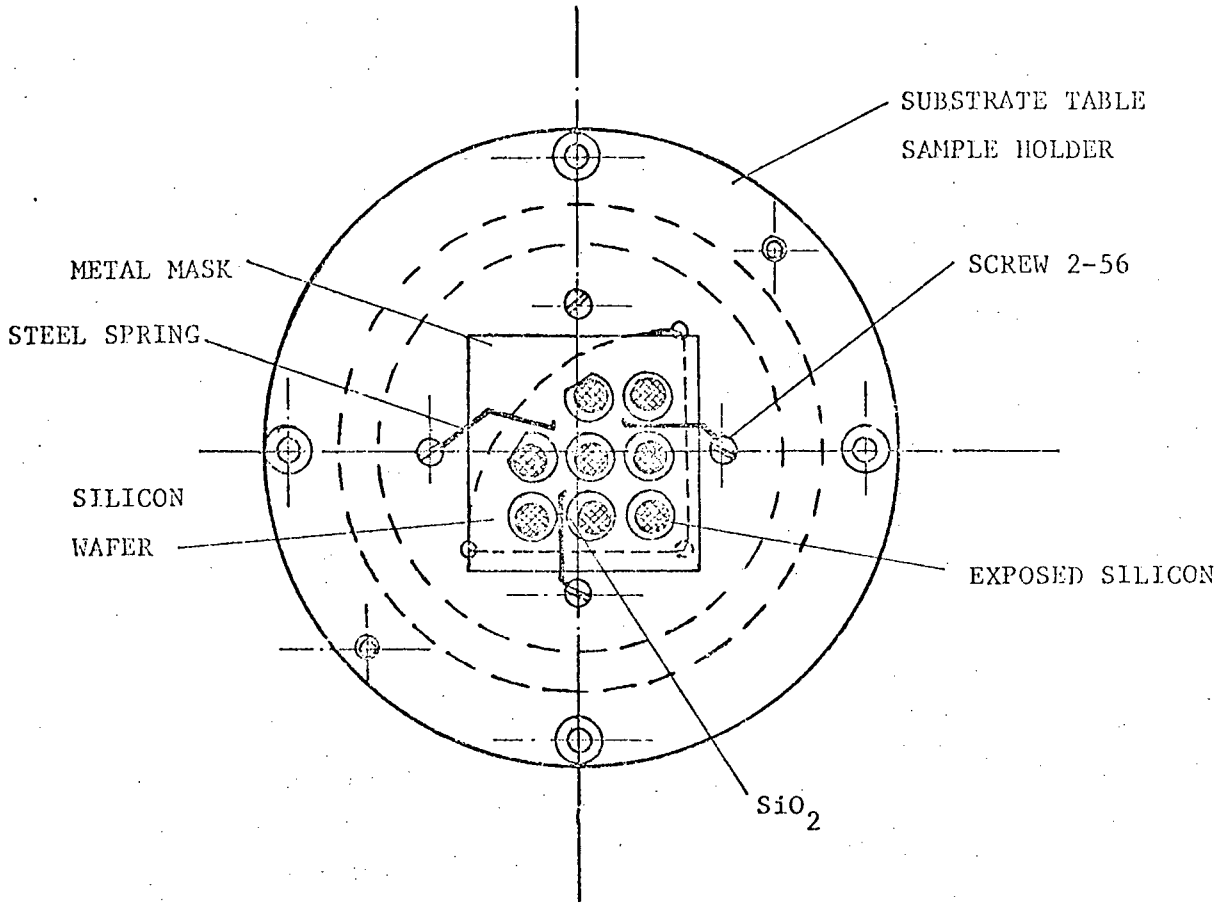

Fig. 6.2 Mask mounting for Cu_2O/Si heterojunction formation

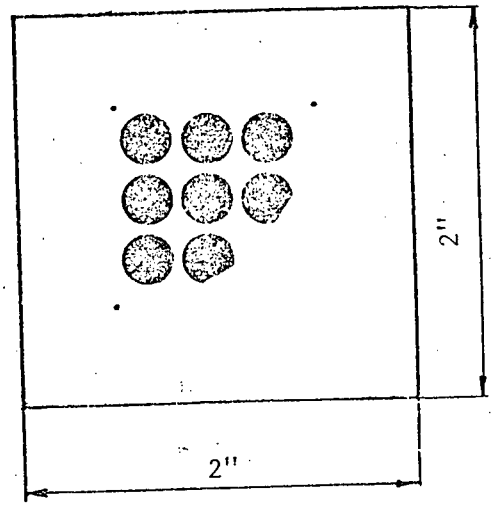

Fig.6.3 Metal mask for Cu_2O/Si heterojunction formation.

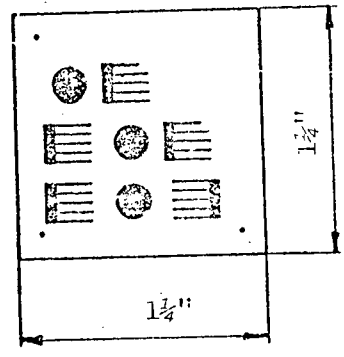

Fig.6.4 Metal mask for top solar cell metallization.

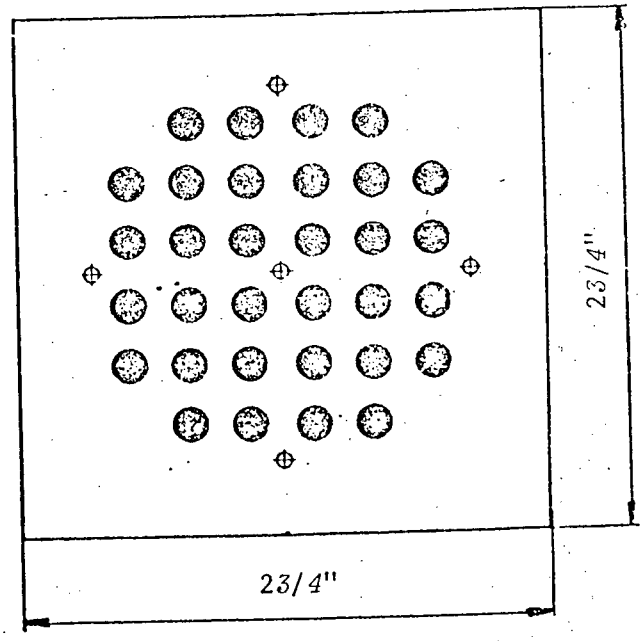

Fig.6.5 Mask for SiO_2 windows formation.

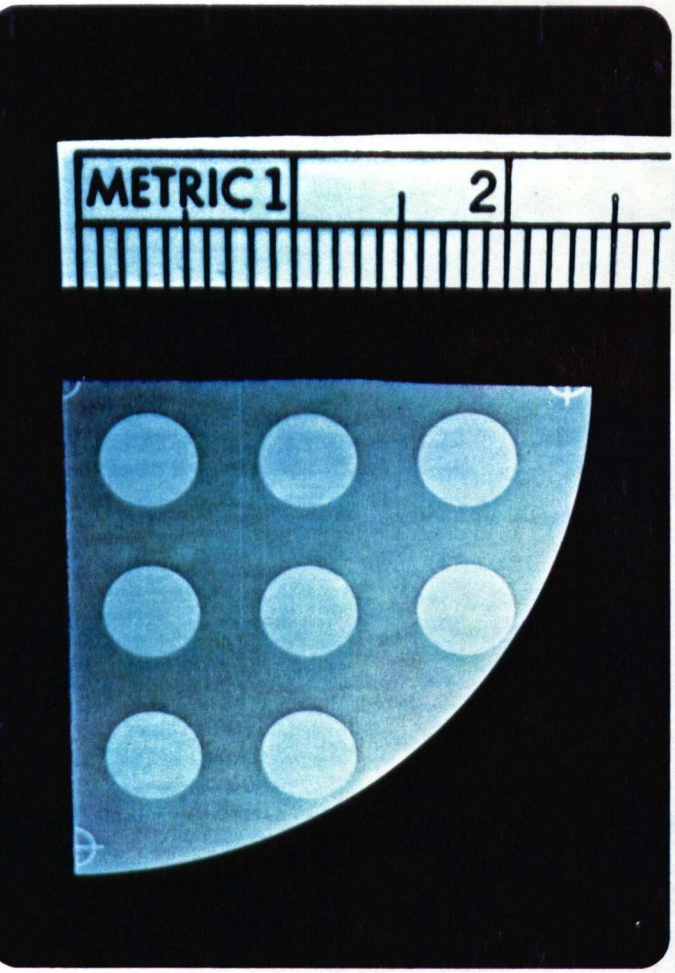

(a) Silicon wafer prepared for Cu_2O deposition.

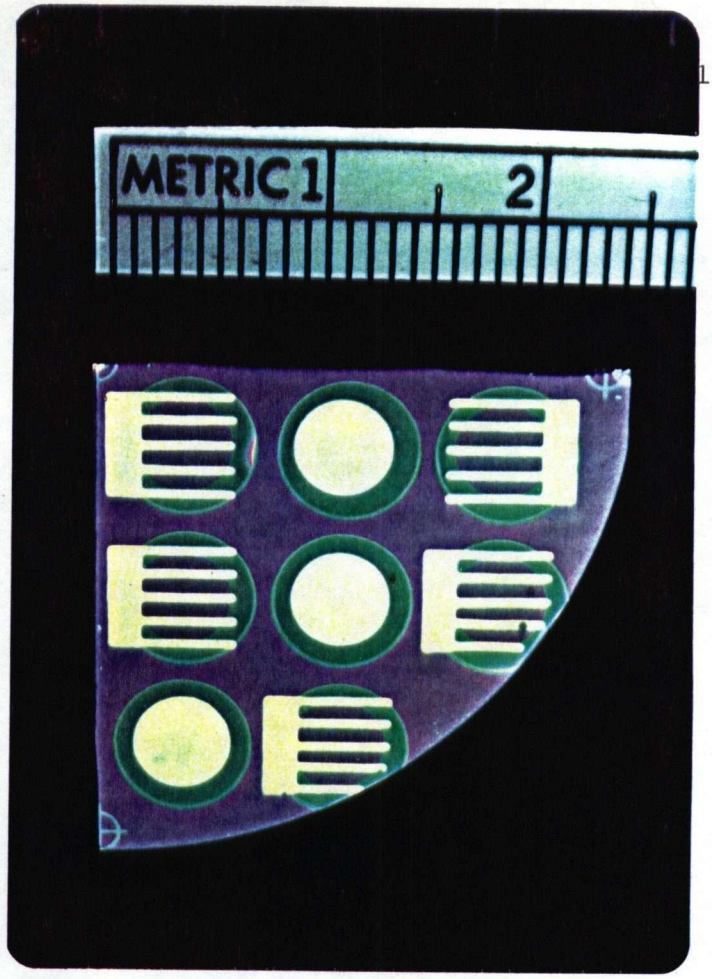

(b) Final Cu_2O/Si solar cell configuration.

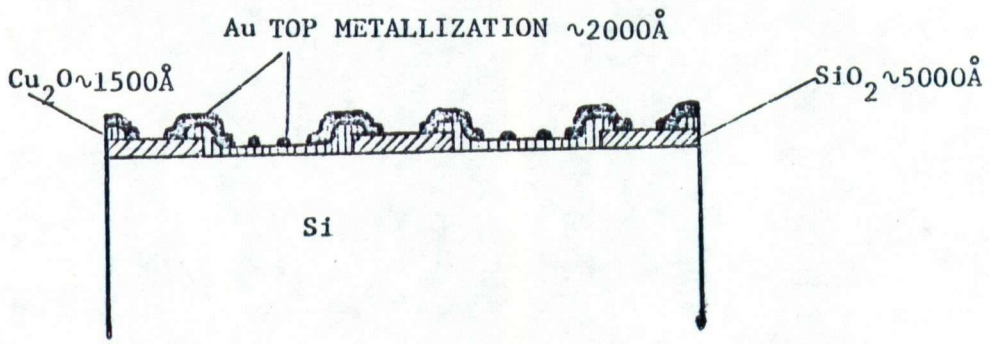

(c) Schematic view of Cu_2O/Si solar cell cross section.

Fig. 6.6 Heterojunction Cu_2O/Si solar cell configuration

comb-like contact grid pattern or a solid circular pattern. Each quarter slice yielded 3 diodes and 5 solar cell devices, each with an active area of 0.106 cm^2 and mutually isolated by the remaining SiO_2 layer (see Fig. 6.6).

6.4 I-V CHARACTERISTICS

I-V measurements were performed on the diodes both in the dark and under 100 $mWcm^{-2}$ of simulated AM1 sunlight obtained from a 3200 K tungsten lamp, filtered by a wide band hot mirror. Rectification was observed with both p-type and n-type silicon substrates, the direction of forward bias being silicon positive for p-type substrates and silicon negative for n-type substrates. Typical characteristics for Cu_2O/nSi devices are shown in Figs. 6.7 and 6.8. The reduction in magnitude of the reverse bias saturation current and the increase in forward "turn-on" voltage with decreasing sputtering power (Fig. 6.7) suggest that the device performance is strongly influenced by the presence of bombardment-induced surface states. This is further evinced by the dark forward bias data plotted in semilog fashion as shown in Fig. 6.9. Similar deviations from linearity of lnI-V plots with increasing sputtering power have been observed in sputtered Mo-Si Schottky diodes [63]. Mullins and Brunnschweiler [63] suggest that during sputter deposition a high density of "donor-like" traps is created in the surface region of silicon. The trap density was assumed to decrease exponentially into the bulk as

$$N_t(x) = N_{ts} \exp\left(-\frac{x}{L}\right) \qquad (6.1)$$

where N_{ts} is the trap density at the surface, L is some characteristic length and $N_t(x)$ is the concentration of these traps at a distance x from the surface. Both, L and N_{ts} depend on the sputtering voltage and the

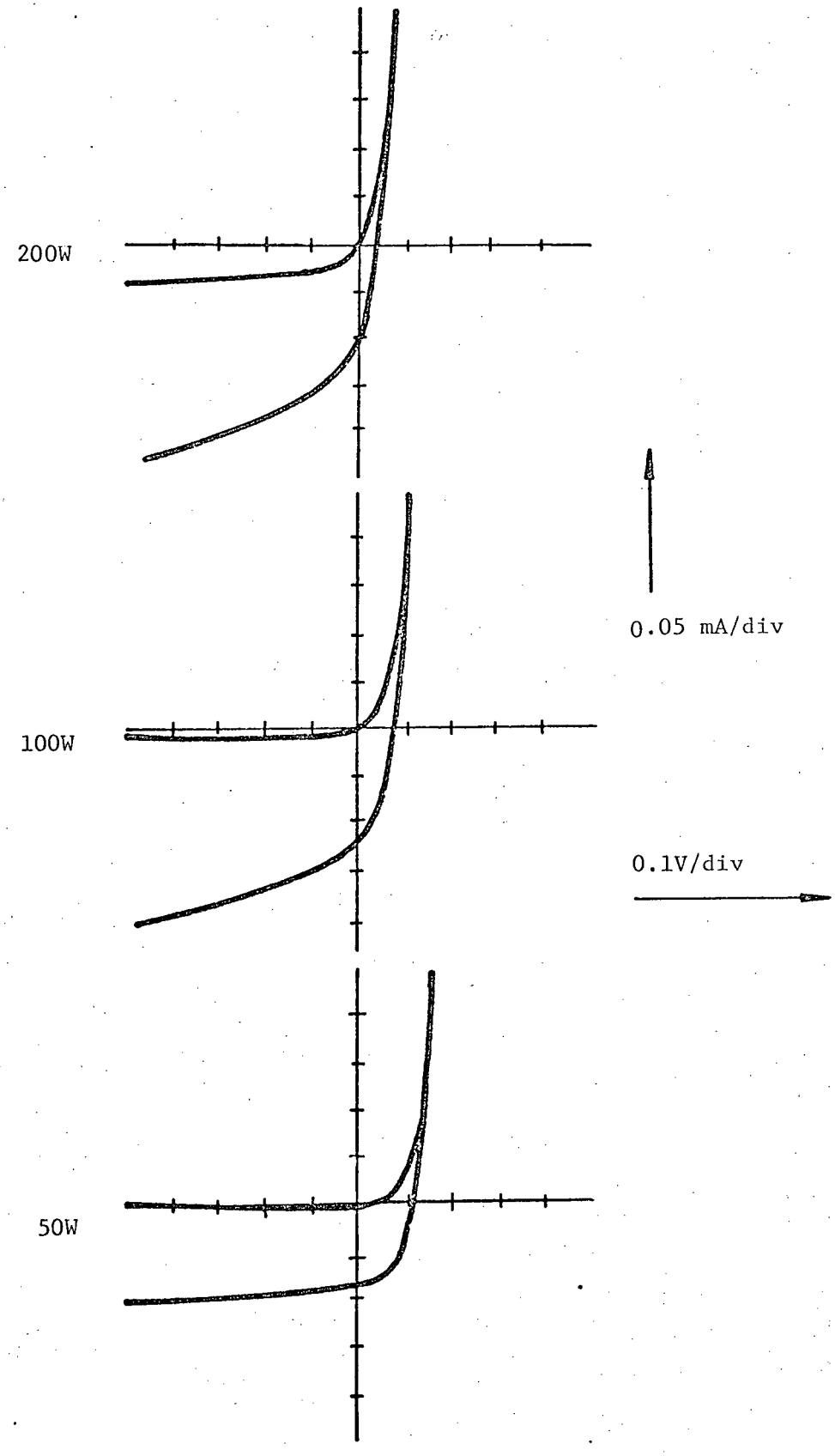

Fig. 6.7 Dark and illuminated (100 mW cm^{-2}) I-V characteristics for Cu_2O/n-Si diodes fabricated at different sputtering power levels.

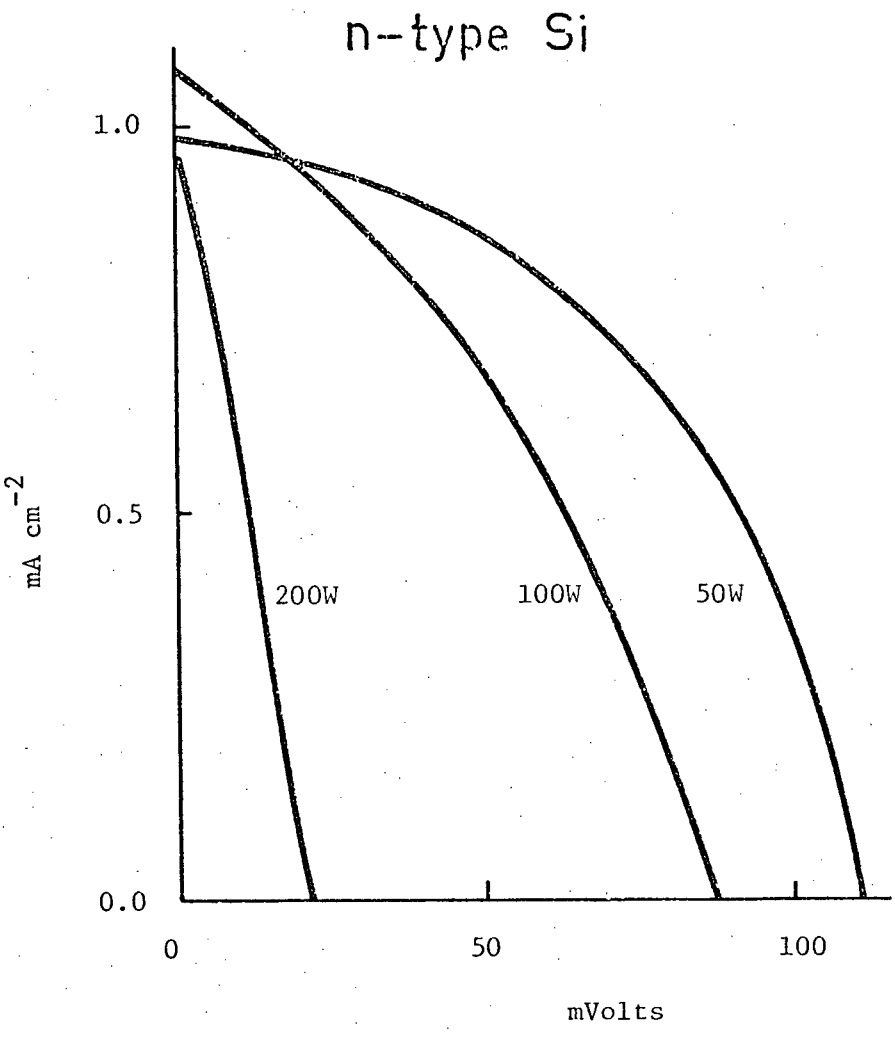

Fig. 6.8 Illuminated (100 mW cm^{-2}) I-V characteristics for Cu_2O/n-Si heterojunction diodes fabricated at different sputtering power levels.

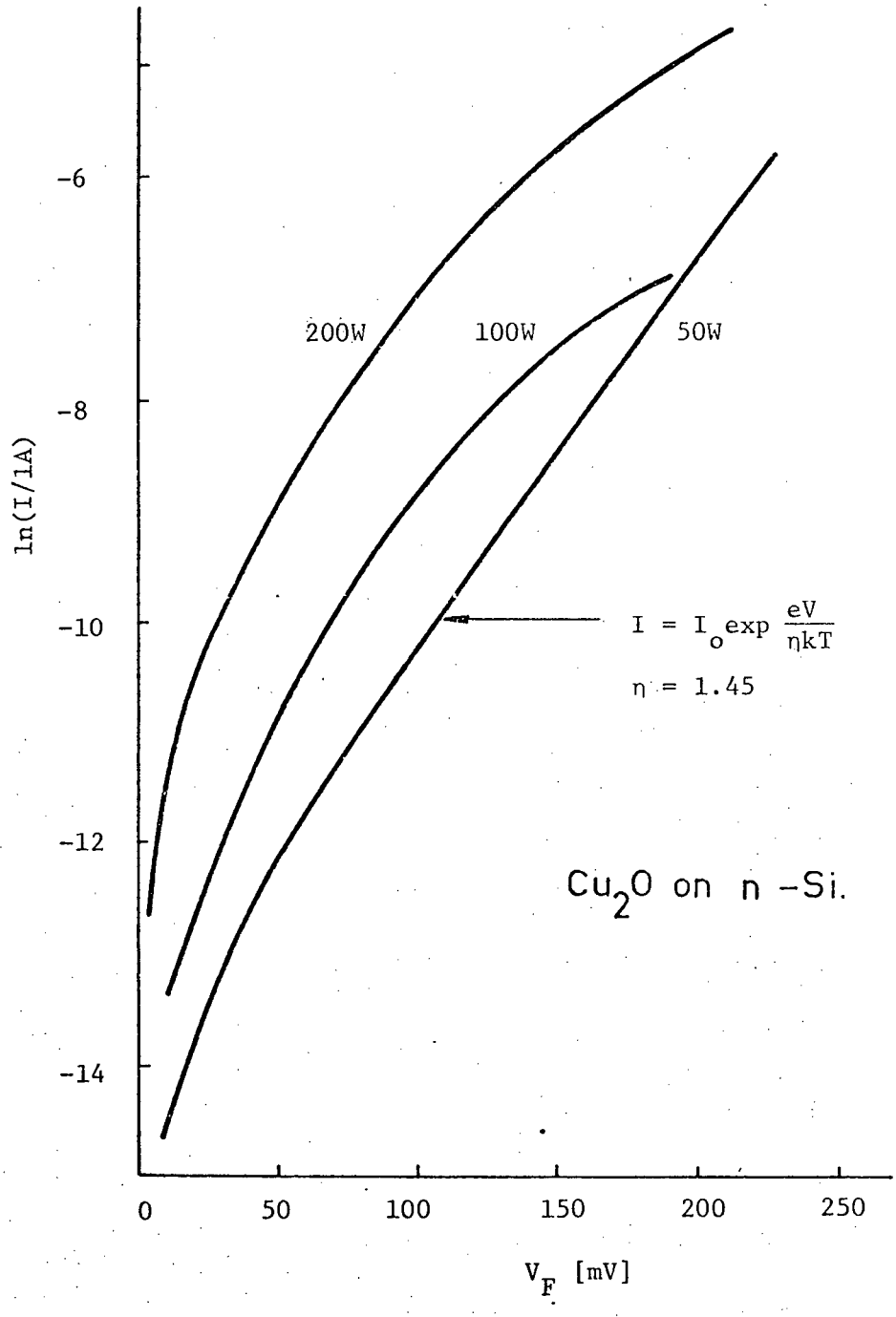

Fig. 6.9 Semilog plot of the forward I-V characteristics from the diodes used to obtain Fig. 6.8.

sputtering time.

Berg, Andersson, Norstrom and Brussel proposed [64] that this high density of donor centres creates a thin region of very high electric field and thus forms a narrow surface barrier. Under such conditions a significant contribution to the dark current can arise from electron tunneling at some representative energy E_{00} smaller than the barrier height energy of $q\Phi_{BO}$, see Fig. 6.10.

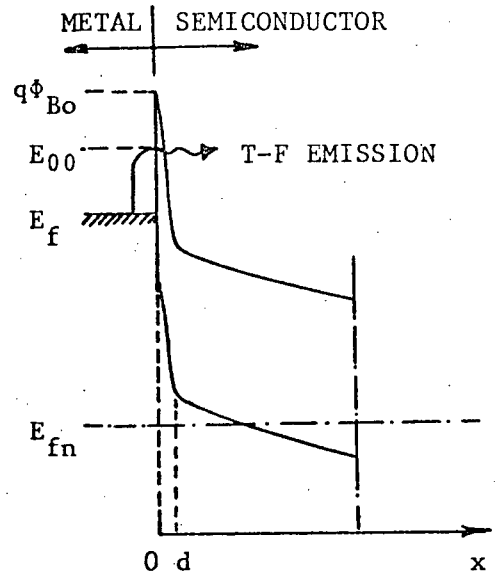

Fig. 6.10 Schematic energy diagram of a reverse biased sputter-damaged Schottky barrier. The damaged region is $0 \leq x \leq d$. The thermionic field emitted electrons are indicated by the arrow. E_f is the Fermi level in the metal and E_{fn} is the quasi-Fermi level for electrons in the semiconductor.

The precise position of E_{00} will depend upon the magnitude of the surface trap density. A low surface trap density gives $E_{00} \tilde{\sim} q\Phi_{BO}$ but increasing the surface density gives a decreasing value of E_{00} and thus leads to an increasing value of the tunnel current which is contributed by thermionic-field emission through the narrow surface barrier. Berg et al.

[64] showed how this current component was revealed in reverse bias I-V measurements and very similar characteristics were obtained from the present diodes, see Fig. 6.11. The reverse bias current at any given bias increases as the sputtering power used during deposition increases, as would be expected from the associated increase in N_{ts} and decrease in E_{00}. Fig. 6.11 thus suggests that thermionic-field emission is the dominating current transport mechanism at room temperature in Cu_2O/nSi diodes formed by r.f. reactive sputtering, and that its contribution to the total current increases with the deposition power. N_{ts} will also depend, for a given deposition power, on the deposition time used. For the diodes with characteristics given by Figs. 6.7-9 and 6.11 both the deposition power level and time were varied in order to produce approximately equal thicknesses of Cu_2O in all cases. It is conceivable that there is an optimum condition for the sputtering power and the time, but this was not deliberately sought at this stage. However some indirect evidence of this effect can be inferred from data taken on Cu_2O/pSi diodes, for which the I-V characteristics did not follow the straightforward relationship with sputtering power shown by the diodes on nSi (see Figs. 6.12 and 6.13 and compare with Figs. 6.7 and 6.8). In the case of the diodes on pSi it is likely that the surface layer of donor-like centres induces an inversion layer in the Si which could improve the photovoltaic performance of such diodes, as is the case in MIS structures [53]. However, for the sputtered Cu_2O/pSi devices, there will obviously be some trade off involved between this possibly advantageous effect and the obviously deleterious effect of the increased dark current as N_{ts} increases. In the present work the highest AM1 conversion efficiency achieved was 1%, and was obtained on a p-type substrate with a Cu_2O layer sputtered at 100W for 5 minutes with an oxygen partial pressure of 0.4

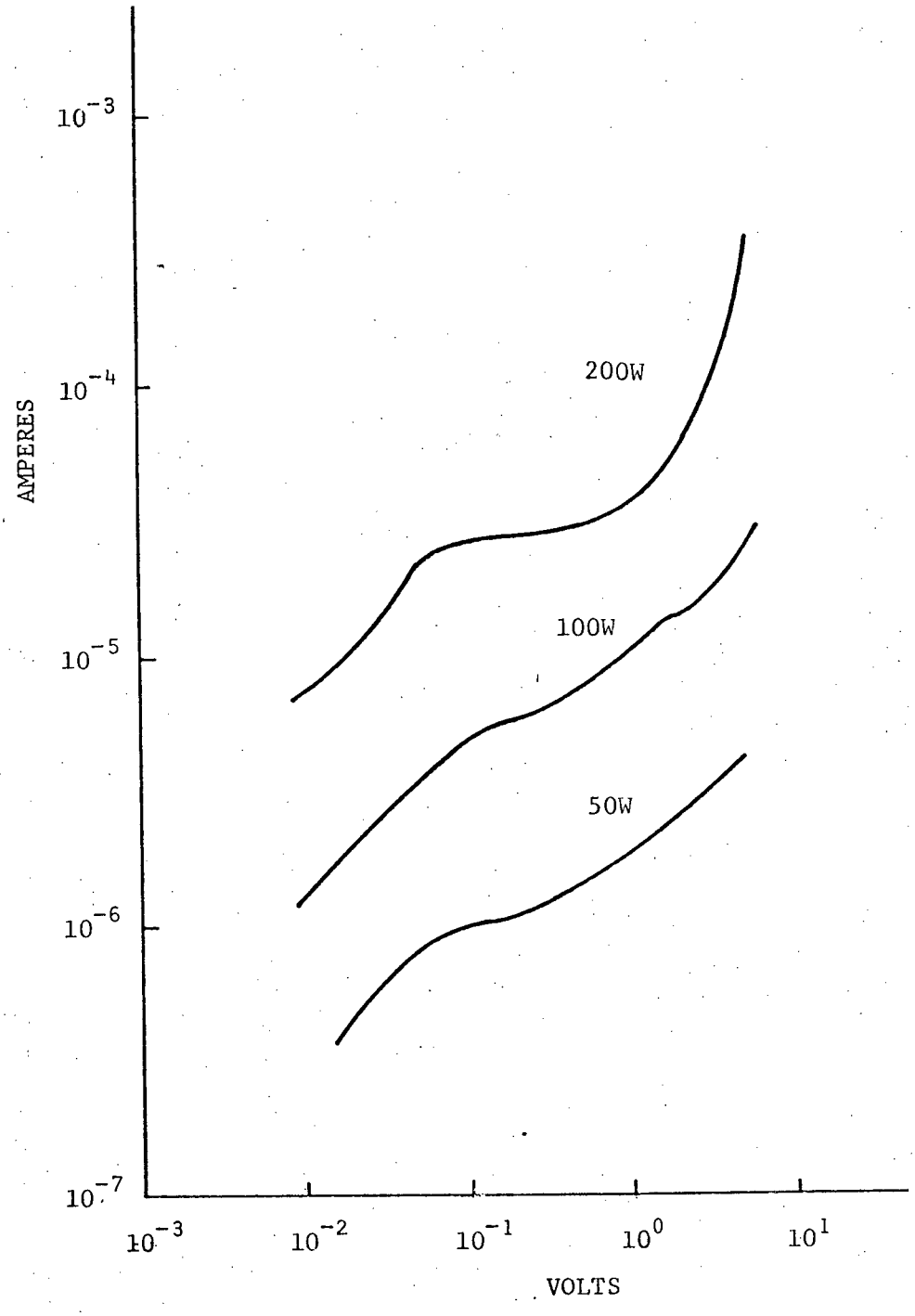

Fig. 6.11 Dark reverse I-V characteristics for Cu_2O/n-Si diodes fabricated at different sputtering power levels.

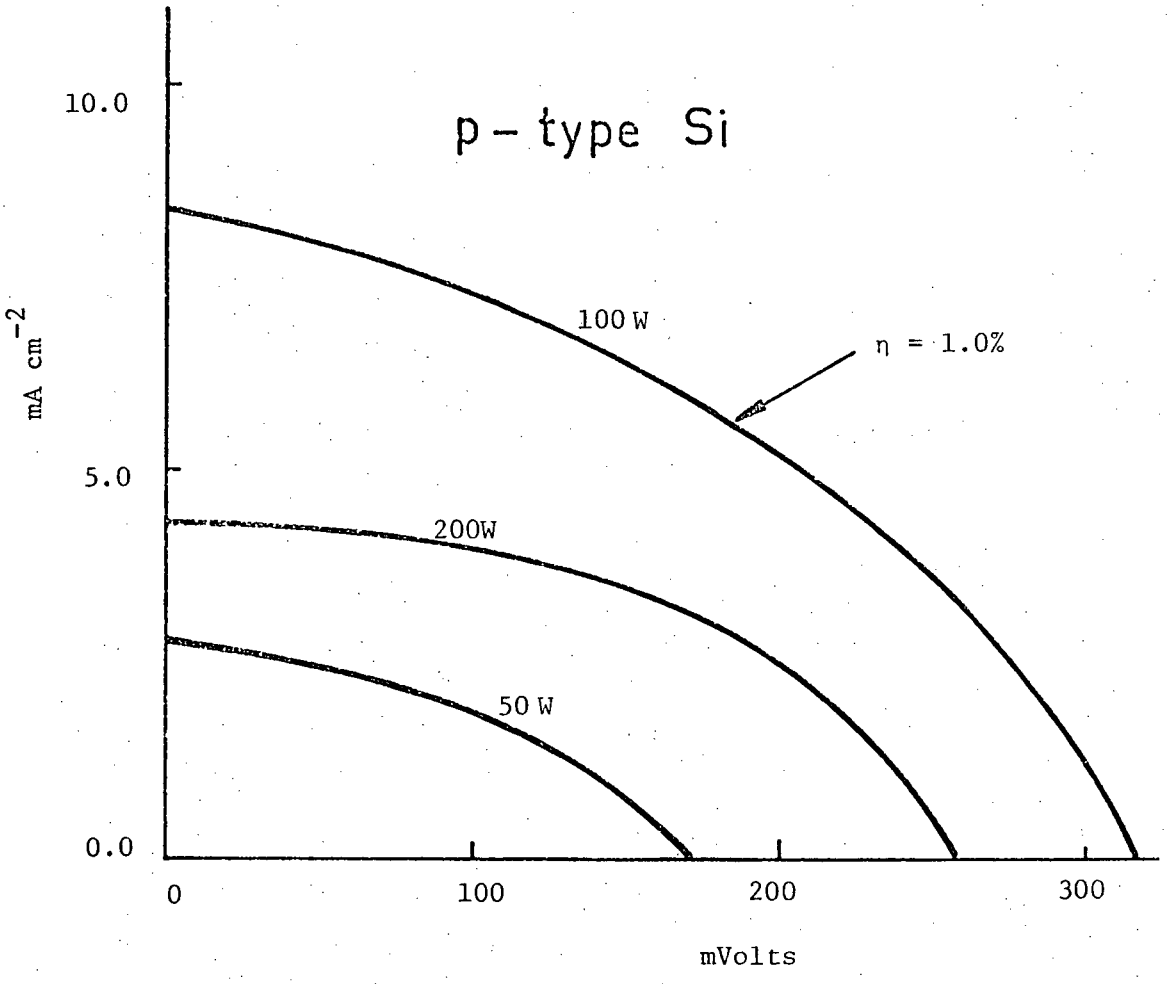

Fig. 6.12 Illuminated (100 mW cm^{-2}) I-V characteristics for Cu_2O/p-Si heterojunction diodes fabricated at different r.f. power levels.

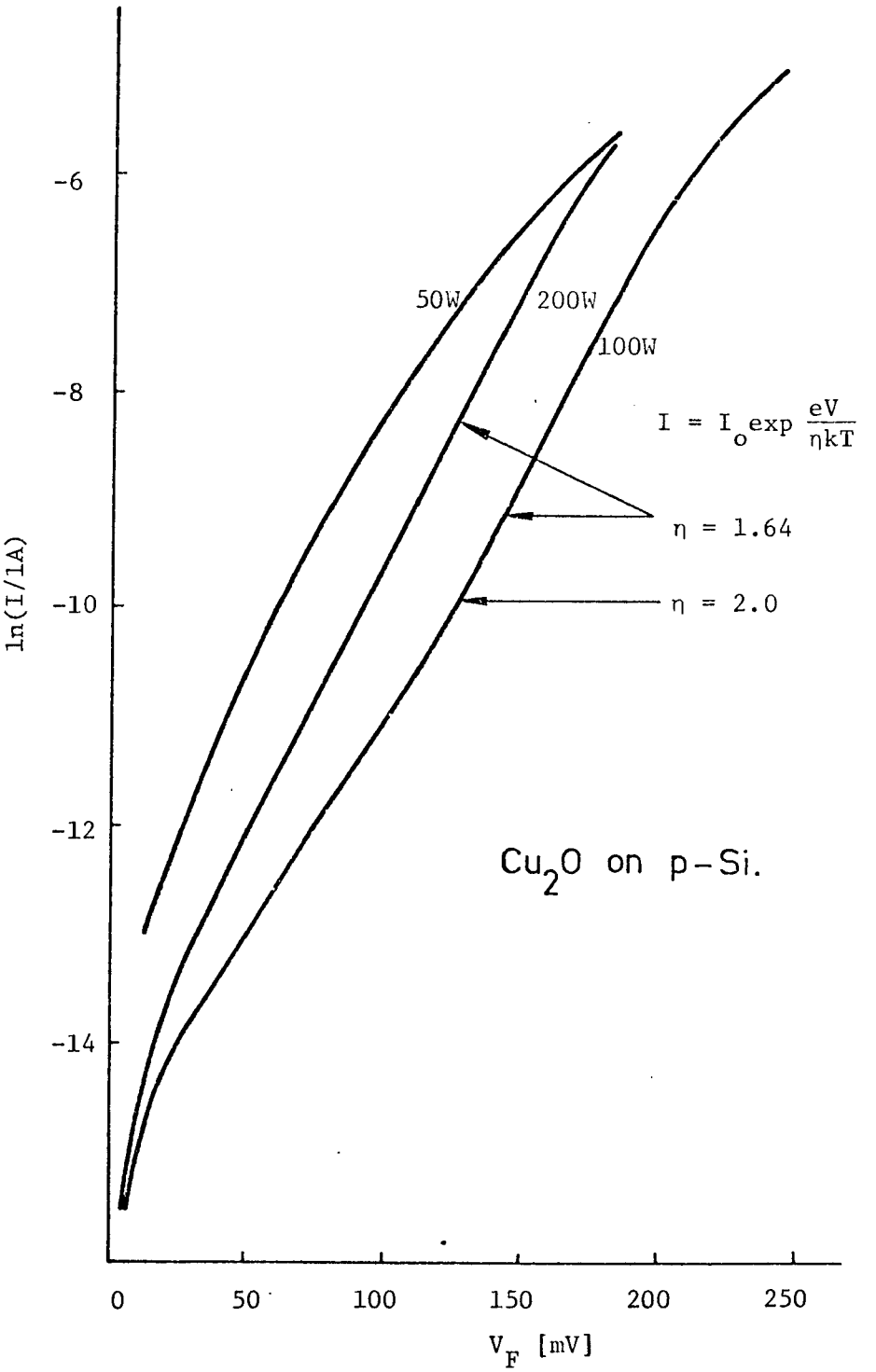

Fig. 6.13 Semilog plot of the forward I-V characteristics of Cu_2O/p-Si diodes formed by reactive sputtering.

mTorr. For this device the short circuit current J_{sc} = 8.7 mA cm^{-2}, open circuit voltage V_{oc} = 315 mV and fill factor FF = 0.40. It is noteworthy that the same efficiency has been obtained from ITO/Si cells in which r.f. sputtering was used for the ITO deposition [65], but that an efficiency of 12% has been attained in ITO/Si cells using neutral beam sputtering for the ITO preparation [57]. In the latter approach high energy electron bombardment of the substrate can be avoided.

7. CONCLUSIONS

A comprehensive theory of reactive sputtering has been developed which allows the absolute composition ratio of deposited films to be related to controllable sputtering parameters. The theory is based on the postulate that the composition ratio of deposited metal oxide films is determined by the relative magnitudes of the fluxes of metal and oxygen atoms at the substrate plane. These fluxes depend on the metal sputtering rate R_M and on the oxygen partial pressure P_o respectively. Variation of these parameters thus provides a convenient experimental arrangement for producing metal oxide films with a range of compositional ratios. Good agreement was obtained between the predictions from the theory and the composition of copper oxide films prepared experimentally by both d.c. and r.f. reactive sputtering in oxygen/argon mixtures. The trend in film composition ratio was

$$Cu \rightarrow Cu + Cu_2O \rightarrow Cu_2O \rightarrow Cu_2O + CuO \rightarrow CuO$$

oxygen partial pressure $\longrightarrow$

copper sputtering rate $\longleftarrow$

Comparison of theoretical and practical data also yielded a value for the sticking coefficient, namely $\alpha_o \tilde{\gtrsim} 0.1148$, of oxygen on copper-coated surfaces.

Copper oxide films of each phase composition possessed different yet characteristic properties as regards optical constants and resistivity. The data on optical constants are the first reported for reactively sputtered copper oxide films. The results for CuO films are similar to those reported for thermally-grown films. Cu_2O films show a characteristic peak in the real part of the refractive index ($n \tilde{\gtrsim} 3.36$) centred at $\lambda = 0.48\mu m$. There is evidence of free carrier absorption in conductive Cu_2O and acceptor level (copper ion vacancy)- conduction band transitions in near-stochiometric

(highly resistive) material. The resistivity of CuO films is unusually low (0.1 - 1.0 ohm cm) and that of Cu_2O films easily controllable, by varying P_o or R_M, within the range of 20 - 60 ohm cm. Cu_2O is a defect-conducting, p-type semiconductor but has been little used outside the laboratory on account of the fact that usual methods of preparation (thermal oxidation and electrodeposition) cannot reproducibly yield low resistivity material. The reactive sputtering method of deposition developed in this work offers a way around this problem. One particular application of promise is in the area of thin film solar cells and devices using a Cu_2O/Si heterojunction structure were fabricated. Rectification with both n- and p-type Si substrates was observed and a solar energy conversion efficiency of 1% was obtained. The solar cells were clearly adversely affected by high energy electron bombardment from the sputtering environment and it is suggested that the employment of neutral beam sputtering could alleviate this problem yet still maintain the attractive features of this deposition method.

APPENDIX A

THERMAL OXIDATION OF COPPER TO COPPER OXIDE

At the outset of this study the formation of copper oxide films by both reactive sputtering and the more traditional method [66-86] of thermal oxidation was carried out. When it became clear that the reactive sputtering method was going to yield new and interesting data the work on thermal oxidation was discontinued. However a brief review of this latter work is in order and is given in this appendix.

Oxidations were performed in the temperature range of 1020 - 1065°C in the vertical quartz furnance shown in Fig. A.1. The electrically controlled valves in the system allowed easy changing of the furnace environment from nitrogen (used when loading and quenching the samples) to air (used at 1.48 l/min for oxidation). Rapid quenching was achieved by allowing the quartz rod supporting the sample to slide through its retaining ring at the top of the furnance until the sample was outside the furnace hot zone.

Prior to an oxidation samples (6x4 cm Cu foils with thickness in the range 5-25 mil) were ultrasonically degreased in chloroform, etched in diluted HNO_3 and rinsed in deionized water. Before a sample was loaded into the furnace the quartz tube was throughly rinsed by nitrogen to avoid CuO formation. After loading, when the temperature of the sample reached the desired oxidation temperature, air instead of nitrogen was allowed into the quartz tube. Because air was used as an oxidation atmosphere, the oxidation temperature was restrained to a range of 1020-1065°C. The lower temperature limit was given by the stability of Cu_2O in air and the higher limit was determined by the eutectic temperature of the Cu/Cu_2O system.

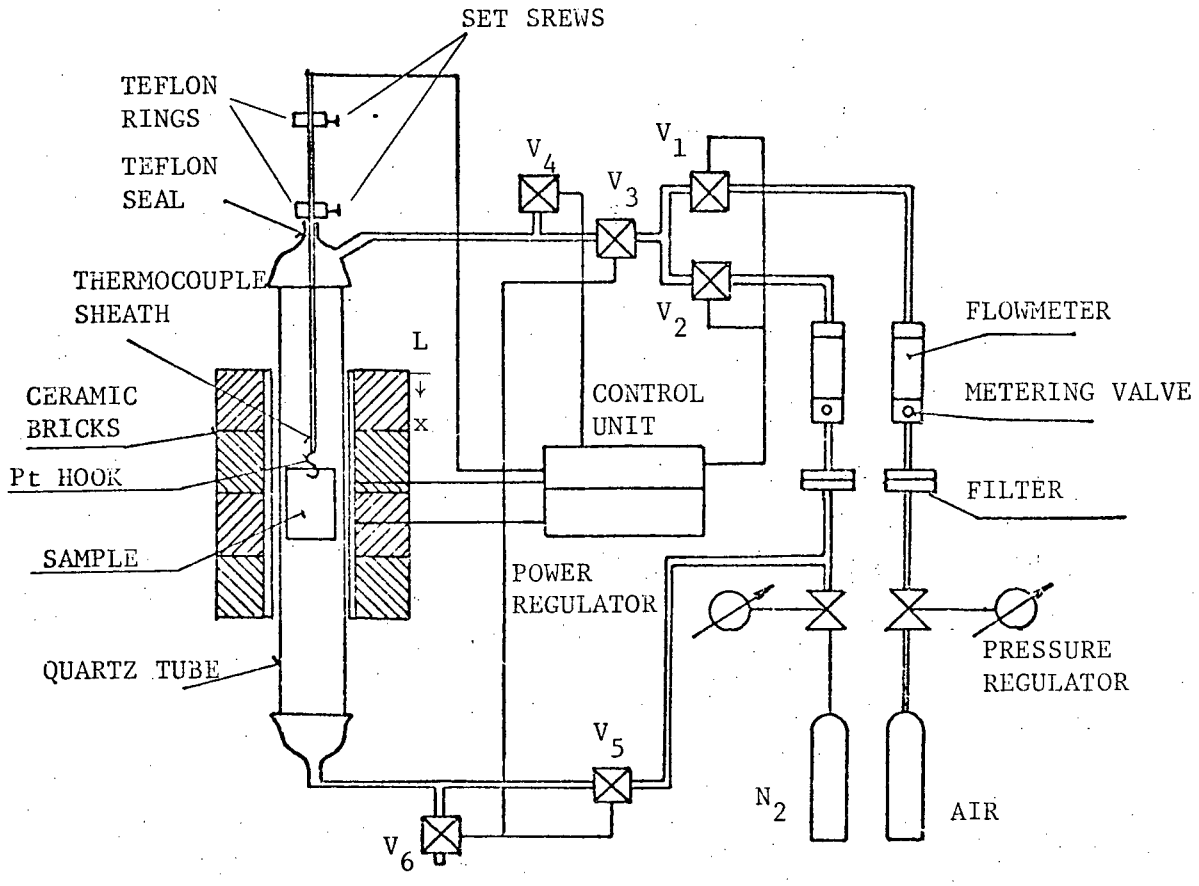

Fig. A.1 Vertical furnace for thermal oxidation and single crystal growth of Cu_2O.

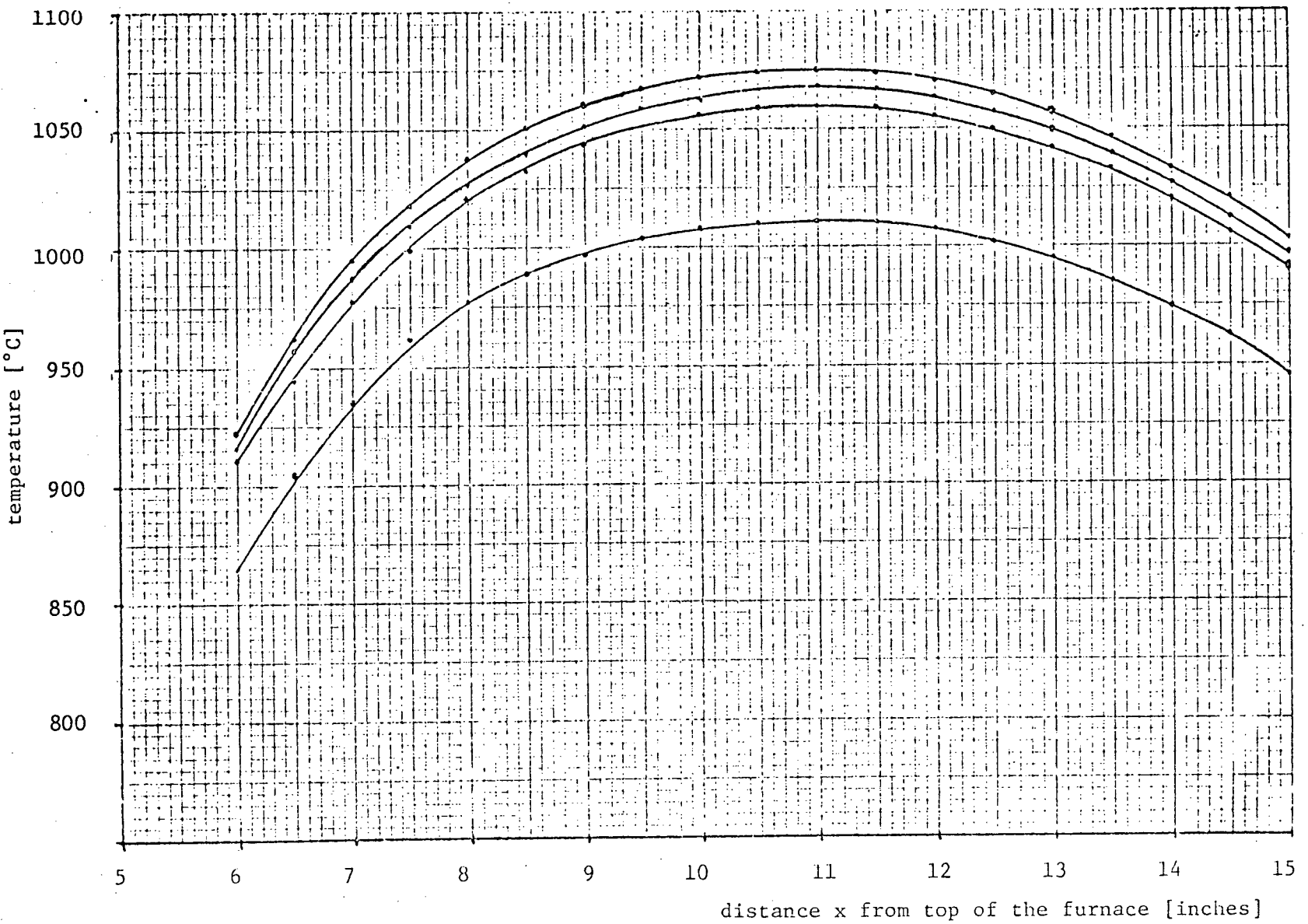

Fig. A.2 Temperature profile of the oxidation furnace at 1.48 l/min. of air flow. The distance is measured from point L, see Fig. A.1.

Because of the thermal gradient in the furnace the upper end of the sample was kept at a temperature of 1062 ± 2°C. Having a thermal gradient along the sample proved beneficial in obtaining large crystals and the desired thermal gradient could be chosen by positioning the sample slightly off the center of the furnace (see Fig. A.2). The length of time for a complete sample oxidation depended on the thickness of the starting copper foil. For 5 mil thick copper typically 10 minutes were required for complete oxidation. Oxidation times followed the expected diffusion theory [96], given by

$$t = \frac{2d^2}{aK} \qquad (A.1)$$

where a is the ratio of the initial copper thickness to the thickness of resulting Cu_2O, d is the initial Cu foil thickness and K an isobaric thermal constant.

After completion of the Cu to Cu_2O conversion, the resulting cuprous oxide had a fine grained polycrystalline structure with an average grain size of 0.02 mm^2, see Fig. A.3. Cuprous oxide grains, during their thermal growth, form a columnar structure, see Fig. A.4. The disordered region which can be seen in Fig.A.5, across the middle part of the sample, is caused by the fact that oxidation proceeds from both sides of the sample. Note that in preparing samples for scanning electron microscropy the crystal structure was revealed by a selective etch in solution of 25% HNO_3, 10% H_2O_2 and 65% H_2O.

It was found that the crystal grain size could be considerably increased by annealing in air at the growth temperature. Presumably this previously unreported phenomenon stems from the temperature gradient present in the furnace which allows significant strain-annealing growth to

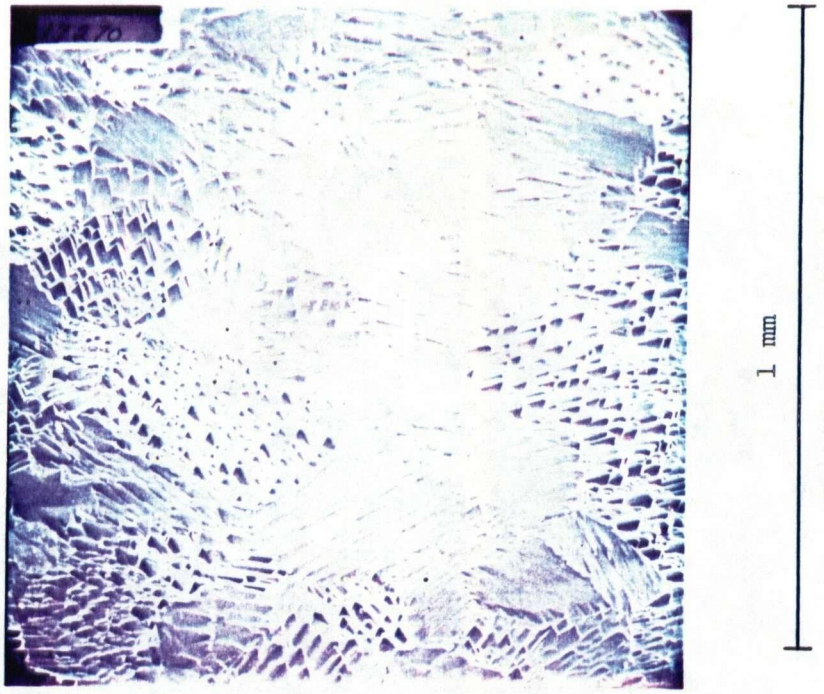

Fig. A.3 SEM print of Cu_2O shortly after the completion of oxidation process. Magnification x 120.

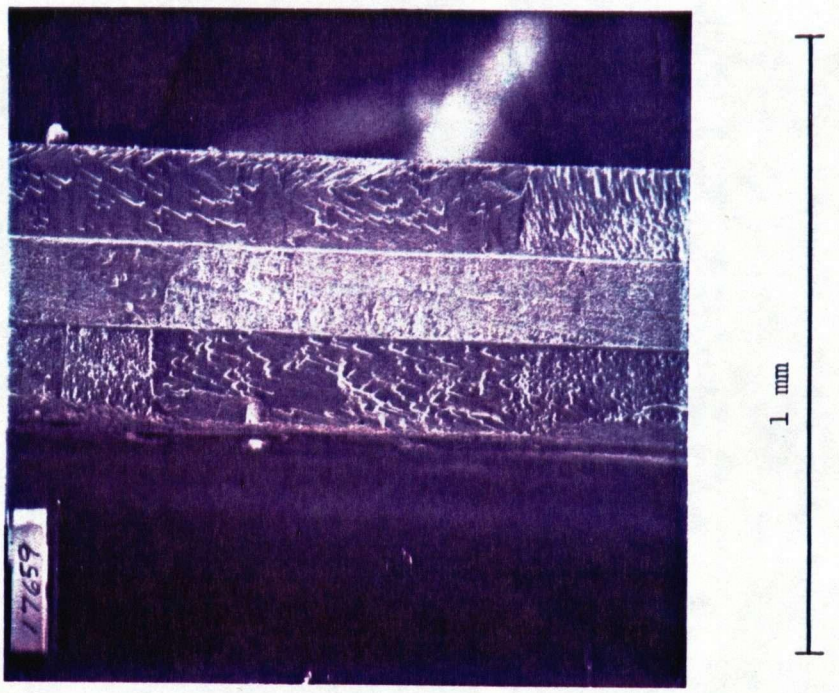

Fig. A.4 Cross section SEM print of partially oxidized Cu plate. Magnification x 125.

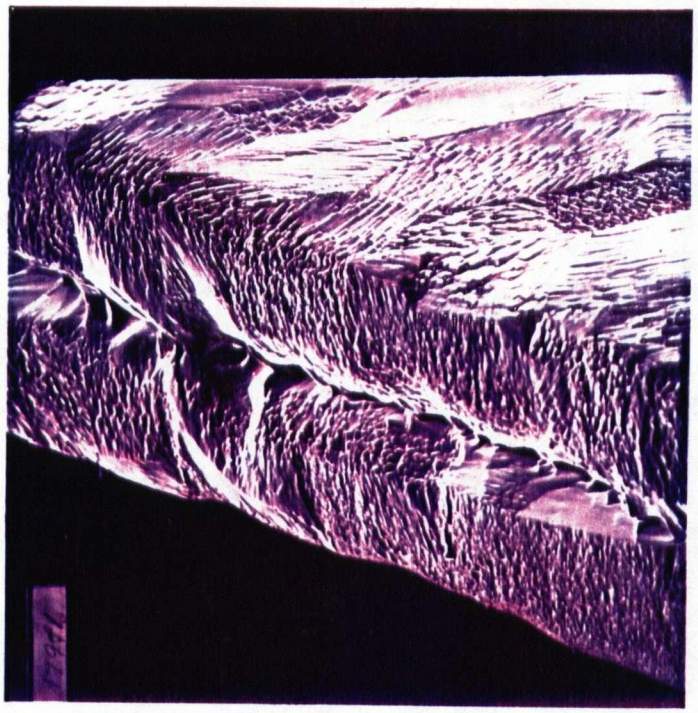

Fig. A.5 Cross section SEM print of completely oxidized Cu foil. Magnification x 110.

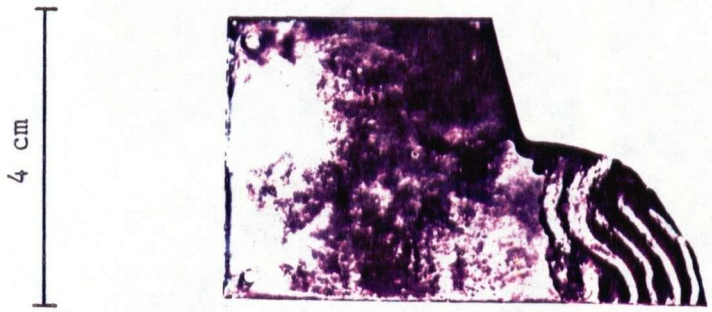

Fig. A.6 Photograph of cuprous oxide plate prepared from 99.999% Cu foil 20 mil thick and annealed for 14 hours.

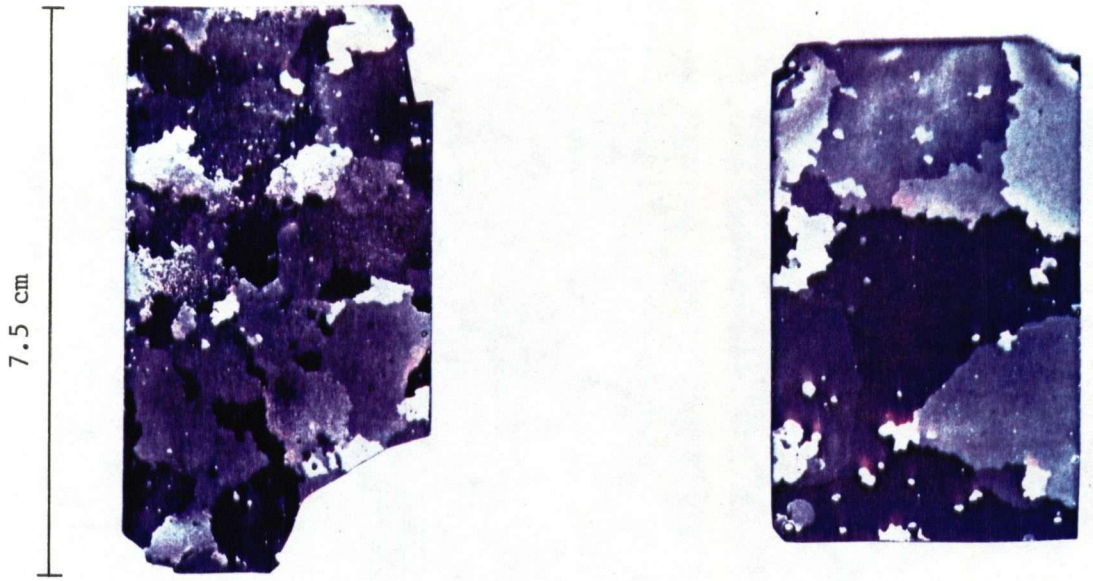

Fig. A.7 Photographs of the Cu_2O samples prepared from 99.99% Cu with 63 ppm of Ni content. The thickness of the initial copper in both cases was 5 mil. (a) - sample annealed for 1½ hours; (b) - sample annealed for 5 hours.

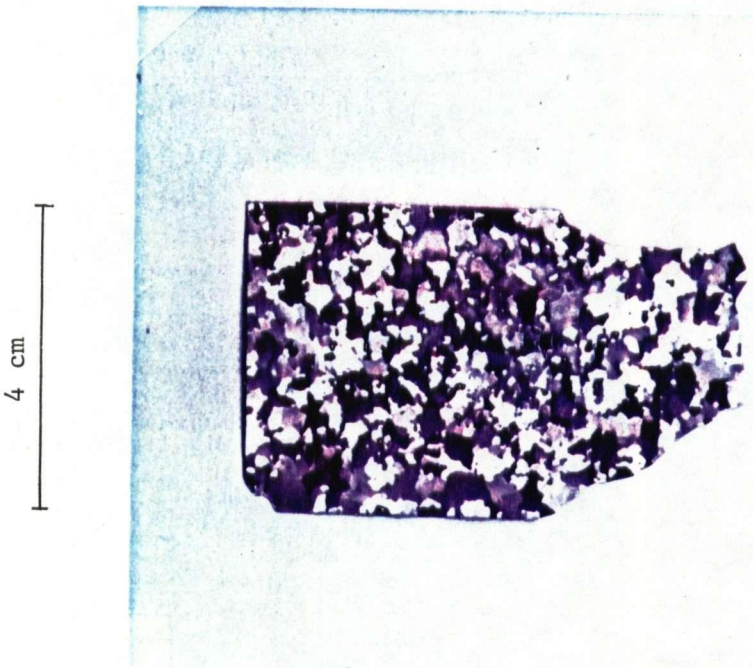

Fig. A.8 Photograph of the Cu_2O sample prepared from 99.9% Cu 5 mil thick, annealed for 7 hours.

occur [94,95]. Annealing times used were related to the thickness of the samples and there was some evidence that the ultimate grain size depended on the purity of the copper foil. This is illustrated by Figs. A.6-8.

The orientation and perfection of crystals was examined by using Laue-pattern X-ray diffraction techniques [93]. In all cases the Laue diffraction pictures taken from well annealed samples had sharp diffraction spots, thus indicating good crystal perfection without significant crystal defects. It was found that large single crystal grains had certain preferred orientations, namely a few degrees from [110], [211], [311], [511] and [231] normal directions. In some cases the [210] orientation was also found. During the grain growth process grains grow not only laterally across the sample but also through the thickness of the sample. Thus the large grains extend through the whole sample thickness, however the memory of the disordered region could never be completely obliterated, see Fig. A.9.

After annealing all samples were abruptly cooled from the oxidation temperature to room temperature in a stream of cold nitrogen, as proposed by Olsen [8], to achieve the lowest possible resistivity. Resistivities and Hall mobilities of samples were determined by the Van derPauw method [97]. Ohmic contacts to the sample were made by gold evaporation. Electrical connections between the probe and the sample were made by tungsten springs. Mobilities were in the range 50-75 $cm^2V^{-1}sec^{-1}$. Resistivities were in the range 5,000 - 60,000 ohm-cm. There was some indication that samples prepared from the least pure copper foil (99.9%) gave lower values of resistivity than samples resulting from 99.999% material. Deliberate doping (by diffusion) of Cu_2O by Zn and Cd has been reported to give, in some cases, enhanced p-type conductivity [7,89] and various attempts were made in the present work to achieve this effect.

Zinc was incorporated in or on the starting copper foil, either by direct evaporation or by utilizing foils of alloy (5% Zn). In both cases vaporization of the zinc occured during oxidation and, although resistivities around 2,000 ohm-cm could be obtained, the reproducibility and uniformity was not satisfactory.

As a reduction in resistivity is essential if thermally grown cuprous oxide films are to find any widespread use in the semiconductor industry it follows that more work might be done in this area of doping. Replacing oxygen by Br, Cl or F may prove more satisfactory than attempting metal ion doping, although the latter might be achieved by the nuclear transmutation of Cu to Zn using thermal neutrons.

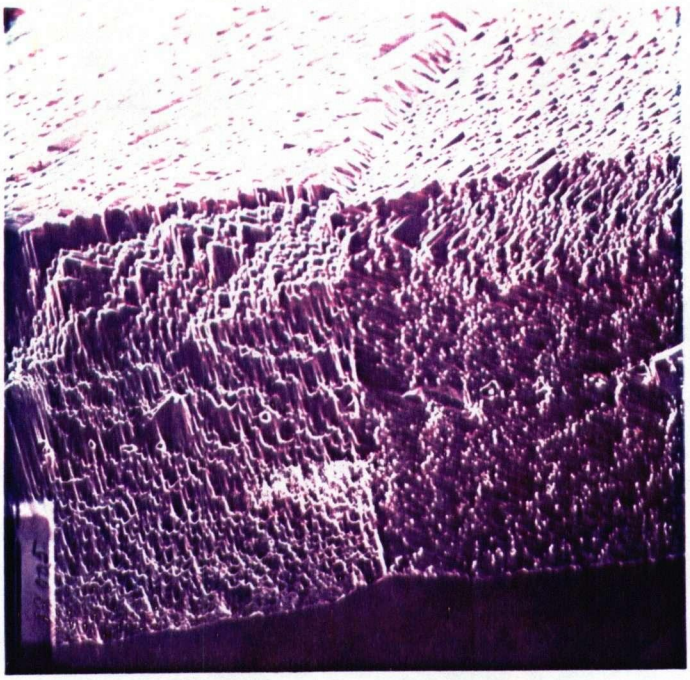

Fig. A.9 Cross section SEM print of completely annealed Cu_2O sample. Magnification x 260.

APPENDIX B

PROGRAM FOR COMPUTATION OF OPTICAL CONSTANTS

```
      C     FORTRAN (FTN) PROGRAM
      C     PROGRAM DESIGNED TO COMPUTE THE OPTICAL CONSTANTS N,K,ALPHA FROM
      C     REFLECTANCE AND TRANSMITTANCE DATA GIVEN IN UNITS OF OPTICAL
      C     DENSITIES FOR MAXIMUM 50 WAVELENGTH POINTS. COMPUTATION IS BASED
      C     ON THE NUMERICAL ITERATION METHOD UTILIZING "NDINVT" ROUTINE
      C     (SECANT METHOD) SUPPLIED BY THE UBC COMPUTING CENTRE.
      C     EQUATIONS WHICH RELATE N,K TO MEASURED R,T VALUES WERE ADOPTED
      C     FROM PUBLICATION BY P.O.NILSSON,APPLIED OPTICS VOL.7,435 (1968).
      C     PROGRAM IS DESIGNED TO BE RUN FROM A CONVERSATIONAL TERMINAL.
      C     THE INPUT DATA ARE: FIRST LINE-FILM THICKNESS IN MICRONS IN FORMAT
      C     (F)(G10.6),FILM IDENTIFICATION F(5A4);ALL NEXT SUBSEQUENT LINES-
      C     WAVELENGTH F(G3.2),REFERENCE MIRROR REFLECTANCE F(G5.4),REFRACTIVE
      C     INDEX OF THE SUBSTRATE F(G6.4),O.D.FOR REFLECTANCE FROM THE FILM
      C     SIDE F(G5.3),O.D.FOR TRANSMITTANCE F(G.3),CONTROL NUMBER: BLANK=
      C     WHEN NEXT POINT EXPECTED,01 FOR LAST POINT,ALL OTHER DATA ARE
      C     SUPPLIED BY OPERATOR DURING THE PROGRAM EXECUTION. THEIR MEANING
      C     AND FORMATS ARE SELFEXPLANATORY FROM THE MESSAGES WRITTEN ON THE
      C     CRT.
      C     DATA ARE EXPECTED TO BE READ FROM UNIT 1, AND RESULTS TO BE
      C     WRITTEN ON UNIT 2.
      C     INSTRUCTION TO RUN THE PROGRAM ARE AS FOLLOWS:
      C     RUN PROGRAM+*NUMLIB I=INPUTDATAFILE 2=OUTPUTDATAFILE
      C     THE RESULTS WRITTEN ON UNIT 2 ARE SELFEXPLANATORY.
      C     ******************************************************************
      C
      C     DEFINING OF ARRAYS, TYPES OF VARIABLES AND BLOCKS OF MEMORY COMMON
      C     TO THE MAIN PROGRAM AND THE SUBPROGRAM:
            IMPLICIT REAL*8(A-H,O-Z)
            DIMENSION ACCEST(2),F(2),X(2),R0(50),RE(50),TR(50),WL(50),YN(50),Y
           1K(50),SN(50),ALPHA(50)
            COMMON/CONUM/DT,PI,R,RN,RNS,RK,SQNS,SQNSM1,SQNSP1,W,T
      C
      C     CONSTANTS DECLARATION
            PI=DPI(0.)
            I=0
            API=40000.*PI
      C
      C     CONSTANTS REQUIRED BY NDINVT ROUTINE
            N=2
            MAXIT=200
            ERR=1.D-06
            EXTERNAL FCN
      C
      C
      C     READING OF FILM THICKNESS AND FILM DESCRIPTION DATA
      C     DATA ARE EXPECTED TO BE ON FILE (UNIT 1)
            READ(1,100)FILMTH,FD1,FD2,FD3,FD4,FD5
            DT=FILMTH
      C
      C     LOOP DESIGNED TO CONTROL READING A DATA FROM FILE
          2 I=I+1
      C     READ FROM FILE: WAVELENGTH, ALUMINUM MIRROR REFLECTANCE, SUBSTRATE N,
      C     OPTICAL DENSITY (O.D.) FOR REFLECTANCE FROM FILM SIDE, O.D. FOR
      C     TRANSMITTANCE, CONTINUATION NUMBER:NEXT DATA=0(BLANK),LAST DATA =1
            READ(1,101)WL(I),R0(I),SN(I),RE(I),TR(I),J
            IF(J.EQ.0) GO TO 2
            NP=I
      C
      C     WRITING THE FILM THICKNESS, FILM DESCRIPTION AND NUMBER OF POINTS ON
      C     FILE (UNIT 2)
```

```
      WRITE(2,204)FILMTH,FD1,FD2,FD3,FD4,FD5,NP
      WRITE(6,204)FILMTH,FD1,FD2,FD3,FD4,FD5,NP
C
      DO 1000 I=1,NP
C     CALCULATION OF ABSOLUTE REFLECATNCE FROM O.D. DATA
      RE(I)=R0(I)*10.**(-RE(I))
C     CALCULATION OF ABSOLUTE TRANSMITTIVITY FROM O.D. DATA
      TR(I)=10.**(-TR(I))
      WRITE(6,104)TR(I),RE(I),I
  104 FORMAT('T=',G12.6,4X,'R=',G12.6,2X,'#=',I2)
 1000 CONTINUE
C
      M=0
      J=0
      I=0
C     READ POINT NUMBERS FOR WHICH THE OPTICAL CONSTANTS ARE TO BE CALCULATED
    3 WRITE(6,200)
      READ(5,102)M,J
C     READ GUESS FOR N
      WRITE(6,201)
      READ(5,103)X(2)
C     READ GUESS FOR K
      WRITE(6,202)
      READ(5,103)X(1)
      IF (J.GT.0) GO TO 5
      IF (M.GT.0) I=M-1
      GO TO 10
C
C
C     LOOP DESIGNED FOR ITERATION COMPUTING OF N,K FOR GIVEN R,T DATA
C     FOR BY OPERATOR GIVEN RANGE OF WAVELENGTH POINTS:
    5 DO 1001 I=M,J
      RNS=SN(I)
      SQNS=RNS**2
      SQNSM1=SQNS-1.
      SQNSP1=SQNS+1.
      R=RE(I)
      T=TR(I)
      W=WL(I)
      CALL NDINVT(N,X,F,ACCEST,MAXIT,ERR,FCN,&20)
      YN(I)=X(2)
      YK(I)=X(1)
      GO TO 10001
C     ERROR OUTPUT FOR NDINVT
   20 YN(I)=0.0
      YK(I)=0.0
      X(1)=.1
      X(2)=3.
C
C      COMPUTATION OF THE ABSORPTION COEFFICIENT:
10001 ALPHA(I)=API*YK(I)/WL(I)
C     DISPLAYING THE RESULTS FOR GIVEN POINT
      WRITE(6,203)WL(I),YN(I),YK(I),ALPHA(I),RE(I),TR(I),I
 1001 CONTINUE
C
C     IF ALL POINTS HAVE BEEN CALCULATED, GO TO 11
    4 IF (I.EQ.NP) GO TO 11
      GO TO 3
C
C     N AND K SINGLE POINT CALCULATION LOOP
```

```
      10 I=I+1
         RNS=SN(I)
         SQNS=RNS**2
         SQNSM1=SQNS-1.
         SQNSP1=SQNS+1.
         R=RE(I)
         T=TR(I)
         W=WL(I)
         CALL NOINVT(N,X,F,ACCEST,MAXIT,ERR,FCN,&21)
         YN(I)=X(2)
         YK(I)=X(1)
         GO TO 10002
C        ERROR OUTPUT FOR NOINVT
      21 YN(I)=0.0
         YK(I)=0.0
         X(1)=.1
         X(2)=3.
C
C        COMPUTATION OF THE ABSORPTION COEFFICIENT
10002    ALPHA(I)=API*YK(I)/WL(I)
         WRITE(6,203)WL(I),YN(I),YK(I),ALPHA(I),RE(I),TR(I),I
         GO TO 4
C
C
C        WRITING THE RESULTS ON FILE (UNIT 2)
      11 I=1
      12 WRITE(2,203)WL(I),YN(I),YK(I),ALPHA(I),RE(I),TR(I),I
         I=I+1
         IF (I.LT.(NP+1)) GO TO 12
C
         WRITE(6,205)
         READ(5,105)K
         IF (K.EQ.1) GO TO 3
C
C
C        READ FORMAT STATEMENTS
  100 FORMAT(G10.6,5A4)
  101 FORMAT(G3.2,G5.4,G6.4,2G5.3,I2)
  102 FORMAT(2I2)
  103 FORMAT(G10.5)
  105 FORMAT(I1)
C
C
C        WRITE FORMAT STATEMENTS
  200 FORMAT('SINGLE P=ITS#; GROUP=##XX; DEFAULT=NEXT P')
  201 FORMAT('GUESS N=? G10.5')
  202 FORMAT('GUESS K=? G10.5')
  203 FORMAT('A=',F6.3,2X,'N=',F6.3,2X,'K=',F6.3,2X,'ALPHA=',1PD10.3,4X,
     1'R=',0PF8.5,2X,'T=',F8.6,3X,I2)
  204 FORMAT('FILM THICK=',G20.8,5X,'SAMPLE: ',5A4,3X,'#',I2)
  205 FORMAT('DO YOU WANT TO REPEAT THIS CALCULATION? YES=1,DEFAULT=NO')
         END
C
         SUBROUTINE FCN(X,F)
         IMPLICIT REAL*8(A-H,O-Z)
         DIMENSION X(1),F(1)
         COMMON/CONUM/DT,PI,R,RN,RNS,RK,SQNS,SQNSM1,SQNSP1,W,T
         RK=X(1)
         RN=X(2)
C
```

```
      C     CALCULATION OF SUBTERMS
      C     NEXT TWO STATEMENTS ARE DESIGNED TO CATCH ANY NUMERICAL OVERFLOW
      C     WHICH CAN OCCUR IN THE ITERATION SUBROUTINE:
            IF (DABS(RN).GT.50.) RN=3.
            IF (DABS(RK).GT.50.) RK=.5
            RNM1SQ=(RN-1.)*(RN-1.)
            RNP1SQ=(RN+1.)*(RN+1.)
            SQK=RK*RK
            SQN=RN*RN
            SQNKP=SQN+SQK
            QNKNSP=SQNKP+SQNS
            QNKNSM=SQNKP-SQNS
            QNP1KP=RNP1SQ+SQK
            QNM1KP=RNM1SQ+SQK
            SQNKM1=SQNKP-1.
            SQNSN4=SQNS*RN*4.
            QKNS8=SQK*SQNS*8.
      C
            A=SQNKP*SQNS*32.
      C
            ARGP=4.*PI*DT/W
            ARN=ARGP*RN
            ARK=ARGP*RK
            A112=SQNSP1*QNKNSP
            A12=A112+SQNSN4
            A1=QNM1KP*A12
            A2=QNP1KP*A12
            C112=SQNSP1*QNKNSM
            B12=C112*SQNKM1
            B1=-2.*(QKNS8+B12)
            B2=2.*(QKNS8-B12)
      C
            RK4=4.*RK
            C122=2.*SQNS*SQNKM1
            C1=RK4*(C122-C112)
            C2=RK4*(C122+C112)
      C
            CF11=A112-SQNSN4
            CF1=QNP1KP*CF11
            CF2=QNM1KP*CF11
      C
      C
            DENOM=(A2*DEXP(ARK)+B2*DCOS(ARN)+C2*DSIN(ARN)+CF2*DEXP(-ARK))
            F(1)=A/DENOM-T
            F(2)=(A1*DEXP(ARK)+B1*DCOS(ARN)+C1*DSIN(ARN)+CF1*DEXP(-ARK))/DENOM
           A=R
            RETURN
            END
END OF FILE
```

Copy of the input data set (example)

```
    1      .105       CU20#3
    2      .80 .854 1.45  .38   .215  0
    3      .78 .857 1.450 .41   .20   0
    4      .76 .859 1.450 .44   .195  0
    5      .74 .862 1.450 .485  .175  0
    6      .72 .864 1.455 .54   .155  0
    7      .70 .867 1.455 .61   .14
    8      .69 .86751.455 .65   .13   0
    9      .68 .868 1.456 .70   .12   0
   10      .67 .86951.456 .75   .11   0
   11      .66 .871 1.456 .805  .10   0
   12      .65 .87151.457 .88   .095  0
   13      .64 .872 1.457 .94   .090  0
   14      .63 .873 1.457 1.00  .085  0
   15      .62 .874 1.457 1.05  .085  0
   16      .61 .875 1.458 1.06  .085  0
   17      .60 .876 1.458 1.025 .095  0
   18      .59 .877 1.458 .91   .11   0
   19      .58 .878 1.458 .83   .135  0
   20      .57 .878 1.459 .73   .17   0
   21      .56 .878 1.459 .65   .21   0
   22      .55 .87851.46  .545  .25   0
   23      .54 .879 1.46  .47  .315  00
   24      .53 .87851.46  .41   .375  0
   25      .52 .878 1.461 .37   .43   0
   26      .51 .87751.461 .35   .51   0
   27      .50 .877 1.462 .33   .585  0
   28      .49 .876 1.46  .33   .67   0
   29      .48 .87551.463 .335  .76   0
   30      .47 .875 1.464 .355  .86   0
   31      .46 .87451.465 .375  .96   0
   32      .45 .874 1.466 .395 1.07   0
   33      .44 .87351.4665.415 1.18   0
   34      .43 .873 1.467 .43  1.28   0
   35      .42 .870 1.468 .44  1.39   0
   36      .41 .867 1.469 .445 1.52   0
   37      .40 .864 1.470 .445 1.66   0
   38      .39 .860 1.471 .435 1.85   0
   39      .38 .858 1.4725.43  2.0    1
END OF FILE
```

Copy of the output data set (example)

78	FILM THICK=	0.10500000		SAMPLE: CU20#3			#38	
79	W= 0.800	N= 2.791	K= 0.029	ALPHA= 4.612E+03		R=0.356006	T=0.609537	1
80	W= 0.780	N= 2.797	K= 0.028	ALPHA= 4.588E+03		R=0.333412	T=0.630957	2
81	W= 0.760	N= 2.751	K= 0.038	ALPHA= 6.330E+03		R=0.311884	T=0.638263	3
82	W= 0.740	N= 2.778	K= 0.035	ALPHA= 5.937E+03		R=0.282168	T=0.668344	4
83	W= 0.720	N= 2.793	K= 0.033	ALPHA= 5.770E+03		R=0.249180	T=0.699842	5
84	W= 0.700	N= 2.803	K= 0.038	ALPHA= 6.733E+03		R=0.212823	T=0.724436	6
85	W= 0.690	N= 2.809	K= 0.037	ALPHA= 6.706E+03		R=0.194209	T=0.741310	7
86	W= 0.680	N= 2.822	K= 0.037	ALPHA= 6.852E+03		R=0.173189	T=0.758578	8
87	W= 0.670	N= 2.827	K= 0.036	ALPHA= 6.723E+03		R=0.154621	T=0.776247	9
88	W= 0.660	N= 2.832	K= 0.034	ALPHA= 6.516E+03		R=0.136464	T=0.794328	10
89	W= 0.650	N= 2.853	K= 0.038	ALPHA= 7.441E+03		R=0.144886	T=0.803526	11
90	W= 0.640	N= 2.858	K= 0.039	ALPHA= 7.752E+03		R=0.100119	T=0.812831	12
91	W= 0.630	N= 2.866	K= 0.039	ALPHA= 7.861E+03		R=0.087300	T=0.822243	13
92	W= 0.620	N= 2.879	K= 0.042	ALPHA= 8.527E+03		R=0.077895	T=0.822243	14
93	W= 0.610	N= 2.950	K= 0.041	ALPHA= 8.358E+03		R=0.076209	T=0.822243	15
94	W= 0.600	N= 2.945	K= 0.045	ALPHA= 9.468E+03		R=0.082700	T=0.803526	16
95	W= 0.590	N= 2.989	K= 0.046	ALPHA= 9.720E+03		R=0.107895	T=0.776247	17
96	W= 0.580	N= 2.994	K= 0.055	ALPHA= 1.198E+04		R=0.129866	T=0.732825	18
97	W= 0.570	N= 3.014	K= 0.067	ALPHA= 1.480E+04		R=0.163491	T=0.676083	19
98	W= 0.560	N= 3.028	K= 0.082	ALPHA= 1.844E+04		R=0.196560	T=0.616595	20
99	W= 0.550	N= 3.069	K= 0.087	ALPHA= 1.983E+04		R=0.250462	T=0.562341	21
100	W= 0.540	N= 3.108	K= 0.111	ALPHA= 2.588E+04		R=0.297844	T=0.484172	22
101	W= 0.530	N= 3.147	K= 0.132	ALPHA= 3.132E+04		R=0.341776	T=0.421697	23
102	W= 0.520	N= 3.177	K= 0.154	ALPHA= 3.719E+04		R=0.374537	T=0.371535	24
103	W= 0.510	N= 3.209	K= 0.203	ALPHA= 4.994E+04		R=0.391965	T=0.309030	25
104	W= 0.500	N= 3.257	K= 0.247	ALPHA= 6.219E+04		R=0.410204	T=0.260016	26
105	W= 0.490	N= 3.290	K= 0.311	ALPHA= 7.988E+04		R=0.409736	T=0.213796	27
106	W= 0.480	N= 3.333	K= 0.382	ALPHA= 1.000E+05		R=0.404815	T=0.173780	28
107	W= 0.470	N= 3.359	K= 0.467	ALPHA= 1.249E+05		R=0.386374	T=0.138038	29
108	W= 0.460	N= 3.330	K= 0.549	ALPHA= 1.500E+05		R=0.368774	T=0.109648	30
109	W= 0.450	N= 3.302	K= 0.635	ALPHA= 1.773E+05		R=0.351975	T=0.085114	31
110	W= 0.440	N= 3.234	K= 0.717	ALPHA= 2.048E+05		R=0.335941	T=0.066069	32
111	W= 0.430	N= 3.170	K= 0.786	ALPHA= 2.296E+05		R=0.324350	T=0.052481	33
112	W= 0.420	N= 3.114	K= 0.856	ALPHA= 2.561E+05		R=0.315878	T=0.040738	34
113	W= 0.410	N= 3.073	K= 0.935	ALPHA= 2.864E+05		R=0.311185	T=0.030200	35
114	W= 0.400	N= 3.050	K= 1.013	ALPHA= 3.183E+05		R=0.310109	T=0.021878	36
115	W= 0.390	N= 3.073	K= 1.116	ALPHA= 3.597E+05		R=0.315863	T=0.014125	37
116	W= 0.380	N= 3.063	K= 1.188	ALPHA= 3.929E+05		R=0.318777	T=0.010000	38

REFERENCES

[1] D.L. Pulfrey,"Photovoltaic Power Generation",Van Nostrand Reinhold: New York (1978), chapter 1.

[2] See reference 1, chapter 4.

[3] L.C. Olsen, Quarterly Progress rept. NSF/RANN/AER75-20501/PR/75/4 (1975).

[4] L.C. Olsen, Research repts. NSF/RANN/AER 75-20501/PR/76/1,2,3 (1976).

[5] D. Trivich, E.Y. Wang, R.J. Komp and F. Ho, Proc. IEEE Photo. Spec. Conf. 12th, 875 (1976).

[6] D. Trivich, E.Y. Wang, R.J. Komp and A. Kakar, Proc. IEEE Photo. Spec. Conf. 13th, to be published.

[7] R. Forman, Research proposal submitted to NSF, Apr. 1975 (unpublished).

[8] L.C. Olsen, Research rept. NSF/RANN/AER 75-20501/PR/76/1 (1976).

[9] L.C. Olsen and R.C. Bohara, Proc. IEEE Photo. Spec. Conf. 11th, 381 (1975).

[10] R.W. Berry, P.M. Hall and M.T. Harris,"Thin Film Technology", D. Van Nostrand Company: New York (1968).

[11] J.L. Vossen,"Transparent Conducting Films",in Physics of Thin Films , 9, G. Hass and R.E. Thun, Eds., Academic Press : New York (1977).

[12] W.D. Westwood, Prog. Surf. Sci. 7, 246 (1976).

[13] L.I. Maissel,"Application of Sputtering to the Deposition of Films", in Handbook of Thin Film Technology, Edited by L.I. Maissel and R. Glang,McGraw-Hill: New York (1970).

[14] E. Hollands and D.S. Campbell, J. Mat. Sci. 3, 544 (1968).

[15] E. Krikorian and R.J. Sneed, J. Appl. Phys. 37, 3674 (1966).

[16] G. Perny, Le Vide 21, 106 (1966).

[17] R.E. Jones, H.F. Winters and L.I. Maissel, J. Vac. Sci. Technol. 5, 84 (1968).

[18] T. Abe and T. Yamashina, Thin Solid Films 30, 19 (1975).

[19] F. Shinoki and A. Itoh, J. Appl. Phys. 46, 3381 (1975).

[20] J. Hrbek, Thin Solid Films 42, 185 (1977).

[21] J. Heller, Thin Solid Films 17, 163 (1973).

[22] P.A. Redhead, J.P. Hobson and E.V. Kornelsen, "The Physical Basis of Ultra-high Vacuum", Chapman and Hall Ltd.: London (1968) , Chapter 2.

[23] J.W. Coburn, E. Taglauer and E. Kay, Japan J. Appl. Phys. Suppl. 2, Pt.1, 501 (1974).

[24] A.J. Purdes, B.F.T. Bolker, J.D. Bucci and T.C. Tisone, J. Vac. Sci. Technol. 14, 98 (1977).

[25] A.F. Trotman - Dickenson and J.A. Kerr, in Handbook of Chemistry and Physics, 50th edn., F-158, Chemical Rubber Co.: Cleveland(1970).

[26] W.D. Westwood, J. Vac. Sci. Technol. 15, 1 (1978).

[27] V.F. Drobny and D.L. Pulfrey, J. Appl. Phys., submitted for publ.

[28] G. Perny, B. Laville-Saint-Martin, P. Roesler and B. Haller, J. Physique 25, 5 (1964).

[29] B. Goranchev, V. Orlinov and V. Popova, Thin Solid Films 33, 173 (1976).

[30] Powder Diffraction File, ASTM Techn. Publication 48-M2 (1963).

[31] V.P. Smirnov, Sov. Phys.-Sol. State 8, 2020 (1967).

[32] A.A. Arafa, M.E. Kenawy and M.F. El-Daoshy, Acta Physica Polonica, A40, 413 (1971).

[33] A.G. Milnes and D.L. Feucht, "Heterojunctions and Metal-Semiconductor Junctions", Academic Press: New York, p. 139 (1972).

[34] See reference 1, Chapter 3.

[35] N.A. Economu, R.S. Toth, R.J. Komp and D. Trivich, Proc. Intern. Photovolt. Solar Energy Conf., Luxembourg, 1180 (1971).

[36] J.M. Bennet and M.J. Booty, Appl. Opt. 5, 41 (1966).

[37] P.O. Nilsson, Appl. Opt. 7, 435 (1968).

[38] O.S. Heavens,"Optical Properties of Thin Solid Films",Butterworth: London (1955).

[39] O.S. Heavens,"Measurement of Optical Constants of Thin Films", in Physics of Thin Films, 2, G. Hass and R.E. Thun, Eds., Academic Press: New York (1964).

[40] F. Abeles,"Methods for Determining Optical Parameters of Thin Films", in Progress in Optics II, E.Wolf ed., North Holland Publ. Co.: Amsterdam, (1963).

[41] S.G. Tomlin, Brit. J. Appl. Phys. (J.Phys.D) 1, 1667, Ser. 2 (1968).

[42] W.N. Hansen, J. Opt. Soc. Am. 63, 796 (1973).

[43] J.E. Nestell, Jr. and R.W. Christy, Appl. Opt. 11, 643 (1972).

[44] D.E. Carlson, C.R. Wronski, J.I. Pankove, P.J. Zanzuchi, and D.L. Staebler, RCA Review 38, 211 (1977).

[45] H.E. Bennet and J.M. Bennet, in Physics of Thin Films 4, G. Hass and R.E. Thun, Eds., Academic Press: New York (1967).

[46] H. Wieder and A.W. Czanderna, J. Appl. Phys. 37, 184 (1965).

[47] M. Tapiero, J.P. Zielinger and C. Noguet, Phys. Stat. Sol. (a) 12, 517 (1972).

[48] J. Gunderman, K. Hauffe and C. Wagner, Z phys. Chem. B37, 148 (1937).

[49] H.C. Lin,"Integrated Electronics",Holden Day: San Francisco (1967), Chapter VI.

[50] H.J. Hovel and J.M. Woodall, J. Electrochem. Soc. 120, 1246 (1973).

[51] J.A. Hutchby and R.L. Fudurich, J. Appl. Phys. 47, 3140 (1976).

[52] A. Rothwarf and K.W. Boer, Progress in Solid State Chemistry 10, 71 (1975).

[53] D.L. Pulfrey, IEEE Trans. Elec. Dev., to be published Nov. 1978.

[54] D.L. Feucht, J. Vac. Sci. Technol. 14, 57 (1977).

[55] S. Franz, G. Kent and R.L. Anderson, "Heterojunction Solar Cells of SnO_2/Si", presented at the Symposium on Solar Energy Conversion of the 1976 Electronics Materials Conference, Salt Lake City, UT, June 23-26, 1976.

[56] T. Nagamoto and O. Omoto, Japan, J. Appl. Phys. 15, 199 (1976).

[57] J.B. DuBow and D.E. Burk, Appl. Phys. Lett. 29, 494 (1976).

[58] J.C. Manifacier and L. Szepessy, Appl. Phys. Lett. 31, 459 (1977).

[59] R.L. Anderson, Research Report, NSF/RANN/SE/AER 76-04168/PR/77/2,3,4 January 1977.

[60] P.A. Iles and S.I. Soclof, Proc. IEEE Photo. Spec. Conf., 12th, 978 (1976).

[61] D.M. Mattox, Optics News, Summer 1976.

[62] E.Y. Wang and R.N. Legge, Pro . IEEE Photo. Spec. Conf., 12th, 967 (1976).

[63] F.H. Mullins and A. Brunnschweiler, Solid State Electron. 19, 47 (1976).

[64] S. Berg, L.P. Andersson, H. Norstrom and E. Grusell, Vaccum 27, 189 (1978).

[65] T. Mizrah and D. Adler, IEEE Trans. Elec. Dev. ED-24, 458 (1977).

[66] A.H. Pfund, Phys. Rev. 7, 289 (1916).

[67] W.W. Coblentz, U.S. Bureau Standards Sci. Papers 18, 603 (1922)

[68] V.P. Barton, Phys. Rev. 23, 337 (1924).

[69] B. Shonvald, Ann. Phys. 15, 395 (1932).

[70] A.W. Joffe and Th. Joffe, Phys. Z. Sowjetunion 11, 241 (1937).

[71] T. Okada and R. Uno, J. Phys. Soc. Japan 4, 351 (1949).

[72] E. Klier, R. Kuzel and J. Pastrnak, Czech. J. Phys. 5, 421 (1955).

[73] J. Pastrnak and R. Kuzel, Czech. J. Phys. 6, 217 (1956).

[74] F.L. Weichman, Phys. Rev. 117, 998 (1959).

[75] J.D. Shick and D. Trivich, J. Electrochem. Soc. 119, 376 (1972).

[76] G.P. Pollack and D. Trivich, J. Appl. Phys. 46, 163 (1975).

[77] E. Fortin, P. Rochon and J.P. Zielinger, J. Phys. Chem. Solids 36, 1299 (1975).

[78] L. O. Grondahl, Science 64, 306 (1926).

[79] L.O. Grondahl and P.H. Geiger, Trans. A.I.E.E. 46, 357 (1927).

[80] B. Lange, Phys. Zeits. 31, 139 (1930).

[81] B. Lange, Phys. Zeits. 31, 964 (1930).

[82] W. Schottky, Phys. Zeits. 31, 913 (1930).

[83] W. Schottky, Phys. Zeits. 32, 833 (1931).

[84] E. Duhme and W. Schottky, Naturwiss. 18, 735 (1930).

[85] E. Duhme, Zeits. F. Elektrochemie 37, 682 (1931).

[86] L.O. Grondahl, Rev. Mod. Phys. 5, 141 (1933).

[87] D. Trivich, E. Wang, R.J. Komp and F. Ho, Proc. IEEE Photo. Spec. Conf. 12th, 875 (1976).

[88] L. Olsen, Annual. rept. NSF/RANN/AER 75-20501/PR/76/3 (1976).

[89] L. Olsen, Quarterly Progress rept. NSF/RANN/AER 75-20501/PR/76/2 (1976).

[90] V.F. Drobny and D.L. Pulfrey, Proc. IEEE Photo. Spec. Conf. 13th, to be published.

[91] See reference 38, p. 4.

[92] R.S. Toth, R. Kilkson and D. Trivich, J. Appl. Phys. 31, 1117 (1960).

[93] B.D. Cullity, "Elements of X-ray Diffraction", Addison-Wesley Reading: Mass. (1956).

[94] J.G. Byrne, "Recovery, Recrystallization and Grain Growth", The MacMillan Company : New York (1965).

[95] J.J. Gilman, "The Art and Science of Growing Crystals", John Wiley and Sons, Inc.: New York (1963).

[96] J. Bardeen, W.H. Brattain and W. Shockley, J. Chem. Phys. 14, 714, (1946).

[97] L.J. Van der Pauw, Philips Research Repts. 13,1 (1958).

[98] J. Pastrnak, Czech. J. Phys. B11, 374 (1961).

[99] I. Pastrnyak, Soviet Physics - Solid State 1, 143 (1959).

[100] E.F. Gross, Nuovo Cimento Suppl. 3, 672 (1956).

[101] A. Compaan and M.Z. Cummins, Phys. Rev. Lett. 31, 41 (1973).

[102] J. Schewchun, J. DuBow, A. Myszkowski and R. Singh, J. Appl. Phys. 42 (2), 855 (1978).

[103] C. Moore Lee "UBC NLE", Computing Center of U.B.C. (1977).